Robust but Flexible: Information Processing and Retrieval in Core Auditory Cortex

Von der Fakultät für Medizin und Gesundheitswissenschaften

der Carl von Ossietzky Universtität Oldenburg

zur Erlangung des Grades und Titels eines

Doctor rerum naturalium (Dr. rer. nat.)

angenommene Dissertation

von Frau **Tina Brigitte Gothner**

geboren am 15.12.1985 in Ansbach

Contents

List of Figures

List of Tables

List of Abbreviations

AAV	adeno-associated virus
A1	primary auditory cortex
AC	auditory cortex
AP	action potential
BF	best frequency
BW	bandwidth
ChR2	Channelrhodopsin-2
CR	correct rejection
DRC	dynamic random chords
EYFP	enhanced yellow fluorescent protein
FA	false alarm
LDA	linear discriminant analysis
MI	mutual information
NS	natural stimuli
PCA	principle component analysis
PV+	parvalbumin-positive interneuron
PSTH	peri-stimulus time histogram
SFO	step-function opsin
SOM	somatostatin-positive interneurons
SSFO	stable step-function opsin
ST	single pure tone stimuli
STRF	spectro-temporal receptive field
VIP	vasopressin-positive interneurons

Zusammenfassung

Die meisten Entscheidungen und Handlungen werden durch unsere Umgebung beeinflusst. Informationen aus unserer Umgebung müssen zuerst festgestellt und bearbeitet werden bevor sie für weitere Handlungen auf Abruf zur Verfügung stehen können. Informationsverarbeitung (information processing) und Informationsabruf (information retrieval) finden in spezifischen sensorischen Arealen des Gehirns statt. Da sie dort dieselben neuronalen Strukturen und Mechanismen des zentralen Nervensystems nutzen, müssen sie jeweils mit spezifischen Herausforderungen zurechtkommen. Auf der einen Seite müssen Informationsverarbeitung und Informationsabruf flexibel auf ihre Umgebung hin reagieren. Auf der anderen Seite müssen sie grundlegende Informationen robust weitergeben. Wie können Robustheit und Flexibilität gleichzeitig innerhalb desselben Systems umgesetzt werden? Die vorliegende Thesis umfasst zwei Studien, die jeweils innerhalb der Informationsverarbeitung bzw. des Informationsabrufs untersucht, wie die zwei gegensätzlichen Funktionen der Robustheit und Flexibilät realisiert werden. Hierfür wurden neuronale Daten aus dem auditorischen Zentrum von Mäusen durch extrazelluläre Ableitungen erhoben.

Die erste Studie untersucht die Rolle der parvalbumin-positiven Interneurone (größte Klasse kortikaler inhibitorischer Interneurone) während der auditorischen Informationsverarbeitung. Hierfür wurden diese Neurone auf einer verhaltens-relvanten Zeitspanne nachhaltig und netzwerkweit optogenetisch manipuliert und die neuronale Aktivität von kortikalen Neuronen auf auditorische Signale hin abgeleitet. Die Ergebnisse aus Einzelzellantworten zeigen, dass die spektralen und temporalen Eigenschaften (Tuning) der kortikalen auditorischen Neurone konserviert bleiben, obwohl die allgemeine neuronale Netzwerkaktivität wesentlich reduziert ist. Diese hauptsächlich dividierende Reduktion der Aktivität konnte sowohl für einfache, als auch für komplexe und naturalistische Stimuli dargestellt werden. Die Ergebnisse weisen darauf hin, dass parvalbumin-positive Interneurone einen Mechanimus für neuronale dividierende Verstärkungsregelung (input-output mapping, gain control) besitzen, der die Eigenschaften d es Stimulus selbst robust erhält.

Die zweite Studie behandelt den kortikalen Informationsabruf verschiedener Aspekte auditorischer Stimuli. Den Mäusen wurden während der extrazellulären Ableitung verschiedene Tiervokalisationen akustisch präsentiert, die entweder verhallt oder unverhallt waren. Mithilfe der Populationsantworten

konnte sowohl die Vokalisationsidentität (welche Tiervokalisation) als auch der Kontext (verhallt oder nicht) erfolgreich klassifiziert werden. Zusätzlich konnten Mäuse in Verhaltensexperimenten mit einem 'Go/No-go' Paradgima erfolgreich verhallte Stimuli detektieren. Diese Ergebnisse führen zur Annahme, dass die Informationen für die Vokalisationsidentität und für den Kontext vollständig und robust vorhanden sind und diese jeweils abgerufen werden können, wenn diese Informationen benötigt werden.

Obwohl beide neuronalen Prozesse (Informationsverarbeitung und Informationsabruf) verschiedene Aufgaben erfüllen, ist ihre Struktur die gleiche. Auf der einen Seite müssen sie ein robustes Fundament schaffen, das bei der Informationsverarbeitung und auch beim Informationsabruf gegenüber ungewollten Einflüssen widerstandsfähig ist. Auf der anderen Seite benötigen die beiden Prozesse die Möglichkeit Einfluss auf die Informationsverarbeitung zu erlauben oder flexibel gezielt auf Informationen zugreifen zu können.

Abstract

Most decisions and behavior depend on our surrounding. These environmental information have to be transduced, processed first and then can be retrieved for further reactions. Information processing and retrieval take place in specific sensory areas of the brain. Since both are sharing the same neuronal structures and mechanism of the central nervous system, they have to cope with particular challenges. On the one hand, information processing and retrieval have to adapt flexibly due to their environment. On the other hand they have to provide basic information robustly. How can robustness and flexibility co-exist within the same system? The present thesis contains two studies, observing how these two contradictory dimensions flexibility and robustness can be realized in information processing and retrieval, respectively. Therefore, neuronal data were collected from the core auditory cortex of mice using extracellular recordings.

The first study investigates the information processing role of parvalbumin-positive interneurons (the largest class of cortical inhibitory interneurons) within auditory cortical computation. Using sustained, network-wide optogenetic manipulation to modulate these interneurons on behaviorally relevant timescales the neuronal activity of cortical neurons due to auditory signals was recorded. Single-unit analysis showed highly conserved spectral and temporal tuning in auditory cortical neurons, despite a profound reduction in overall network activity. The profound reduction was predominantly divisive, and consistent across simple, complex, and naturalistic stimuli. These results suggest that parvalbumin-positive interneurons may provide a means for divisive gain control (input-output mapping), which enables flexible adaption while conserving stimulus characteristics robustly.

The second study obtains the cortical information retrieval of different aspects of auditory stimuli. During extracellular recordings of mice, different animal vocalization, which were reverberated or not, were acoustically presented. Here, the vocalization identity (which animal vocalization) and context (reverberated or not) were successfully classified using population responses. Additionally, mice successfully detected reverberated stimuli in behavioral 'Go/No-go' experiments. These results lead to the assumption that information for both vocalization identity and context entirely robustly exist and can be flexibly retrieved if required.

Although both computational procedures (information processing and information retrieval) fulfill

different tasks, they are structured the same way. On the one hand, they need to create a robust fundament which maintains basic features (information processing) or information (information retrieval) and resists unwanted influences and disturbances. On the other hand, both processes have to allow essential influences (information processing) or have to precisely extract required information (information retrieval) for a particular behavior.

1. Introduction

Hearing, sight, touch, smell and taste are the five basic senses of human. With the help of these senses we can perceive our environment. This is important because most of our decisions and behavior like action or reaction depend on our surrounding.

The information from the surrounding therefore have to be transduced, processed and then provided for further reactions. The first step is to transduce the information from the environment to neuronal signals. Depending on the kind of information, a highly specialized sensory organ is in charge of the transduction. For instance, ears are capable of transducing sounds. The second step is to process these transduced information. At this stage, information processing enables to combine various information. For instance, in order to locate the source of a sound it is necessary to process the information transduced by both ears. The third step is to provide these processed information in order to retrieve them for a behavior. For instance, after information processing it is possible to turn the head towards the source of the sound. All three steps (information transduction, processing and retrieval) are necessary to interact with and react to the environment and forms the fundament of any behavior. This is the task of which the sensory nervous system is capable of.

Where do information transduction, processing and retrieval take place within the sensory nervous system? Information transduction arises by a highly specialized sensory organ. This has the advantage, that the organ is particularly designed for its functional task and thus is able to manage challenges quite well. In contrast to information transduction, information processing and retrieval take place at specific areas of the brain. On the one hand, this is a logistical advantage for both information processing and retrieval. For processing, necessary information from different brain areas can easily be provided and sent to one site in the brain. Furthermore, processed information can be supplied fast for information retrieval. On the other hand, processing and retrieval have to share the same neuronal mechanisms (like neuronal connections) in the brain, although processing and retrieval aim different goals. As information processing and retrieval share the same neuronal structures, they have to use different strategies in order to fulfill their particular tasks. Hence, the context of this thesis is to observe possible strategies for both information processing and retrieval while they are sharing

the same neuronal structures. In the following, information processing and retrieval deserve more detailed explanation.

The task of information processing is to integrate various information. Hereby the kind of information does not matter. On the one hand, information that have to be processed can be arose by the same sensory organ. For example, the ability to identify different musical instruments within one musical piece: the ear arises all acoustic sounds of the musical piece but information processing makes it possible to distinguish between different musical instruments. On the other hand, processing information from different sensory organs can enlarge the perceived environment and can help to detect any possible danger. For example, to hear an approaching car and to see an icy road can convince somebody to stay on the pavement and not to cross the road. All in all, information processing combines various information and brings them into the right context.

After information have been processed they can be retrieved and hence used for further actions. Information retrieval is the ability to extract required information which have been processed before. The function and task of information retrieval can be illustrated well with an example of listening to a music band while being in the audience. After processing, identifying the sound of the guitar only is possible. Maybe the guitar player is too far away from the audience and the sound is not as loud as expected. Hence, the soft sound level (this is the retrieved information) of the guitar player wants to make a listener move towards the stage. At the same time, all other musicians of the band make music as well. The information of these musicians have been processed as well but does not play a role for the listener. All information from the whole music band are provided by information processing, but only those information are retrieved (the sound level of the guitar) which are necessary for the listener's interest or for his actions and reactions.

To sum up, information processing and retrieval have different responsibilities. Information processing combines various information in order to provide them for information retrieval. Out of it, information retrieval extracts only necessary and required information. Both information processing and retrieval take place in the brain using the same neuronal structures. Since they are sharing the same neuronal structures and mechanisms, they have to use different strategies in order to fulfill their particular tasks and cope with specific challenges.

What are the requirements of information processing and retrieval and how do they meet their specific challenges? On the one hand, both have to be flexible and adaptable due to different scenarios like the number and kind of combined information (information processing) or the retrieval of required information for a behavior (information retrieval). On the other hand, both have to be robust in the meaning of rejecting disturbances (information processing) or providing all available information for further actions (information retrieval). Are robustness and flexibility a contradiction? Robust

but flexible at once - the aim of this thesis is to investigate the role of robustness and flexibility for information processing and retrieval with the help of the auditory system.

The overall purpose of this thesis is to characterize how robustness and flexibility interact to each other in both information processing and retrieval in the auditory system. Therefore, neuronal data were collected from the core auditory cortex (AC) of mice using extracellular recordings. Information processing and retrieval were regarded in two separate studies. By analyzing information processing (chapter 4), the computational role of a specific type of neuron was examined. By analyzing information retrieval (chapter 5), the information content due to a presented stimulus (e.g. reverberated sound and non-reverberated sound) was observed. In order to prepare the reader for both studies, the following two chapters provide detailed information. Chapter 2 informs about the auditory system and provides a view of the neuronal data which were collected for both studies. Chapter 3 refers to both experimental and analysis methods of both studies.

2. How does neuronal activity in the auditory cortex arise?

"The auditory system is one of the engineering masterpieces of the human body." (Purves et al., 2004) From the translation of acoustic sound waves to neuronal information, the ear makes a lightning start in auditory processing. Neuronal integration of both ears enables not only to localize the source of a sound but also to identify different sound sources within an environment full of acoustical distraction and noise. We can receive auditory information from distances and spots which the eyes cannot see. Spoken words and music can change our moods, can make us happy or sad. In order to realize this engineering masterpiece, the auditory pathway is a sophisticated system of parallel processing and intense crosslinks that makes complex processing on high level possible. For all of this, the nervous system allocates a large number of neurons which differ in morphology and molecular structures but can be categorized into only two functional groups of neurons: excitatory and inhibitory neurons.

This chapter provides an overview of the biological formation from physical acoustic wave forms to neuronal signals and its way to the AC in mice. For this thesis, activity from neurons of the AC were recorded and furthermore local parvalbumin-positive interneuron (PV+) cells of the middle cortical layers got optogenetically manipulated. Hereafter, the auditory system is introduced.

2.1. From the outside to the brain: the ascending pathway of the auditory system

Acoustic sound waves get transferred from air pressure to mechanical vibrations via the tympanic membrane. After amplification by the middle ear bones,the vibrations enter the fluid-filled cochlea (inner ear) at the oval window. Vibrations at the oval window cause an oscillation of the basilar membrane which is a part of the cochlea. Oscillations of the basilar membrane get translated into electrical impulses (hair cells) as action potential (AP) within the organ of Corti. Receptor hair cells

are placed between the basilar membrane and the tectorial membrane. The movement of the basilar membrane causes shear forces on top of the hair cells and depolarizes the hair cells by mechanical opening of ion channels. As a result, hair cells induce frequency-depending transmitter release, which binds to the receptors of the auditory nerve fibers (mechanoelectrical transduction). Thenceforth, neuronal transmission via AP begins (Hudspeth, 1997; Robles and Ruggero, 2001; LeMasurier and Gillespie, 2005).

All fibers of the auditory nerve synapse on further neurons within the cochlea nuclei complex, which is part of the brainstem (Fig. 2.1 left). From there on, the ascending auditory pathway runs on three parallel traces. Most axons of the dorsal cochlear nuclei cross over and connect to the nuclei of the lateral leminiscus (pons) contra-laterally (dorsal acoustic striae). Some neurons from the posteroventral cochlea nuclei synapse on the contralateral nuclei of the lateral leminiscus (intermediate acoustic striae). A small part of the anteroventral cochlea nuclei connect ipsi-laterally, whereas the main part of the nuclei complex (ventral acoustic striae) cross over and synapse contra-laterally on the superior olivary nuclei complex. Axons from the superior olivary complex ascend with the intermediate and some fibers of the dorsal acoustic striae and axons of the nuclei of the lateral leminiscus as a bundle of fibers (lateral leminiscus). This bundle connects to the inferior colliculus in the midbrain. Before auditory information enter cortical structures, all ascending fibers (mostly from the inferior colliculus) have to pass the medial geniculate complex of the thalamus and are involved in multisensory processing. From the thalamus, radiations run to the primary auditory cortex (A1) in the temporal lobe (Thompson and Schofield, 2000; Cant and Benson, 2003; Malmierca, 2003; Keifer et al., 2015).

Summing up, acoustic environmental information gets translated to AP in the cochlea of the inner ear and ascend to the primary auditory cortex via several pathways, passing the cochlea nuclei complex and the medial geniculate complex of the thalamus. Parallel pathways enable to integrate multisensory input like bi-aural information for sound localization or allows descending circuits to regulate motor neurons. The auditory cortex as central target provides higher-order processing of sound and its perception.

Figure 2.1.: The auditory cortex contains different neuronal cell types (red box): Exc: excitatory pyramidal cells; PV: inhibitory parvalbumin-positive interneurons; SOM: inhibitory somatostatin-positive interneurons; VIP: vasopressin-positive interneurons; TC: thalamo-cortical projections neurons; Open circles: excitatory synapse; closed circles: inhibitory synapse (Blackwell and Geffen, 2017). Neuronal recordings enable to calculate the spectro-temporal receptive field (STRF) of single neurons (grey circle). Yellow areas mark excitatory fields while dark blue areas mark inhibitory fields of the neuronal response (read from left to right) and the average stimulus that elicit and AP (read from right to left).
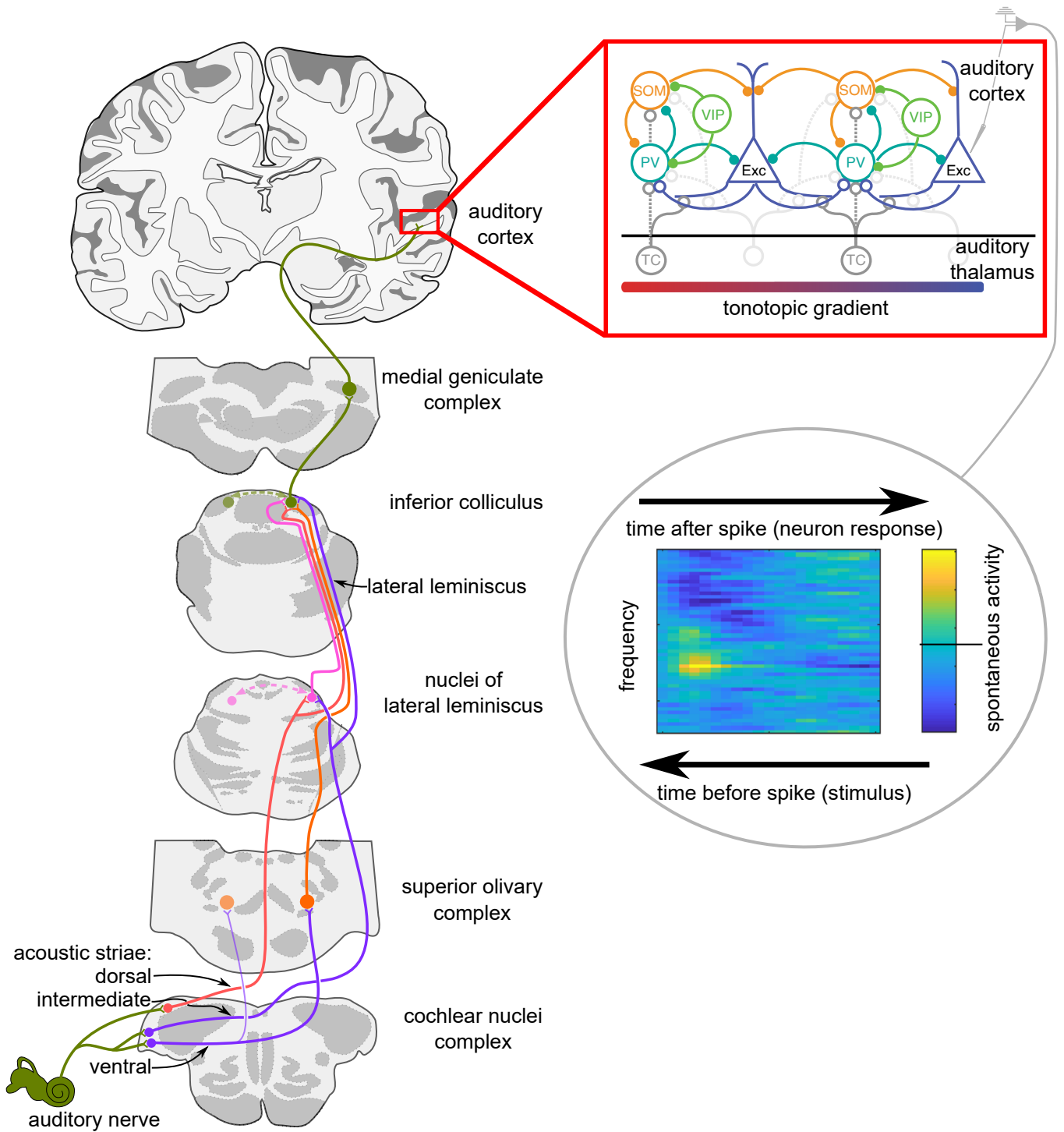
Figure 2.1.: **Auditory pathway and cortical structures.** On the way to the auditory cortex auditory processing passes different subcortical structures via three parallel pathways (brain slices and cochlea, adapted from Purves et al. (2004)).

2.2. Structures and neurons of the auditory cortex

The mouse AC is located in the superior temporal-parietal lobe and can be divided in five areas. The neurons within these areas respond mainly to specific frequencies, such as the A1 represents tone frequencies from 2 kHz to 45 kHz. These frequencies are arranged tonotopically among the rostral-caudal plane (Caviness, 1975; Stiebler, 1987; Stiebler et al., 1997).

As all neocortical structures, the A1 is horizontally arranged in six layers. Efferent nerve fibers to other cortical areas arise from layer II/III and to subcortical areas from layer V/VI. Afferent nerve fibers from the thalamus enter the A1 in middle layers. Vertically, groups of neurons in all six layers can be outlined to single columns of a neuronal network: Columns receive neuronal input, compute them and send those processed information to further areas. Unlike other sensory cortices, the AC receives input from both ears, ipsilaterally and contralaterally (Mountcastle, 1997; Linden and Schreiner, 2003; Harris and Mrsic-Flogel, 2013).

Those networks are managed by excitatory and inhibitory neurons (Fig. 2.1 red box). Up to 80 % of all cortical neurons are excitatory principal cells. The most prominent group of principal cells are pyramidal neurons. Pyramidal cells are mostly located in layers III and V and form, among other things, long-range axons to further sensory cortices. Pyramidal cells in layer II/III show low firing rates and are highly influenced by GABAergic interneurons. Those inhibitory interneurons are the remaining 20 % of cortical neurons. They can be classified into three major subgroups, which differ morphologically and molecular-biologically: PV+, somatostatin-positive interneurons (SOM) and vasopressin-positive interneurons (VIP) neurons (DeFelipe, 1997; Cruikshank et al., 2001; Linden and Schreiner, 2003; Markram et al., 2004; Xu et al., 2010; Moore and Wehr, 2013; Harris and Mrsic-Flogel, 2013; Tremblay et al., 2016).

The largest subgroup of interneurons (40 %) forms PV+ neurons. Parvalbumin proteins in those neurons are considered as intracellular calcium buffer with a high affinity to calcium but at a slow speed. Most PV+ neurons are fast-spiking basket cells, which synapse on the soma and proximal dendrites of pyramidal cells and other interneurons (especially PV+ cells). Chandelier cells are connected to the initial segment of pyramidal cells. Both groups together form a fast and strong influence on the excitatory output of pyramidal cells. Since both pyramidal cells and PV+ neurons receive thalamic input, PV+ neurons are involved in the feed-forward inhibition of pyramidal cells: Pyramidal cells receive excitatory input from the thalamus and delayed inhibitory input by the PV+ neurons. This circuit permits to stabilize the inhibited cell and forms a buffer system for changed spectral input (DeFelipe, 1997; Caillard et al., 2000; Cruikshank et al., 2001, 2007; Moore and Wehr, 2013; Harris and Mrsic-Flogel, 2013; Tremblay et al., 2016).

About 30 % of inhibitory interneurons are SOM cells. They mainly receive input from local and distant cortical areas and synapse on PV+ neurons and pyramidal cells. They are strongly involved in lateral inhibition. Therefore, they inhibit pyramidal cells they were excited from and in addition they inhibit further local pyramidal cells (Harris and Mrsic-Flogel, 2013; Tremblay et al., 2016; Riedemann, 2019).

The smallest major subgroup of interneurons are VIP neurons (10 %). Theses neurons primarily synapse on SOM neurons and with less influence on PV+ cells. Activation of VIP neurons (from higher-order cortical areas like motor cortex) lead to a disinhibition of pyramidal cells due to inhibited SOM neurons (Harris and Mrsic-Flogel, 2013; Tremblay et al., 2016; Posluszny, 2019).

2.3. Spectro-temporal receptive fields of the auditory cortex

Sherrington (1906) evoked in cervical transected dogs a scratch-reflex by electrical stimulation of certain areas of the dog's skin. He called this area the receptive field of the scratch-reflex and can be described as the sensory area in which a stimulation can elicit a neuronal response.

Since then, receptive fields of single neurons have been described in several sensory systems (e.g. visual (Hubel and Wiesel, 1962), olfactory (Wilson, 2001) and have been estimated in form of spike-triggered averages (Fig. 2.1 grey circle). Hence, receptive fields give information about the average stimulus that triggers a spike (what it needs to evoke a spike) as well as the response pattern of the neuron after an appropriate stimulation (how the neuron responds to a stimulus). In the auditory system, both the proper stimulus and response pattern depend on temporal and spectral aspects of an acoustic stimulus (spectro-temporal receptive fields, STRFs).

Based on the balance between neuronal excitatory and inhibitory circuits, the STRF is a dynamic structure that shares the attributes of the cortical plasticity like age-related reorganization, learning or context-depending environment. On that account, the STRF adapts to the sensory environment (Fritz et al., 2003; Keuroghlian and Knudsen, 2007; de Villers-Sidani et al., 2010; Froemke and Jones, 2011).

3. How to make auditory information accessible?

The comprehension of the theoretical background is required to understand and interpret the collected data correctly. In order to provide this knowledge, the aim of this chapter is twofold: On the one hand, this chapter gives an overview of the subjects and methodical tools used in both research parts (chapter 4 and 5) unless otherwise stated. On the other hand, this chapter provides space to focus on further information about specific topics: The mechanism about the used optogenetic tool and electrophysiological analyzing methods are spotlighted here.

Contents of this chapter (sections 3.1, 3.2) are published in Gothner et al. (2020).

3.1. Mouse strain

All data presented here were obtained from male B6.Cast/PVALB-Cre mice. This line is a cross between B6.CAST-Cdh23 (Stock number 002756, Jackson Laboratory, Bar Harbor, ME, US) and PVALB-IRES-Cre mice (Stock number 008069, Jackson Laboratory, Bar Harbor, ME, US), crossed and reared in the animal facilities of the University of Oldenburg. These animals are not susceptible to developing the early-onset age-related hearing loss typical of the standard C57BL/6J strain due to a major gene responsible on chromosome 10 (Johnson et al., 1997). Cre-recombinase was expressed in inhibitory PV+ (Hippenmeyer et al., 2005), enabling to manipulate those neurons optogenetically following injection of an cre-dependent viral vector (chapter 4). All mice were housed separately following surgical implantation with recording devices and maintained on a reversed 12 h/12 h light-dark cycle at approx. 23 °C with access to free water and food.

All procedures were performed in accordance with the animal welfare regulations of Lower Saxony and approved by the local authorities (State Office for Consumer Protection and Food Safety / LAVES).

3.2. Surgery

Mice were equipped with a 32-channel self-made chronic implant (probe) for extracellular recordings (chapters 5 and 4) and additional optogenetics (see chapter 4) at the age of 8 to 12 weeks. Animals were injected subcutaneously with 0.1 mg/kg meloxicam pre- and post-operatively to reduce pain and inflammation. During surgery, the animals were anaesthetized with 1.5 % isoflurane (initial: 2 %). Body temperature was monitored and held at approx. 37 °C. Eyes were covered with ophthalmic ointment. Anaesthetized mice were fixed in a stereotaxic apparatus (Model 900, Kopf instruments, Tujunga, CA, US) with zygomatic clamps. After skull exposure, a trepanation was drilled in the dorsal skull (relative to Bregma: anterior-posterior -2.6 mm, medial-lateral -2.9 mm, injection angle 24 °, right hemisphere) to allow tangential access to the region designated AC in the Allen Mouse Brain Atlas (2011, www.mouse.brain-map.org). For optogenetic experiments, 1000 nl of adeno-associated virus (pAAV-EF1/a-DIOhChR2-(C128S/D156A)-EYFP, serotype 5, Vector Core, University of North Carolina, US; Fig. 3.1 A) was injected (Nanofil 10 µl, WPI, Hertfordshire, UK) at 150 nl/min at each of two depths within auditory cortex (z=3.7 and z=3.9-4.0 mm from entry point in dorsal cortex). aftter virus injections, the probe was implanted with the electrode tips placed at the 3.7 mm depth initially (Fig. 3.1 B). This placement resulted in a path of the electrodes that was tangential to the cortical surface at a depth of approximately 400µm, so most of our recordings likely stem from middle layers of core auditory cortex. In order to fix the implant microdrive onto the skull, five to six screws were drilled into the skull, one of which over the contra-lateral pre-frontal cortex served as reference for the recordings. The implant microdrive was then secured to the skull and screws with dental acrylic (Vertex SC, Vertex Dental, Zeist, Netherlands). After surgery, mice were given a recovery period between 7 and 14 days before recordings began (Fig. 3.1 C).

3.3. Optogenetic design

Optogenetic is a tool which enables to control light-sensitive ion channels embedded in the cell membrane of specific neurons and permits a fast regulation of the activity of those neurons in *in vivo* experiments (Nagel et al., 2003; Boyden et al., 2005; Deisseroth et al., 2006). This technique was used in chapter 4.

3.3.1. Manipulating PV+ neurons optogenetically using the cre-loxP system

Using the Cre/loxP system (Metzger and Chambon, 2001) to express light-sensitive ion channels in neurons of interest, two components are required: The transgentic mouse strain B6.Cast/PVALB-Cre

provides the expression of cre-recombinase in any neurons expressing parvalbumin (Hippenmeyer et al., 2005). Cre-recombinase is an enzyme from bacteriophage P1 for site-specific recombination within a DNA sequence (Sauer and Henderson, 1988). The used viral vector pAAV5-EF1/α-DIO-hChR2-(C128S/D156A)-EYFP is an adeno-associated virus (AAV) which carries the gene for a light-sensitive ion channel hChR2-(C128S/D156A) (Fig .3.1 A box). This gene is inserted in the viral vector in inverted orientation and flanked by two sets of different lox-sites (DIO). Lox is a site-specific area that the cre-recombinase requires for recombination. Using one set of lox-sites, the cre-recombinase first flips the inverted gene sequence. Using the second set of lox-sites, the cre-recombinase deletes either one lox site of both sets in order to terminate the function of cre-recombinase. This enables the transcription of light-sensitive ion channels in specific PV+ neurons using a non-neuron specific but robust promoter EF1/α (Zhang et al., 2006). The production of light-sensitive channels can be evaluated afterwards due to the binding of enhanced yellow fluorescent protein (EYFP) to the transcribed channel using fluorescence microscopy with an excitation peak of 514 nm and an emission peak of 527 nm (Shaner et al., 2005). In the absence of cre-recombinase, the transcription of the inverted gene sequence leads to a nonsense protein without any functions (Gopaul and Duyne, 1999; Guo et al., 1999; Tronche et al., 2002; Yizhar et al., 2011a).

For most optogenetic experiments AAV is a well-established and safe viral vector that enters neurons via PDFG receptors by binding to sialic acid (Di Pasquale et al., 2003). Within the host neuron, AAV remains in an extra-chromosomal state and does not interact with the host genome (Flotte and Berns, 2005). Compared to other serotypes, the diffusion of serotype 5 of AAV(AAV5) within tissue is wide-ranging and provides the transcription of the desired light-sensitive ion channel to a large cortical area (Paterna et al., 2004).

3.3.2. Double-mutant of Channelrhodopsin-2 offers a stable step-function opsin for optogenetics

The ion channel hChR2-(C128S/D156A) is a light-sensitive unspecific cation channel (Yizhar et al. (2011b); Fig. 3.1 d) and a modified variant of the wild-type ChR2 from the green algae *Chlamydomonas reinhardtii* (Nagel et al., 2003). As a part of the rhodopsin-family, ChR2 is a transmembrane protein that consists of a light-sensitive microbial-type chromophore and an unspecific cation channel. After absorbing light at a wavelength of 480 nm, the chromophore isomerizes and the channel pore opens. Those open channels permit diffusion of further cations and modify the membrane conductance: the cell depolarizes. Channel closing occurs within 11 ms due to channel kinetics (Nagel et al., 2003; Zhang et al., 2006; Bamann et al., 2008; Berndt et al., 2009; Yizhar et al., 2011a).
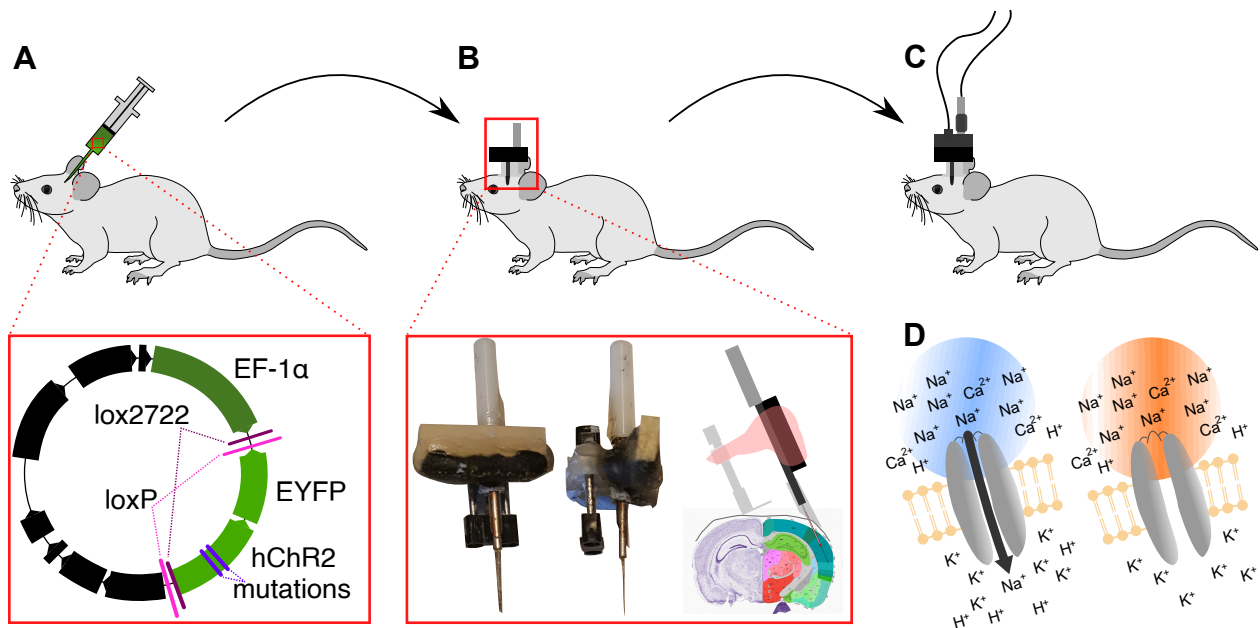
Figure 3.1.: **Outline of optogenetic experimental procedure. (a)**: Injection of viral DIO-vector for optogenetic experiments at core auditory cortex. Cre-recombinase in PV+ neurons inverts the gene of ChR2 within the double lox sites for correct transcription (box). Vector adapted from everyVECTOR (2009). **(b)**: Customized movable probe (box) **(c)**: Electrophysiological recording and optogenetical control are separate parts of the implant. **(d)**: Function of SSFO in PV+ neurons: activation of unspecific ChR2 cation channel using blue light, deactivation using orange light (left channel adapted from Yizhar et al. (2011a)). Mouse adapted from Encyclopaedia Britannica (2010)

The genetic modification of the wild-type ChR2 allows to adapt the channels kinetics in regard to experimental designs: The most effective adaption of ChR2 is the mutation of cysteine-128 to serine (C128S). On the one hand, the C128S-channels do not close immediately after light-offset and remain open for more than 100 s. Based on this characteristic, this mutant ChR2 was designated as step-function opsin (SFO). As a result, the neurons resting membrane potential depolarizes towards the spiking threshold and increases the excitability of the neuron. On the other hand, it is possible to close the channel manually using a light pulse with a wavelength of approx. 540 nm. Using pulses of blue and yellow light enables to manifest a fast bi-stable optogenetic SFO switch (Berndt et al., 2009; Yizhar et al., 2011a). Further mutation of aspartic acid-156 to alanine (D156A) prevents the closing of ChR2-channels after light-offset for more than 30 min and hence stabilizes the SFO-characteristics as SSFO (Yizhar et al., 2011b). In the end, replacing algal codons with mammalian codons (humanized ChR2, hChR2) enhances the expression of the ChR2-(C128S/D156A)-channels (Zhang et al., 2006; Yizhar et al., 2011a).

3.4. Electrophysiological Analysis

All recorded data from AC are continuous raw voltage data collected by eight tetrodes (32 channels) at a sample rate of 30 kHz. For further analysis, spike times for single units were identified.

3.4.1. Spike detection and sorting

Identifying spike times for single units from continuous raw voltage recordings includes two steps: first, typical spike wave forms have to be detected in individual voltage traces (spike detection) and second, detected spike wave forms have to be grouped based on different aspects of their shapes in order to distinguish between individual neurons (spike sorting). For spike sorting fitting models were created based on a sub-sample of data (10 minutes of recordings) and afterwards applied to the whole recorded data set of the experimental day.

In a first step, generalized noise (external interference factors) recorded in all channels was removed from every channel. Therefore, the arithmetic mean of each recorded voltage sample over all channels was calculated and subtracted from each individual channel. Then, spike detection, model fitting and applying was carried out tetrode-wise.

Voltage traces from all four channels were highpass-filtered (finite pulse response filter, 256th order) and upsampled for spike detection. For each event higher than a certain manually adjusted threshold and specific condition of the event (peak alignment within event snippet, size), the center of mass was calculated to determine the timing of the detected spike. For spike-sorting, a principle component analysis (PCA) was used to distinguish spike cluster in reduced dimensions (for detailed information, see Sahani (1999); Hildebrandt et al. (2017)). Hence, spike times were extracted and classified into single-units.

3.4.2. Single-unit and population responses

Behavior is the result of neuronal interactions and integration of different networks of local and/or global processing. The functional role of individual neurons in those networks depends on several cellular factors like protein expressing and structure of the cell membrane as well as on network factors like place and strength of connected neurons (Bean, 2007; Tremblay et al., 2016; Blackwell and Geffen, 2017).

A neuronal network is supported by individual neurons with individual encoding properties. Single-unit analysis can uncover those properties to distinguish different roles of neurons within the network. Perel et al. (2015) observed in recordings of the motor cortex in Rhesus monkeys, that individual

encoding properties of single-units are necessary to provide information about the aspect direction in movement, but in order to complete the whole behavior (e.g. speed and velocity), further information beside single-unit properties (e.g. local field potential) are mandatory.

Single-unit analysis (chapter 4) can produce immense information processing content across time but not across neurons. For this, population response analysis (chapter 5) offers additional computational tools like population-based stimulus decoding for information retrieval, which can be a more natural estimator for fast reaction outcome within few milliseconds (Panzeri et al., 2015).

3.4.3. Mutual information in population response

The mutual information (MI) describes the amount of information that the neuronal response carries about the stimulus. The statement of MI of a population response can be provided by the number of neurons instead of the number of repeated measurements. This allows to estimate instantaneously a reaction due to an input stimulus. Analyzing the information content across neurons enables to observe different time fractions during the stimulus, which can provide multiplex coding strategies of a neuronal network.

The MI is given by the overall response entropy minus the average noise entropy, whereby entropy represents the average information of a random variable:

$$MI = \underbrace{-\sum_r p(r) \; log_2 \; p(r)}_{overall \; response \; entropy} \; - \; \underbrace{-\sum_s p(s) \sum_r p(r|s) \; log_2 \; p(r|s)}_{average \; noise \; entropy}$$

where $p(r)$ denotes the probability of observing neural response to any stimulus, $p(s)$ is the probability of presentation of stimulus s and $p(r|s)$ donates neural response r when the stimulus s is presented.

MI was computed in chapter 5 by using the information breakdown toolbox for fast information analysis (Magri et al., 2009).

3.4.4. Stimulus classification in population response

Population decoding across neurons is a powerful analyzing tool in order to answer the question: Does the collected data contain important feature information about the stimulus? The task of population decoding is the prediction of a presented stimulus or observed behavior from recorded neuronal activity. In chapter 5, population decoding was used to categorize (classify) neuronal activity into different subtypes of auditory stimuli (stimulus classification).

The heart of stimulus classification is a pattern classifier. This is an algorithm (e.g. maximum correlation coefficient classifier, support vector machine, Euclidean distance classifier) that learns the relationship between neuronal population response across neurons and its referring stimulus. For this, a subset of data (population response and its referring stimulus) serve as training data for the pattern classifier in order to associate both inputs. Afterwards, the remaining subset of data is used for testing the adjusted pattern classifier. Here, the result of the pattern classifier is the predicted stimulus of the test data. Comparison of the predicted stimulus to the presented stimulus indicates the success of the pattern classifier and hence gives an outlook of feature information content in the neuronal population response due to the stimulus (Zhang et al., 2011; Meyers, 2013).

3.4.5. Stimulus reconstruction

Like stimulus classification, stimulus reconstruction is a decoding tool that reassembles a stimulus based on its population response. In contrast to the stimulus classification, for stimulus reconstruction the spectrogram of presented stimuli to the population response is required (not only the information about the stimulus). Consequently, stimulus reconstruction predicts the spectrogram of the stimulus of the neuronal input in order to draw conclusion about the stimulus features encoded by the population response.

In particular, we used stimulus reconstruction in chapter 5 in order to compare the reconstructed stimuli for original and reverberated sound to their original spectrograms. The reconstructed spectrograms were developed by linear mapping of a reconstruction filter applied to a neuronal data set. The filter was computed by minimizing the mean-squared error between the stimulus and the linear discriminant analysis (LDA) components of the population response for vocalization differentiation.

LDA is a method for dimensionality reduction and data classification. Reducing dimensions enables to remove redundant and dependent features for an enhanced data classification for different classes. Therefore, new projection lines (lower dimension spaces, at least one dimension less than the original data contain) are drawn within the data set that maximizes the between-class distances (the mean of each class to each other) and simultaneously minimizes the within-class variances (the scatter within a class). For vocalization discrimination in chapter 5, four dimensions (LDA components) are necessary to classify five vocalizations.

As described above, the reconstruction filter was first established using a subset of the neuronal data set before the filter was transmitted to predict the reconstructed stimulus from the remaining data set (Mesgarani, 2013; Mesgarani et al., 2014; Tharwat et al., 2017).

Part I.

Cortical auditory information processing

The following study provides the basis for discussion of flexibility in auditory information processing. Here, cortical responses were experimental influenced by increasing the activity of a specific class of inhibitory interneurons (PV+ neurons). This manipulation imitates the integration of diverse influences on auditory processing which should have a flexible impact on the neuronal activity. Beside the neuronal flexibility, is there something robust hidden as well?

The following chapter of the thesis is a part of the published study Gothner et al. (2020).

4. Sustained Activation of PV+ Interneurons in Core Auditory Cortex Enables Robust Divisive Gain Control for Complex and Naturalistic Stimuli

4.1. Introduction

Sensory processing in the cortex requires flexible and reliable mechanisms for adjusting computations and information flow according to context. Both internal states and external requirements can reliably trigger changes of the most fundamental cortical computations, and these modulations can also generalize across stimulus conditions. The different subtypes of cortical inhibitory interneurons are candidate mediators of contextual modulation because they are in an exquisite position to produce such changes (Markram et al., 2004; Kepecs and Fishell, 2014; Tremblay et al., 2016; Cardin, 2019).

Three major interneuron cell classes in the neocortex include parvalbumin-positive (PV+) cells, somatostatin-positive (SOM+) cells, and cells expressing vasoactive intestinal peptide (VIP+). Each of these cell classes is differentially targeted by neuromodulation (Swanson and Maffei, 2019), and has a unique, class-specific expression profile of neuromodulatory receptors (Paul et al., 2017), which can produce class-specific modulation of interneurons depending on behavioral context, for example, state of arousal, attention, learning, or locomotion (Kawaguchi and Shindou, 1998; Alitto and Dan, 2012; Polack et al., 2013; Toussay et al., 2013; Poorthuis et al., 2014; Pakan et al., 2016). In order to obtain a functional understanding of neuromodulation, a more detailed description of network effects of the activation of specific interneuron classes is desirable (Edeline, 2012). Great progress in understanding the functional role of modulation of PV+ cells and other interneuron classes has recently been made with the help of optogenetic tools (Atallah et al., 2012; Lee et al., 2012; Wilson et al., 2012; Hamilton et al., 2013; Aizenberg et al., 2015; Seybold et al., 2015; Moore et al., 2018).

These previous optogenetic experiments have indicated that PV+ interneurons play an important, albeit complex, role in controlling excitability in sensory cortices.

So far, most studies of the effects of precise class-specific manipulation of inhibitory populations have focused on fast timescales, typically locked to sparse and transient stimuli. However, contextual modulation may act both at fast subsecond timescales (Munoz and Rudy, 2014; Poorthuis et al., 2014; McGinley et al., 2015) and over longer timescales of several seconds to minutes (Metherate et al., 1992; Kawaguchi and Shindou, 1998; Petrie et al., 2005; Alitto and Dan, 2012; Schneider et al., 2014). Moreover, there is evidence that PV+ inhibition may mediate very different network dynamics in sensory cortices depending on the timescale of stimulation (Ozeki et al., 2009; Haider et al., 2010). To investigate the functional role of modulation of PV+ activity not only at fast, but also at slower timescales, a precise but sustained manipulation of PV+ cell activity is needed in addition to the more commonly used fast and transient optogenetic activation or deactivation techniques (Atallah et al., 2012; Lee et al., 2012; Wilson et al., 2012; Hamilton et al., 2013; Aizenberg et al., 2015; Seybold et al., 2015; Moore et al., 2018). Here, we employed a variant of Channelrhodopsin 2 that allows for sustained, low-level activation at the timescale of minutes (stable-step function opsin, SSFO, Berndt et al. (2009); Yizhar et al. (2011a)) to ask how the sustained activation of PV+ cells affects cortical computation.

We hypothesized that sustained, low-level activation of PV+ cells (Tremblay et al., 2016) provides a means for divisive scaling of neural responses in core auditory cortex. Divisive scaling describes ratio-changes in neuronal response profiles (e.g. tuning curves) due to specified factors. Divisive scaling has been proposed to be one of the canonical cortical computations (Carandini and Heeger, 2011), with functional roles ranging from context-dependent modulation of sensory processing (Rabinowitz et al., 2011, 2013) to task-dependent top-down control (Ruff and Cohen, 2017). Concretely, a mechanism for divisive scaling in a cortical area should (1) produce divisive changes in firing rate across single-unit responses, (2) leave basic neuronal response properties such as tuning and receptive-field structure intact, and (3) generalize across different stimulation paradigms, including complex and naturalistic stimulus sets.

To investigate the impact of sustained PV+ cell activation on auditory cortical processing, we expressed SSFO in PV+ cells in the core auditory cortex (AC) of mice. We recorded responses of populations of single units in awake mice during presentations of three different stimulus sets: single tones (ST), dynamic random chords (DRC) and animal vocalizations (natural stimuli, NS). The combination of sustained PV+ cell activation and reliable long-term recording allowed us to quantify the effects of PV+ modulation on cortical responses to complex and naturalistic sounds, and to test for changes in single-unit response properties that generalized across the different stimulus sets.

We show that sustained activation of PV+ cells in AC produces coherent divisive scaling, with minimal changes in spectral or temporal tuning of neuronal responses. This divisive scaling generalizes across complex and naturalistic stimuli on both population and single-unit levels. Overall, our findings demonstrate that sustained activation of PV+ interneurons may constitute a powerful neural instrument for context-dependent scaling of cortical responses.

4.2. Materials and Methods

4.2.1. Subjects and Surgery

All electrophysiological data from optogenetic experiments (see section 3.3) were obtained from eight male mice. Animals were kept as described in section 3.1. At the time of surgery (see section 3.2), the mice were between 8 and 12 weeks old.

4.2.2. Implant design

Implants were custom-made at our laboratory. The implant consisted of eight twisted-wire tetrodes (17 μm, Platinum/10% Iridium California Fine Wire Company, Grover Beach, CA, US) concentrically arranged around a 105 μm optic fiber (FG105LCA Multimode Fiber, Thorlabs, Newton, NJ, US) for optogenetic manipulations and was attached to a microdrive (Axona) to move the probe within AC. The electrode tips protruded 400 μm from the tip of the fiber.

4.2.3. Optogenetic strategy

In the Cre-expressing PV+ cells of the mouse line, infection by the injected Cre-activated recombinant viral vector produced expression of a bistable ChR2 variant (Stable Step-Function Opsin, SSFO). Expression was confirmed via histological examination of brain tissue after the experiments. Expression spread through all layers of the AC and extended at least with a diameter of 1.5 mm radially in the medial-lateral and caudal-rostral dimensions. Efficiency of expression in PV+ cells was >95% (confirmed in 3 animals using imaging of immunostained PV+ cells and cells expressing the virally transmitted yellow fluorescent protein).

SSFO was used to achieve prolonged, stable, low-level depolarization of PV+ cells (Yizhar et al., 2011a), and has the advantage of its activation/deactivation interfering minimally with the timing of the sensory stimulus. Activation of SSFO was achieved with a pulse of blue light (447 nm, 2.5 mW for 2 s). SSFO cation channels remain open and induce a depolarizing input current until deactivation

with a pulse of orange light (594 nm, duration 5 or 10 s at 2.5 mW). All experimental sessions started with a stimulus block in control condition (no SSFO activation). Activating and deactivating light pulses were subsequently delivered in silent periods between stimulus blocks, starting directly after the previous stimulus block had finished. The next stimulus block began directly after offset of the activating or deactivating light pulse. At the end of every experimental session, PV+ cells were deactivated to return to control condition.

4.2.4. Electrophysiology

We recorded neural data extracellularly during auditory stimulation in alternating blocks of trials either without or with PV+ cell activation (hereafter, control and SSFO • PV trial blocks, respectively). These trial blocks each lasted between 3 and 5 min. Continuous raw voltage traces were amplified and digitized using a 32-channel headstage (RHD2132, Intan Technologies, Los Angeles, CA), recorded using an acquisition board (OpenEphys, www.open-ephys.org), and saved on a personal computer at a sample rate of 30 kHz for offline spike sorting and analysis. After an experimental session was completed, the probe was moved approximately 65 μm along the middle cortical layers using the microdrive attached to the implant and the tissue was allowed to settle for at least 3 h (more typically, overnight). Data collection could last up to four months, recording from 2-17 positions in each animal. Data collection was stopped when no primary-like responses could be detected anymore; criteria for primary-like responses were latency below 20 ms and reliable, clearly tuned responses to pure tone stimuli.

4.2.5. Experimental setup

All experiments took place in a customized double-walled sound-attenuated chamber (workshop of the University of Oldenburg). Animals were monitored throughout experiments using an infrared camera (Pi NoIR, Raspberry Pi foundation, Cambridge, UK). Mice were placed on a custom horizontal and acoustically transparent running wheel made out of wire mesh and were free to run during the experiments. In a subset of recordings from two animals, rotations of the running wheel were recorded using a black and white pattern at the base of the wheel and a custom-built light detector. The light-detector signal was recorded along with the electrophysiological signal, so that rotations could be determined on a trial-by-trial basis. Running data was used to confirm that the main conclusions from our analysis did not depend on the activity of the animal (Supplementary Fig. S1).

Sound delivery and optogenetic manipulation were both controlled using MATLAB (MathWorks, Natick, MA, US). Sound stimuli were generated digitally at a sample rate of 192 kHz using custom

MATLAB software and were D/A converted by a USB sound device (Fireface UC, RME, Haimhausen, Germany). Sound signals were amplified (A-S501, Yamaha, Hamamatsu, Japan) and then delivered via a loudspeaker (XT 300 K/4, Vifa, Viborg, Denmark) attached 45 cm above the running wheel. For activation of PV+ cells a blue laser was used (MDL-III-447 PSU-III-FDA, Changchun New Industries, Changchun, China), whereas deactivation of PV+ cells was achieved with an orange laser (Cobolt Mambo 50 594 nm, Cobolt AB, Solna, Sweden) using a shutter driver (Model SR474, Stanford Research Systems, Sunnyvale, CA, US). The optic fibers from both lasers were merged (TM105R3F1A, Thorlabs, Newton, NJ) and plugged onto the single optic fiber incorporated into the animal's implant. After a block of auditory stimuli was presented, laser pulses activated or deactivated SSFO for the next stimulus block (see Fig. 4.1 A). The number of blocks for each SSFO condition varied depending on the stimulus protocol.

4.2.6. Auditory stimuli

We used three different types of auditory stimuli: (1) simple single pure tone stimuli (ST), (2) natural stimuli (NS), and (3) dynamic random chords (DRC). We presented these stimuli sequentially within the same experimental session. ST were presented randomly at 70 dB SPL between 4 and 70 kHz using eight frequencies per octave. The tones had a duration of either 0.5 or 1 s including 2 ms ramps and were generated with an inter-stimulus interval of 1 s or 2 s respectively. Each tone frequency was repeated three times within one stimulus block. The stimulus block was repeated ten times for each SSFO condition, resulting in at least 30 repetitions of each tone pulse. For NS, we extracted five natural animal vocalizations from an audio disc ('Die Stimmen der Tiere 1 - Europa', Cord Riechelmann, 2007; tracks: 13-tundra vole, 18-european pine vole, 40-yellowhammer, 45-european robin, 71-long eared owl) with frequency spectrum centered between 4 and 25 kHz and up-sampled their sample rate to 192 kHz. The vocalizations were repeated in total 30 times in 3 to 6 blocks in each SSFO condition. DRC stimuli were similar to those described in previous studies (deCharms et al., 1998; Linden et al., 2003). The chords consisted of short tone pulses 20 ms in duration (including 5 ms ramps) with center frequencies varying between 4.1 and 62 kHz in 1/12-octave steps and sound levels varying between 25 and 70 dB SPL in 5 dB steps. Tone frequencies and levels were chosen randomly for each chord, with an average tone density of 2 tone pulses per octave. The DRC protocol lasted for 60 s and was repeated 5 times within a stimulus block. The stimulus block was repeated 4 times for each SSFO condition.

4.2.7. Data analysis

All analyses were performed offline using MATLAB, unless otherwise noted.

Continuous raw voltage traces were spike-detected and -sorted using a latent-variable spike-sorting algorithm (Sahani, 1999) as previously described (Hildebrandt et al., 2017). For spike characterization, we set the waveform baseline at 0.23 ms before peak (Keller et al., 2018) and normalized the unfiltered waveform with respect to the peak. We extracted the trough amplitude and measured spike width at 50 % peak amplitude, tested for significant differences in medians between the subgroups using the Kruskal-Wallis test, and analyzed results further using the post-hoc Tukey-Kramer test. To compare optogenetic effects between units grouped by spike width, we used the Mann-Whitney U-Test.

Criteria for exclusion and classification of units

For all of our analysis we only included units with a significant response during tone presentation. A unit with a significant response was defined as a unit for which the firing rate during tone presentation was significantly greater than spontaneous firing rate for at least 3 tested tone frequencies. Significance was tested by Student's paired t-test to compare tone response with pre-tone firing on each of the repeated trials for each tone frequency in windows of 50 ms (p < 0.05 with Bonferroni correction for multiple tests). To classify the effect of PV+ activation on the neuronal responses, we calculated the mean firing rate over entire stimulus blocks, including periods of tone presentation at all tested frequencies and silent periods in between. Then, the distributions of the mean rate during stimulus blocks for SSFO-PV and control condition were compared for each unit (Student's paired t-test, single tail for decrease and enhancement respectively, $p < 0.05$, with Bonferroni correction).

Single tones (ST)

To create a frequency-response profile, we computed the mean onset response over trials (40 ms window starting 15 ms after stimulus onset) for each tone frequency. The resulting iso-intensity frequency-response curves are hereafter referred to as (frequency) tuning curves. Tuning curves were smoothed using a Hanning window (width 3). Before extracting the tuning width and the best frequency (BF), we computed a frequency-response profile for spontaneous activity and subtracted it from the tuning curves. The tuning bandwidth (BW) was measured at 50 % of the amplitude.

To test for significant changes in BF and BW in single units, a bootstrap approach was used as follows. For each unit, all trials from both SSFO-PV and control conditions were pooled separately at each sound frequency; subsamples (30 trials) were drawn randomly from this combined pool; and BW and

BF were estimated as above. This procedure was repeated 1000 times to estimate the distribution of tuning parameters BW and BF. The values obtained from the separate analysis of control and test conditions were compared to these distributions at a $p < 0.05$ level with a Bonferroni correction for multiple tests.

To compare the tuning curves between control and PV-activated conditions, the tuning curves were first normalized to the unit's maximum firing rate in the control condition and then correlated by using major-axis regression (i.e., two-dimensional least-mean-squares linear fit). From the major-axis regression, we extracted slope and y-intercept. In order to avoid floor effects, rates within the tuning curve lower than 10 % of the maximum rate were discarded from the fit. In order to analyze the suppression of the tuning curves after PV+ cell activation, we calculated the value of the t-statistic t_{val} with $t_{\text{val}} = (m - m_{\text{ref}})/\sqrt{\sigma^2/n}$, where m is the regression parameter (either slope or y-intercept), m_{ref} either 1 (slope) or 0 (y-intercept), σ the standard deviation of the regression parameter and n the number of points that went into the regression. The result was then compared to the t-distribution (single tail) and units categorized accordingly: divisive suppression in case of $p_{\text{slope}} < 0.05$ and $p_{\text{intercept}} > 0.05$; subtractive suppression for $p_{\text{slope}} > 0.05$ and $p_{\text{intercept}} < 0.05$.

Dynamic random chords (DRC)

For each cell and SSFO condition, the average response to the DRC stimulus was used to estimate the respective spectro-temporal receptive fields (STRFs). STRFs were estimated with automatic smoothness determination (Sahani and Linden, 2003) within Python module 'lnpy' (`https://github.com/arnefmeyer/lnpy`). We set the dimensionality of the STRF to be 48 frequency channels and 15 time steps spanning 300 ms, chose a minimum STRF smoothness of 0.5 and tolerance of 10^{-5}, and ran the optimisation for 100 iterations. For control trials, the spectral, temporal and overall smoothness scales were initialised at 4, 4 and 7 respectively. For PV-activated trials, the smoothness parameters were fixed at the optimised smoothness parameters obtained in the corresponding control trials, to ensure that comparisons between control and PV-activated trials were not confounded by differences in STRF smoothing parameters.

We included in the final DRC analysis all cells that were both: (1) responsive to pure tones (see above) and (2) responsive to the DRC stimulus (i.e., signal power of DRC response at least 1 standard error above zero (Sahani and Linden, 2003; Williamson et al., 2016)).

We used the same major-axis regression procedure as with ST to compute correlations in STRF-predicted activity between control and PV-activated conditions.

4.3. Results

4.3.1. Consistent Effects of Sustained Activation of PV+ cells Across Trials and Paradigms

Many behavioral and brain-state dependent modulations of PV+ activity occur over timescales of several seconds to minutes (Metherate et al., 1992; Castro-Alamancos and Connors, 1996; Kawaguchi and Shindou, 1998; Petrie et al., 2005; Alitto and Dan, 2012; Schneider et al., 2014). In order to mimic such modulations and to probe their functional significance for cortical computation at the network level, we decided to employ a stable step-function variant of ChR2 (stable step-function opsin, SSFO) expressed in PV+ interneurons. SSFO allows for constant depolarisation of the targeted cells for minutes after applying a single, short pulse of light (Berndt et al., 2009; Yizhar et al., 2011a). This mode of action not only allowed for more modulatory-like activation of PV+ cells, but also enabled us to examine the effect of PV+ cell activation on the encoding of extended auditory stimuli of greater complexity. Thus, we could compare effects of PV+ activation during prolonged DRC stimuli to effects observed with more traditional ST paradigms (Aizenberg et al., 2015; Seybold et al., 2015; Phillips and Hasenstaub, 2016; Moore et al., 2018).

To determine whether sustained activation of PV+ interneurons produces consistent changes in neural responses across trials and stimulus paradigms, we first compared overall firing rates of single-unit responses to ST and DRC stimuli recorded in awake mice (Fig. 4.1 A) with (SSFO $^\bullet$ PV) and without (control) activation of PV+ cells. Using blue and orange light to activate/deactivate SSFO, we found a robust and reproducible effect of sustained PV+ activation in single units (Fig. 4.1 B). Among the recorded units, we observed both robust decreases and increases in firing rate (Fig. 4.1 C). These changes were consistent for ST and DRC stimuli when looking at overall firing rates during either stimulus paradigm (correlation coefficient r=0.42, $p = 2 * 10^{-63}$, n=1422) with no systematic difference in single-unit modulation under DRC and ST stimulation (Fig. 4.1 D, $p = 0.367$, Wilcoxon rank-sum test, $n = 1422$). At the population level, we observed on average a decrease in population firing rate during PV+ activation for both ST and DRC stimulation (rate change mean (SD) = -22.93% ($\pm 67.79\%$) for ST, -26.98% ($\pm 36.18\%$) for DRC). Effects of sustained PV+ activation on firing rates in single units ranged continuously from complete suppression to robust elevation.

4.3.2. Are the Enhanced Units PV+ Interneurons?

A small proportion of the recorded units showed an enhancement of firing rate with sustained PV+ activation rather than a reduction (Fig. 4.1). Because SSFO depolarizes directly activated cells, we
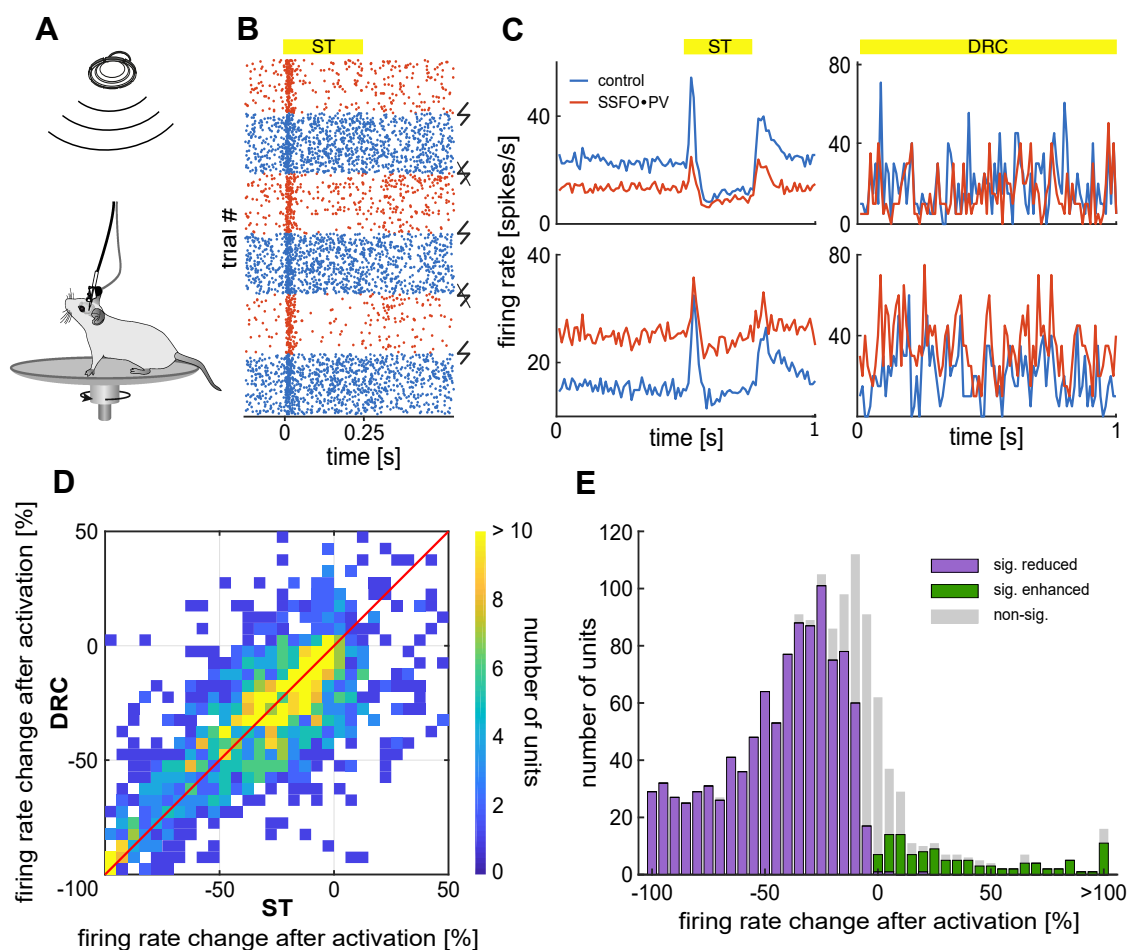
Figure 4.1.: **Sustained activation of PV+ cells results in consistent changes of firing rates across trials and paradigms.** (**A**): Recording setup. Mice were implanted with a combined opto-electrode implant and were able to freely move on a horizontal running wheel while sound was presented from above. (**B**): Responses of an example unit to sound (yellow bar) in control (blue) and SSFO • PVtrials (red). Spiking activity changes immediately after activation of PV+ cells (flash) and lasts until deactivation (strikeout flash). (**C**): Example PSTHs of two units (top, bottom) during ST (left) and DRC (right). PV+ activation resulted both in decreased (top) and increased (bottom) firing rates in individual units. (**D**): Comparison of the percentage firing rate change in individual units after PV+ activation during ST and DRC (n = 1422 units). The red diagonal line indicates equal firing rate changes with PV+ activation in both stimulus paradigms. (**E**): Distribution of percentage firing rate change after PV+ activation during ST stimulation. Classification of units into two groups for further analysis: units with a significantly reduced firing rate (reduced units, purple, n = 1027) and units with a significantly enhanced firing rate (enhanced units, green, n = 111) during sustained PV+ activation.

hypothesized that a large proportion of the enhanced cells were directly-activated PV+ cells rather than pyramidal cells or non-PV+ inhibitory neurons in the cortical network. In order to test this, we

analyzed extracellular spike shapes separately for significantly enhanced and reduced units.
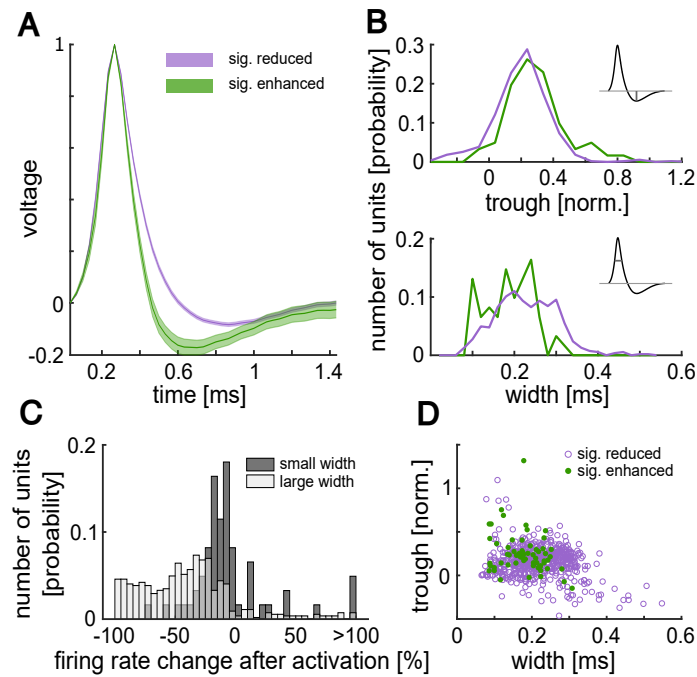
Figure 4.2.: **Reduced and enhanced units display different spike shapes.** (**A**): Mean normalized waveforms grouped into reduced (purple line, n = 545) and enhanced (green line, n = 61) units. Shaded area depicts SEM. (**B**): Histograms of trough amplitude (top, normalized to peak) and spike width (bottom, at 50 % of peak amplitude) within the subgroups. (**C**): Distribution of firing rate changes after PV+ activation for units with a spike width smaller (light grey, n = 61) and larger (dark grey, n = 545) than 0.12 ms. (**D**): Relationship of width and trough for reduced (purple circles, n = 545) and for enhanced units (green dots, n = 61).

Previous work reported that most of PV+ cells have narrow spike duration (fast-spiking cells, Keller et al. (2018)) and an increased peak-to-trough ratio (Moore and Wehr, 2013; Kim et al., 2016), criteria that we used to find putative PV+ cells in the group of enhanced units. We extracted spike width and trough amplitude in normalized waveforms and compared these between reduced and enhanced units (Fig. 4.2 A). Mean trough amplitude for the enhanced units was significantly larger (Fig. 4.2 B, top; mean (SD) = 0.2513 ($\pm$ 0.2285)) than for reduced units (mean (SD) = 0.1522 ($\pm$ 0.1713), Tukey-Kramer Test, $p = 0.0021$). Furthermore, enhanced units did have significantly smaller mean spike widths (Fig. 4.2 B, bottom; mean (SD) = 0.1804 ms ($\pm$ 0.0552 ms)) compared to reduced units (mean (SD) = 0.2190 ms ($\pm$ 0.0741 ms), Tukey-Kramer Test, $p = 10^{-4}$). The distribution of spike widths for enhanced units exhibited a local minimum at approximately 0.12 ms. We observed substantially different optogenetic modulation for neurons with spike widths falling above and below this value (Fig. 4.2 C). Units with a spike width larger than 0.12 ms exhibited a highly significant reduction in

firing rate during sustained PV+ activation (mean (SD) = -40.64 % ($\pm$ 38.88 % ms), Mann-Whitney-U-Test, $p = 3.14 * 10^{-15}$) compared to units with a smaller spike width (mean (SD) = -5.61 % ($\pm$ 32.82 % ms)). Thus, we found clear evidence for a relationship between spike shape and rate modulation during SSFO $^\bullet$ PV trials. However, we did not find a clear bimodal distribution of any of these features or a combination of them in our data (Fig. 4.2 D). Narrow spiking units were more often enhanced than other units, but often reduced in their firing. Similar mixed effects on PV+ cells due to indirect network effects have been reported previously (Moore and Wehr, 2013).

Since no clear separation between putative PV+ and PV- units was possible, we decided to group units on a functional basis reflecting the direction of firing rate change instead (reduced units; n = 1027; enhanced units; n = 111, Fig. 4.1 E). Based on the analysis of spike shapes, we expect the enhanced group to contain mostly directly activated PV+ cells, but many PV+ cells to be contained in the reduced group as well.

4.3.3. Activation of PV+ cells Preserves Frequency Tuning Properties of Neurons in Auditory Cortex

We next asked whether sustained PV+ activation would conserve basic encoding properties in AC, as would be expected for general divisive gain control mechanisms harnessed by contextual modulation, or whether it might instead sharpen or shift tuning. To address this question we recorded responses to isolated single tones of varying frequency. We constructed frequency response curves using the onset responses of the units for both control and SSFO $^\bullet$ PV conditions.

We observed a wide range of changes to the frequency response curves in the recorded units (Fig. 4.3). Fig. 4.3 A depicts the change in tuning curves after PV+ activation, ordered by the change at best frequency (BF). In the group with overall enhanced units, units could show increased firing rates over all test frequencies (example in the lower left box, Fig. 4.3 A) or even a reduction of firing at BF but increased rate at off-BF sound frequencies (Fig. 4.3 A, upper left example). A similar range of effects could be observed in the group with overall reduced firing rates: some units showed a general reduction of firing rates (Fig. 4.3 A, upper right example), others were reduced mostly at off-BF frequencies (Fig. 4.3 A, lower right example).

A selective reduction at off-BF frequencies could result in narrower overall tuning as measured by the bandwidth (BW). We found a small(albeit significant) reduction of BW in the reduced group (Fig. 4.3 C, right panel, median change in bandwidth 0.06 octaves, $p < 10^{-25}$, Wilcoxon sign-rank test, single-tail). This small changes was reflected in changes within a few individual units; BW was reduced in only 25 out of 876 units at a $p = 0.05$ level (bootstrap estimated with Bonferroni
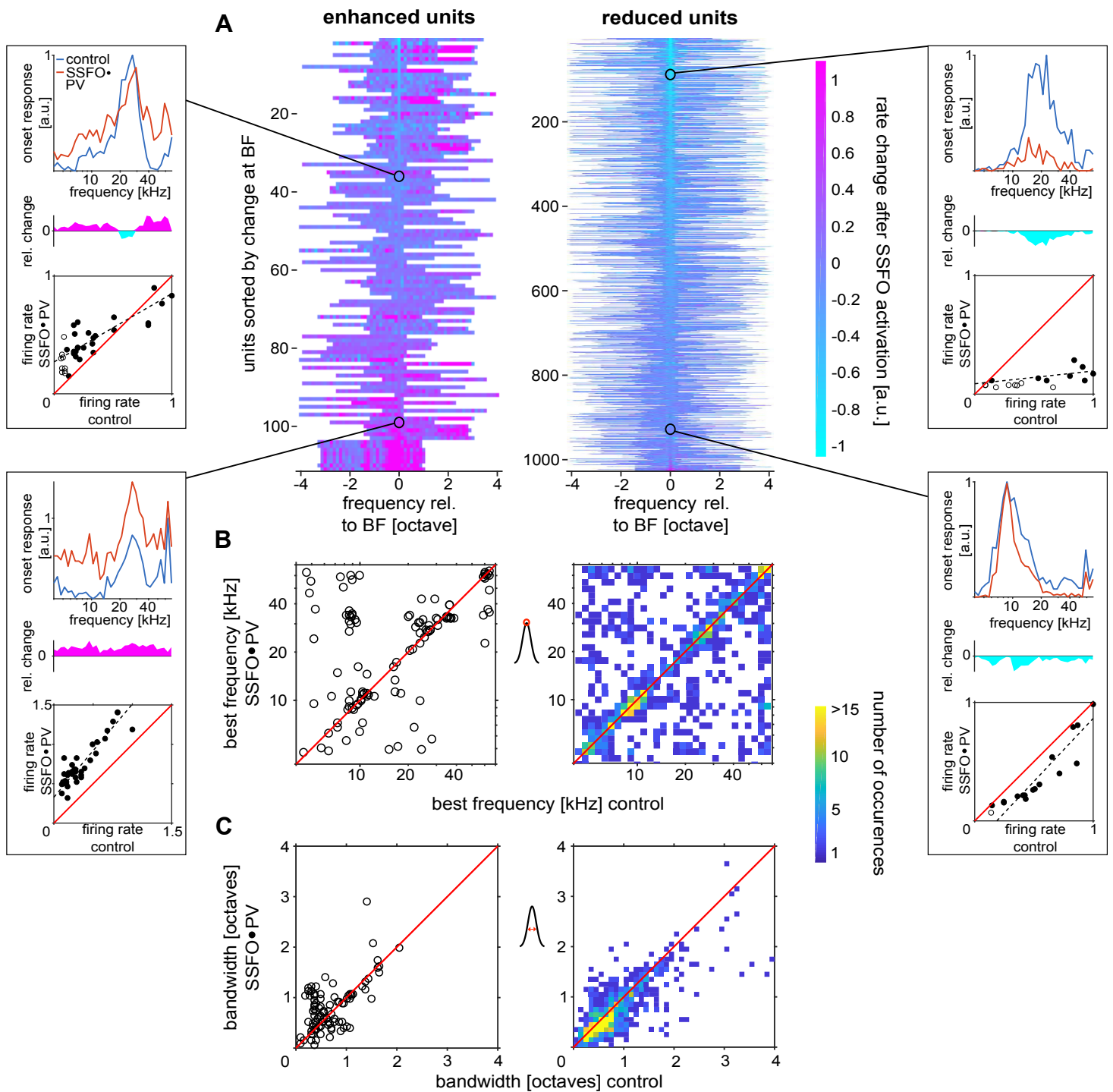
Figure 4.3.: **Sustained activation of PV+ cells has minimal effects on tuning best frequency and bandwidth.** Tuning curves were generated for each unit from the mean firing in a short window after stimulus onset (15-55 ms relative to sound onset).

Figure 4.3.: **(A)**: Overview of tuning curve changes during SSFO • PV trials, grouped by the mean effect the manipulation had on the unit (left: enhanced units, n = 111 units; right: reduced, n = 1027 units). Within each group, units are sorted by the amount of change in SSFO • PV trials at their BF: units with a large decrease in the response (light blue) at BF are located at the top, units with a large increase (purple) at BF are located at the bottom (examples boxes). Boxes at the side: tuning curves of example units for control condition (blue) and during SSFO • PV trials (red); relative change in the tuning curves (center); and difference in firing rate between the two conditions (bottom). The black dashed line marks the result of a major axis regression between control and SSFO • PV trials. To avoid threshold effects, only frequencies with a firing rate greater than 10% of the maximum rate in both conditions were used for the major axis regression (filled circles). Black circle and line indicates which unit in A is shown in the box. **(B)**: Best frequency during SSFO • PV vs. control trials (left: enhanced units, n = 111 units; right: reduced units, n = 1027 units). **(C)**: Bandwidth (measured at 50 % of peak amplitude) for SSFO • PV trials plotted against the bandwidth for control trials (left, n = 93 units; right, n = 876 units). Because of the large number of enhanced units (right panels in (B) and (C)), data from these was plotted as histograms, while data for reduced units is presented in scatter plots.

correction, see methods for details). We did not find a significant change in bandwidth for enhanced units at the population level ($p = 0.92$, signrank test) and at the individual unit level only 7 out of 93 single units showed a significant increase in BW ($p < 0.05$).

While BW was slightly affected, activation of PV+ cells did not alter the units' best frequency tuning at the population level (Fig. 4.3 B, median change in frequency in each group = 0 octave). Accordingly we found only two units out of 876 with a significant change of BF ($p < 0.05$, Bonferroni-corrected).

Thus, despite a considerable reduction of the overall firing rate during sustained PV+ activation (Fig. 4.1), both BF and BW where well conserved during SSFO • PV trials, with BW changes of less then a semitone on average and almost no change in BF (Fig. 4.3).

4.3.4. Reduction of Firing is Predominantly Divisive

Since we observed very little change in neuronal frequency tuning, we hypothesized that sustained activation of PV+ interneurons may provide a means for the context-dependent modulation of divisive gain control. Divisive action on tuning curves should result in little or no change in tuning characteristics due to the firing-rate-dependent adjustment for each frequency in the tuning curve. Conversely, previous studies using short-term optogenetic stimulation have reported that PV+ activation results in a mixture of divisive and subtractive changes (Seybold et al., 2015; Phillips and Hasenstaub, 2016). Here we asked whether sustained activation would also result in mixed effects or provide means for predominantly divisive modulation.

To address this question, we first calculated the tuning curves for each unit for both control and SSFO • PV trials and normalized them to the peak of the control tuning curve. Units with tuning curves that were too poorly correlated for effective comparison were excluded from further analysis (exclusion criterion: tuning curve correlation coefficient <0.5; qualitatively similar results obtained when criterion correlation coefficient lowered to 0.25). For the remaining units, we compared the normalized firing rate per frequency for tuning curves from SSFO • PV trials to those from control trials using major axis regression (see Fig. 4.3, example boxes, bottom). We then extracted the slope and the y-intercept from the regression fit. If there were no difference between the tuning curves in the control condition and after PV+ activation, the slope would be 1 while the y-intercept would be 0 (Fig. 4.4 A, red horizontal and vertical lines).
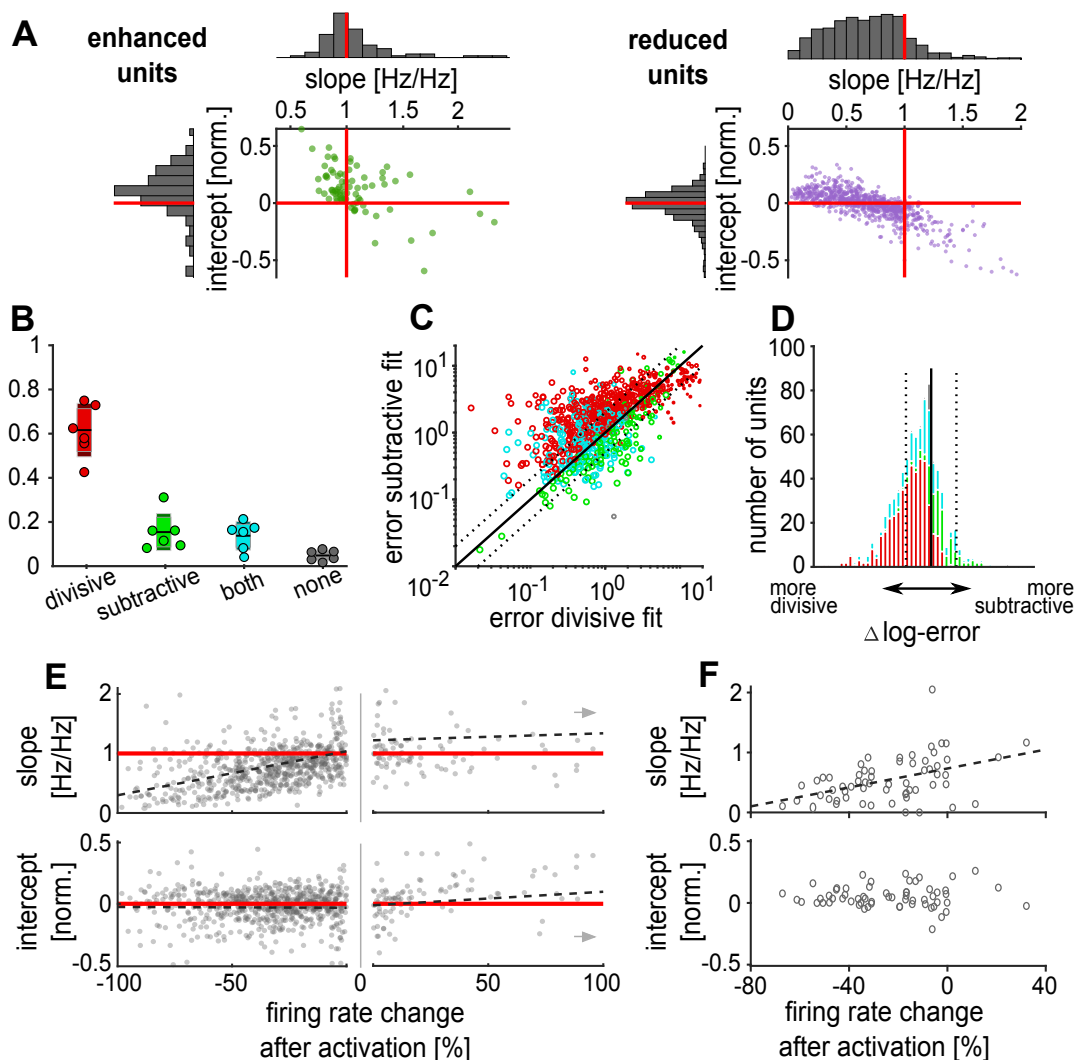

Figure 4.4.: **Sustained activation of PV+ cells has minimal effects on tuning best frequency and bandwidth.**

Figure 4.4.: **(A)**: Distribution of parameters of the linear fits between tuning curve in control and SSFO • PV trials (fig. 4.3 example boxes) for enhanced units (left, n =111) and reduced units (right, n = 1027). Units with tuning curve correlation coefficient r < 0.5 were excluded from further analysis of the fit. The red lines indicate no change in the slope (top) or shift of the y-intercept (sides). **(B)**: Proportion of units with significant divisive and/or subtractive effects in SSFO • PV trials compared to control (mean ± SEM (light shading) and ± standard deviation (dark shading). Circles represent the proportion in each individual animal (n = 7). **(C)**: Summed errors of the tuning curve fits using only divisve or subtractive terms. Each circle represents a single unit, colors correspond to classification in B. Dotted lines are plotted as a reference for the axis in D. **(D)**: Histograms of divisiveness of single units quantified as the log-error difference between purely divisive and subtractive fits, dotted lines and color of circles correspond to C . **(E)**: Relationship between firing rate change in each individual unit and the slope (top) and intercept (bottom) parameters of the linear fits. Dashed lines represent linear regressions, separately fit for reduced (n = 694) and enhanced (n = 110) units. For illustrative purposes, units with a change > 100% are not displayed (grey arrows), but were included in the fit. **(F)**: Same as in (E) for the median rate change and median fitted parameters of all units recorded in each recording position (n = 61).

Results of this analysis suggest that at the population level, sustained PV+ activation produced mostly divisive modulation in reduced units and additive modulation in enhanced units. The reduced units (Fig. 4.4 A, right) displayed very little subtractive change based on the y-intercept, but a clearly reduced slope (y-intercept median (IQR) = -0.01 (0.14), slope median (IQR) = 0.75 (0.41)), indicative of divisive gain control. In contrast, for enhanced units (Fig. 4.4 A, left), the y-intercept values show that tuning curves were mostly additively shifted upwards, with slope values broadly distributed but on average close to 1 (y-intercept median (IQR) = 0.11 (0.2), slope median (IQR) = 0.99 (0.53)).

These findings at the population level held also at the level of individual units. We quantified whether the effect of sustained PV+ activation was divisive or subtractive in individual units by determining whether the regression slope and/or y-intercept differed significantly from 1 and 0 respectively. We then calculated the fraction of units recorded from each animal that exhibited divisive, subtractive, both or neither modulation (Fig. 4.4 B, n = 7 mice). In all animals tested, significant divisive suppression was clearly the dominant effect (proportion of purely divisive units: mean (SD) = 0.62 (± 0.12), SEM = 0.05). In contrast, we observed fewer units with a subtractive suppression (mean (SD) = 0.15 (± 0.084), SEM = 0.03), a combination of both (mean (SD) = 0.14 (± 0.06), SEM = 0.03), or neither (mean (SD) = 0.05 (± 0.03), SEM = 0.01). Since locomotion and other motor activity have been shown to directly impact inhibitory circuits in AC (Schneider et al., 2014), we repeated our analysis for a subset of recordings (from 12 sites in 2 animals) during which running activity was monitored. We split the data into trials when the animals were running or at rest to examine the influence of locomotion on sustained PV+ modulation of firing rate in individual units (Supplementary Fig. S1).

Despite a considerable reduction in firing rate during trials when the animals were active (Supplementary Fig. S1 B), the effects of sustained PV+ activation remained consistent, with no significant changes in the distributions of slope and y-intercept values between running and rest trials (Supplementary Fig. S1 C, D). Thus, our conclusions from analysis of the full dataset are likely to be robust to any variations in the activity level of the animals across trials.

Further analysis of individual unit responses confirmed again that divisive modulation was the dominant effect of sustained PV+ activation. For individual units, overall reduction in firing rate could be well explained by a reduction of slope (Fig. 4.4 E, top, correlation coefficient $r = 0.34$, $p = 1.2 * 10^{-19}$, $n = 694$). On the other hand, we did not find a correlation between rate changes and y-intercepts for individual units (bottom, correlation coefficient $r = -0.01$, $p = 0.847$, $n = 694$), although variance of the intercepts was reduced with stronger reduction in firing rate (correlation between reduction and residuals of the linear fit: $r = 0.36$, $p < 10^{-22}$).

It has been suggested that the relative strength of divisive and subtractive action mediated by PV+ cell activation could be related to the extent of activation (Seybold et al., 2012; Lee et al., 2014). As an indirect measure of PV+ cell activation, we compared median firing rate change within single experiments to the median slope and y-intercept by pooling data from all units recorded at the same site (Fig. 4.4 F, $n = 61$). The results of this analysis confirmed our finding from the individual units; we again observed a high correlation of the slope and mean rate reduction (top, correlation coefficient $r = 0.45$, $p = 3 * 10^{-4}$) and a mostly constant intercept (bottom, correlation coefficient $r = 0.01$, $p = 0.93$). Thus, most suppression of firing is mediated by divisive changes. Moreover, division scaled linearly with the amount of suppression, indicating that sustained activation of PV+ units results in a divisive scaling of neuronal output, and depends on the strength of inhibitory drive.

Figure 4.5.: **(A)**: STRF for a reduced unit (upper) and an enhanced unit (lower) in control and PV-activated conditions. The STRF predicted activity for the reduced unit is divisively modulated in PV-activated compared to control conditions. The STRF-predicted activity for the enhanced unit shows a multiplicative enhancement. **(B)**: For reduced (top) and enhanced (bottom) units, slopes (left) and intercepts (right) of linear fits to STRF predicted activities in PV-activated versus control conditions. Only units with a correlation coefficient $r > 0.5$ are included (enhanced units $n = 44$ and reduced units $n = 419$). We note that a small fraction of units (1 to 2% of reduced units, and 5 to 9% of enhanced units) lie outside the plotted bounds and are excluded from the histograms to enable better visualization of the bulk of the data. **(C)**: For most units, sustained PV-activation does not shift the STRF in time and frequency. 1 % of reduced units and 2 to 5 % of enhanced units lie outside the plotted bounds and are excluded for better visualization of the rest.
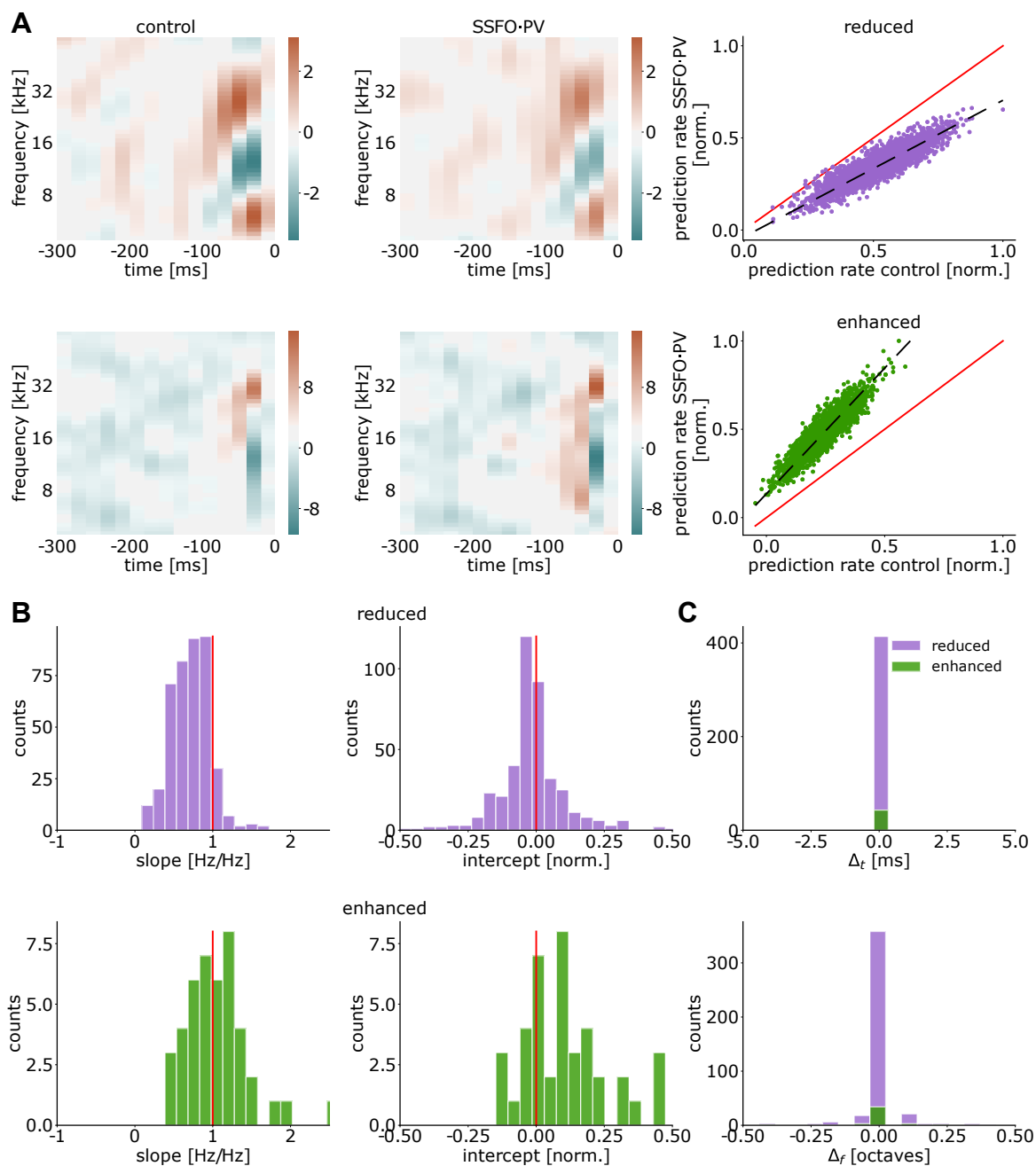
Figure 4.5.: **Spectro-temporal receptive fields are divisively scaled by sustained PV+ activation, but their structure is preserved.**

4.3.5. Spectro-Temporal Receptive Fields are Divisively Scaled and Their Structure Conserved

The prominent divisive effect of sustained PV+ activation on tuning curves, with minimal impact on tuning BF and bandwidth led us to the question of how such effects would generalize to more complex stimuli. Therefore, we investigated the impact of SSFO manipulation of PV+ activity on STRFs estimated from responses of cortical cells to DRC stimuli.

We found that many STRFs estimated from DRC responses were divisively or multiplicatively modulated for reduced and enhanced cells respectively, which in turn meant that DRC responses predicted from the STRFs were divisively suppressed or multiplicatively enhanced (Fig. 4.5 A).

Linear fits to the STRF predictions for PV-activated versus control conditions show that most reduced cells were strongly modulated through the slope, that is, divisively (Fig. 4.5 B top; slope median (IQR) = 0.72 (0.33) and y-intercept median (IQR) = -0.02 (0.09)). In contrast, enhanced cells showed more heterogeneous effects, with some units exhibiting strong modulation through the intercept, that is, additively (Fig. 4.5 B bottom; slope median (IQR) = 1.01 (0.44) and y-intercept median (IQR) = 0.09 (0.20)). However, as previously explained, for the majority of cells both DRC responses and single-tone responses were reduced, not enhanced, by sustained PV+ activation (Fig. 4.1 D). Overall, therefore, the STRF analysis of DRC responses reveals predominantly divisive effects of sustained PV+ activation, in agreement with analysis of ST responses. We note that restricting the analysis to the subset of units with the highest coefficients of determination of the estimated STRFs confirms these results (Supplementary Fig. S2).

We also found that for the majority of cells, sustained PV+ activation did not shift the STRF in time and frequency (Fig. 4.5 C). We quantified this by computing the lag in time and frequency that maximized the cross-correlation between the STRFs in the PV-activated and control conditions. These time and frequency lags were tightly concentrated near 0 ms and 0 octaves (Fig. 4.5 C; for both reduced and enhanced units, time lag median (IQR) = 0.0 (0.0) ms and frequency lag median (IQR) = 0.0 (0.0) octaves). Thus, the minor impact of sustained PV+ activation on the best frequency and bandwidth of responses to pure tones generalized to a minimal impact of the manipulation on spectrotemporal tuning.

4.3.6. Divisive Scaling Generalizes to Naturalistic Stimuli

We found consistently divisive scaling of single-unit responses both for ST (Fig. 4.3) and DRC stimuli (Fig. 4.5), conserving the receptive fields of the units. We next asked whether divisive scaling would

transfer to more naturalistic stimuli. To address this question, we recorded auditory cortical responses in a subset of the animals (n = 4) to a set of animal vocalizations varying in temporal and spectral structure, applying the same manipulation as for ST and DRC stimuli. We recorded from a total of 513 responsive units in all 3 paradigms.

Many units locked their spiking activity to the envelope of the NS (Fig. 4.6 A). During SSFO $^\bullet$ PV trials, responses were similar and typically a scaled version of the responses in the control trials (Figs. 4.6 B,C, left panels). When we compared spike rate modulation in all three paradigms, we observed highly conserved divisive scaling in the majority of units. Units that were enhanced in one paradigm, also were enhanced in the other two (Fig. 4.6 B), and units with decreased activity during SSFO $^\bullet$ PV trials scaled divisively in all three paradigms (Fig. 4.6 C).

This finding was confirmed when we looked at divisive and subtractive changes in SSFO $^\bullet$ PV trials compared to control (Fig. 4.6 D). Neither slopes nor intercepts changed between the ST and DRC paradigms in single units (Fig. 4.6 D). Slopes were slightly less reduced for the vocalizations, but still highly correlated for single units (Fig. 4.6 D, upper panels). The medians of the intercepts were close to zero for all paradigms, with a much larger variance in estimates from the ST paradigm than from DRCs and vocalizations (Fig. 4.6 D, lower panels).

Figure 4.6.: **(B)**: Effect of sustained PV-activation on the responses of one enhanced unit to all three different paradigms (from a population of 513 cells with recordings in all three paradigms). Top left: Animal vocalizations – 500 ms snippets from all five vocalizations used. Top center: DRC – 2 second snippets taken from continuous DRC stimulation. Top right: Tones – tuning curves obtained from tone onsets (see Fig. 4.3). Lower panels show comparison of firing rate in control and SSFO $^\bullet$ PV trials in the respective paradigm, including the full recording. Dashed line depicts the linear fit. **(C)**: Same as (B), but for one unit with decreased firing rates in the SSFO $^\bullet$ PV condition. **(D)**: Relationship between linear fit parameters observed in different stimulus paradigms. Scatter plots depict slope and intercept fits for single units, comparing tones and DRC stimulation (left) or tones and vocalization stimuli (center). Grey, open markers are units for which the respective linear fit parameter was not significantly different from what would be expected if PV-activation had no effect (slope=1, intercept=0); filled, black markers are those with parameter value significantly different from the null condition (one sided, $p < 0.05$). Right, histograms of fit parameter values for all three stimulus paradigms.
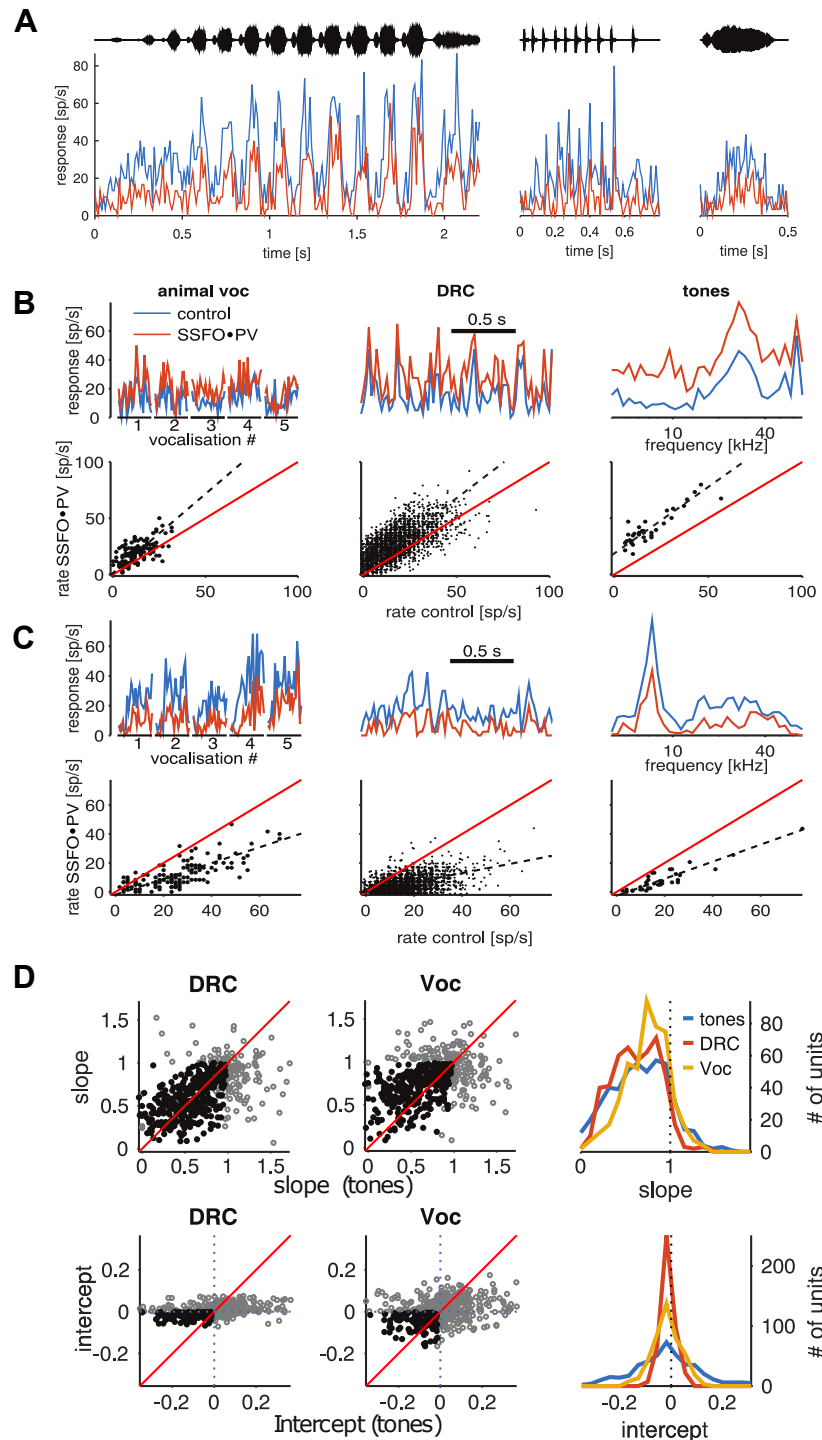
Figure 4.6.: **Divisive action generalizes to naturalistic stimuli and is consistent across stimulus paradigms.** **(A)**: Example responses to three different animal vocalizations. On the top, the time course of the respective vocalization is depicted (vocalizations 1-3 in panels B and C). Blue line: control, red line: SSFO • PV.

4.4. Discussion

Here we asked whether sustained activation of PV+ cells, on timescales much longer than previously tested, could serve as a general mechanism for implementing divisive gain control. We used a bistable variant of Channelrhodopsin (SSFO) to activate and deactivate PV+ cells on the multi-second time scales that are typical for contextual modulation of PV+ cells (Metherate et al., 1992; Kawaguchi and Shindou, 1998; Petrie et al., 2005; Alitto and Dan, 2012; Schneider et al., 2014). This approach enabled us to test effects of PV+ activation not only on brief sounds such as ST, but also on prolonged sounds including complex NS and DRC. Our results show that sustained activation of PV+ interneurons produces divisive modulation of cortical responses (Fig. 4.3) which is consistent across trials (Fig. 4.1), single units, electrode positions (Fig. 4.4), and greatly differing stimulus paradigms (Fig. 4.6). Furthermore the divisive change preserves the main response properties of cortical units in both the spectral (tuning curves Fig. 4.3; receptive fields Fig. 4.5) and temporal domains (Fig. 4.5).

4.4.1. Cell-to-Cell Variability in Effects of Sustained PV+ Activation

Although sustained PV+ activation produced strong suppression of neuronal responses in a large majority of neurons ("reduced units"), a subset of recorded cells instead showed enhancement of firing rate during SSFO • PV trials ("enhanced units") (Fig. 4.1). The distribution of modulatory effects was essentially unimodal across the recorded population, with no clear separation between reduced and enhanced units. However, in individual units, modulatory effects were reproducible and consistent across different auditory stimuli, and at the population level, a similar diversity of modulatory effects was observed in different experimental animals. Moreover, diverse effects of sustained PV+ activation were observed even among neighboring neurons at a single electrode position within individual mice. These observations suggest that cell-to-cell variability in effects of sustained PV+ activation might arise not only from differences in viral expression or spread of light at different electrode positions and in different mice, but also from locally heterogeneous synaptic strength of (PV+) inhibitory connections or locally heterogeneous activation of PV+ cells. Units with strong PV+ inputs might be more strongly affected by the activation of PV+ cells than neighboring units with weak PV+ inputs.

For cells with reduced activity during sustained PV+ activation, the extent of reduction was associated solely with the strength of divisive modulation (Fig. 4.4). In contrast, cells with enhanced firing rates predominantly showed an additive change in their responses (Fig. 4.4 A). It is conceivable that these units were primarily PV+ cells that had been directly activated. This interpretation is consistent with the observation that spike waveforms for enhanced units had narrower peaks and deeper troughs than

for reduced units (Fig. 4.2). If PV+ units were enhanced and non-PV+ units reduced in firing rate, why did we not observe a clear bimodal distribution of firing rate changes? It has been shown that activation of PV+ cells in some layers can functionally disinhibit PV+ cells in other layers (Moore et al., 2018). These indirect disinhibitory effects, along with variable activation of PV+ cells and variability in PV+ to non-PV+ cell connections, could produce high variation in effective firing rate changes in PV+ units.

4.4.2. Comparison with Previous Findings on Optogenetic PV+ Manipulation in AC

In comparison with previous studies on the computational roles of cortical inhibitory interneurons in the AC (e.g., Seybold et al. (2015); Phillips and Hasenstaub (2016)), we found a more divisive and less broadly mixed effect of PV+ activation.

Our optogenetic approach differed most significantly from previous work in the timing of the optogenetic manipulation. While other studies have combined standard ChR2 and stimulus-synchronized light activation, the SSFO variant used here allows for decoupling of light activation and sensory stimuli. It has already been shown for visual cortex that the effect of PV+ activation depends on the relative timing of the circuit manipulation and the sensory stimulus (Atallah et al., 2012; Lee et al., 2012, 2014; Wilson et al., 2012). Similar factors may explain some of the differences between our results and previous findings (Seybold et al., 2015; Phillips and Hasenstaub, 2016). Both transient, stimulus-locked activation and slowly varying, sustained activation may be important for contextual processing and top-down control. While modulatory effects on PV+ cell activity related to locomotion (Polack et al., 2013; Schneider et al., 2014; Pakan et al., 2016) and vigilance (Kawaguchi and Shindou, 1998; Kuchibhotla et al., 2017) typically last for several seconds to minutes, some forms of neuromodulation may also include fast, transient components at the time scale of tens of milliseconds (Munoz and Rudy, 2014; Poorthuis et al., 2014; McGinley et al., 2015). An exact description of timescales for contextual modulation of sensory computation may be crucial for a detailed understanding of these processes (Edeline, 2012).

A second technical aspect that differed between our study and previous related work was the location of the optogenetic stimulation site within the AC. A study using local stimulation of PV+ cells in different layers showed that activation in one layer may have deactivating effects on PV+ cells in other layers and vice-versa (Moore et al., 2018). Other studies stimulated at the surface of the cortex using low light levels ($< 0.5\,\mathrm{mW/mm^2}$ Aizenberg et al. (2015); Seybold et al. (2015); Phillips and Hasenstaub (2016)). Since light transmission drops in brain tissue by $50\,\%$ every $200\,\mu\mathrm{m}$ (Yizhar

et al., 2011a), surface illumination may have activated mainly PV+ cells in superficial cortical layers, potentially mostly Chandelier cells with large arborizations in layer I (Inan and Anderson, 2014). In contrast, our fiber tip was typically placed in middle layers (IV and adjacent) and oriented tangentially to the cortical surface, probably mostly activating PV+ cells throughout middle layers. These layers contain more PV+ cells than layer I and predominantly Basket rather than Chandelier cells (Miyamae et al., 2017). Chandelier and Basket cells synapse onto different segmental areas of their target cells, and may thus differ in their impact on synaptic integration in the post-synaptic cell (Markram et al., 2004). Activating different proportions of these distinct PV+ cell types could well result in different proportions of subtractive (Chandelier cells, axonal targeting) and divisive (Basket cells, preaxonal targeting) firing rate changes, further explaining some differences between our results and previous findings.

4.4.3. Use of Bistable Optogenetic Tools for Probing Cortical Inhibition

Standard optogenetic tools allow for manipulation of cell activity during laser illumination only, and the duration of illumination is limited to a few hundred milliseconds by the potential for photodamage and temperature increase (Yizhar et al., 2011a). This limitation means that most optogenetic manipulations of sensory processing are performed using short and low-complexity stimuli. The SSFO variant we used here allowed us to manipulate PV+ cells during complex and naturalistic stimuli and to explore how effects of PV+ activation generalize across stimulus sets and over time.

In addition, bistable optogenetic tools as we used here may be an important means of understanding the effects of neuromodulation of cortical circuitry (Edeline, 2012) mediated by differential activation of distinct groups of interneurons at slower timescales (Paul et al., 2017). Several neuromodulators have been shown to specifically affect cortical PV+ cells (e.g. serotonin (Puig et al., 2010), acetylcholine (Metherate et al., 1992; Alitto and Dan, 2012), norepinephrine (Toussay et al., 2013)) on timescales of seconds to minutes. Thus, using SSFO enabled us not only to implement complex and prolonged auditory stimuli and to avoid laser onset and offset artifacts, but also to attain an activation of PV+ cells at new and physiologically relevant timescales.

4.4.4. Functional implications for cortical computation

Divisive gain control has been proposed to be one of the canonical neural computations performed by cortical circuits (Salinas and Thier, 2000; Carandini and Heeger, 2011). A range of computationally important functions in sensory processing are attributed to divisive gain control, including adaptation to stimulus statistics (Rabinowitz et al., 2011)), invariant stimulus encoding (Rabinowitz et al., 2013),

optimized sensory discrimination (Guo et al., 2017), foreground-background separation (Busse et al., 2009), and selective attention (Ruff and Cohen, 2017).

Most of these functions depend on behavioral and sensory context and therefore need to be under control of modulatory mechanisms. We show here that prolonged, low-level activation of PV+ interneurons provides a means for flexibly modulating such gain control in AC. PV+ neurons are the target of neuromodulators such as serotonin (Puig et al., 2010) and acetylcholine (Metherate et al., 1992; Alitto and Dan, 2012), and are differentially activated in specific behavioral states such as task engagement (Kuchibhotla et al., 2017) and locomotion (Schneider et al., 2014; Zhou et al., 2014), putting them in an optimal position to mediate necessary changes in sensory processing at the timescale of seconds to minutes. Our results demonstrate that sustained activation of PV+ interneurons in AC on this timescale produces robust divisive gain control, not only for brief tones but also for continuous, complex and NS.

Part II.

Cortical auditory information retrieval

The following study provides the basis for discussion of robustness in auditory information retrieval. Here, reverberated and non-reverberated (dry) vocalizations of different animals were presented to the experimental subjects. How do information for vocalization identity (different animals) and context (reverberated or not) robustly exist within the neuronal code? Beside the robustness of information storage, is there something flexible hidden as well?

5. A Multiplexed Population Code for Sound Identity and Context in Core Auditory Cortex

5.1. Introduction

Auditory recognition involves more than labeling sound identities. Furthermore, it is possible to characterize the context of a sound like the reverberated piano play in a great hall. Therefore, the acoustic relevant information has to lead to a neuronal code which has to differ robustly between different sound identities but should contain an invariant representation as well: Different sound identities mandatorily vary in temporal and spectral features which are represented in a variant neuronal coding of the different sound identities (Smith and Lewicki, 2006) as auditory objects (Bizley and Cohen, 2013). However, recognizing the sound identity depending on the context like reverberation, the neuronal information should have to be invariant due to the original context-free acoustic template (Mesgarani et al., 2014).

How can variant and invariant representations of different aspects of the same sound coexist? Information of both sound identity and context (reverberation) could lead to different cortical areas by separate pathways (two-stream hypothesis) as it is already described for the visual (where- and what pathways, (Goodale and Milner, 1992)) and auditory system for simple and complex word recognition (DeWitt and Rauschecker, 2012) and spoken language (Gow, 2012).

Another solution to maintain different aspects of sound is that coding for sound identity and reverberation is presented in the same cortical area as neuronal multiplexed representation.

Multiplex coding has been shown for simple elements like the timing of individual spikes and their accuracy and precision, interspike-intervals and absolute spike rates (Fairhall et al., 2001; Lundstrom and Fairhall, 2006). These features encode timber, pitch or spatial location (Walker et al., 2011)

or relative features normalized to the stimulus ensemble (Fairhall et al., 2001) on short or longer time-scales. Accordingly, a multiplexed representation of information at the level of single-neurons (Fairhall et al., 2001; Lundstrom and Fairhall, 2006; Walker et al., 2011) or population (Bathellier et al., 2012; Mizrahi et al., 2014) can provide a powerful tool for the efficient use of limited neuronal capacity.

Therefore, we hypothesize that information about both, sound identity and reverberation is encoded in AC via multiplex representation and can be used by the animals if required. In detail, we want to show that neuronal information about sound reverberation is generally traceable in the neuronal code other mammals besides humans can have access to that information if it is required (1). Furthermore, we want to observe the neuronal dynamics in AC involving how reverberation is presented there (2) and if both reverberation and sound identity are preserved within the same population of neurons (3).

In order to explore if reverberation detection is a general physiological neuronal mechanism (1), we wanted to confirm that other mammals besides humans are also able to detect reverberation. Therefore, we performed behavioral experiments on mice, using a Go/No-go task for reverberation discrimination. The mice had to detect reverberated stimuli embedded in a continuous set of non-reverberated (dry) stimuli for five different sets of animal vocalizations. In order to observe if reverberation is presented in AC (2) and how the same population of neurons is able to preserve both reverberation and vocalization ID (3), we presented those dry and reverberated vocalizations to passively listening and awake mice and recorded neuronal responses of populations of single units in AC. We show that mice are able to detect reverberation from dry stimuli and that the diversity of neuronal response within a population response provides means for this discrimination. Furthermore, our results present that both reverberation and sound identity is encoded in AC at different time windows within the same population response. Overall, our findings provide a conclusive explanation for a multiplex representation of reverberation and sound identity for that mammals have access to if required.

5.2. Materials and Methods

In order to observe the mechanism behind reverberation recognition, we performed both, behavioral and electrophysiological experiments. Subjects were housed as described in section 3.1 unless otherwise noted.

5.2.1. Behavior

Subjects

All behavior data were obtained from four mice: two naive mice and two mice which were involved in sound localization experiments beforehand. Mice were kept at an inverted 12/12 day/night cycle, all training and experiments were performed during the dark period. The mice were food-deprived for operant conditioning to the auditory target stimulus. Their weight was daily monitored and held at approx. 10 % below basic weight (measured before food-deprivation and updated regularly) before the first behavioral session of a day. The animals were involved in behavioral sessions (with food reward) up to two times a day and were additionally fed in the afternoon at least 30 minutes after their last session of the day. At the beginning of the training, the mice were 3 and 5 months old.

Experimental setup

The subjects were trained (operant conditioning) to identify a target (reverberated) stimulus in a set of background (non-reverberated / dry) stimuli (Go/No-go paradigm). Training and experimental sessions took place in an acoustically transparent doughnut-shaped cage (out of wire mesh, diameter 30 cm) with a pedestal and a food dish for food reward from a customized feeder apparatus opposite each other.

The doughnut-shaped cage was placed in the middle of a customized double-walled sound-attenuated chamber (workshop of the University of Oldenburg). A loudspeaker (Vifa/Peerless XT-300 K4, Tymphany Sausalito, CA) was attached 45 cm above the cage's pedestal and delivered sound from audio files (sample rate 96 kHz), which were D/A converted (Fireface UC, RME, Haimhausen, Germany) and amplified (PM7004, Marantz, Kawasaki, Japan). A light barrier at the pedestal detected the movement of the subject on the pedestal and was connected to the PC and the feeder apparatus via an Arduino (Arduino UNO, Arduino s.r.l., Monza, Italy). The experiment control was performed by our PsychDetect software framework for MATLAB running on a Microsoft Windows PC. The subjects were monitored throughout behavioral sessions using an infrared camera (Pi NoIR, Raspberry Pi foundation, Cambridge, UK).

Auditory stimuli

For dry and reverberated (target) stimuli, we used a set of five different natural animal vocalizations (fig. 5.1 a). In each behavioral session, we presented only one out of these five vocalizations. The target stimulus was randomly placed within continuously presented dry stimuli. In order to eliminate

unwanted auditory cues, we randomly changed the sound pressure level of the dry stimuli up to 9 dB SPL (max. 79 dB SPL). Additionally, we trimmed all stimuli to 1 s.

All dry vocalizations were extracted from an audio disc ('Die Stimmen der Tiere 1 - Europa', Cord Riechelmann, 2007; tracks: 13-tundra vole = mouse 1, 18-european pine vole = mouse 2, 40- yellowhammer = bird 1, 45-european robin = bird 2, 71-long eared owl = bird 3) and were sampled to 96 kHz. For reverberation, we convolved the dry vocalizations using a room impulse response generator (RIR, v.1.3.0.0, McGovern, S. (2020)).

Experimental design

After initiating a trial (ascending the pedestal), a target stimulus was presented with a random delay time between 1.25 to 5.25 s (fig. 5.1 b). By jumping from the pedestal within 1 s after the target stimulus started, the subject received a food reward (hit) otherwise the subject did not receive a food reward and the trial resulted in a miss. In order to prevent hits by chance, we included sham trials. These trials did not contain any target stimuli and only presented dry stimuli. Staying on the pedestal during the designated response window during a sham trial was evaluated as a correct rejection (CR) while jumping from the pedestal was counted as a false alarm (FA). One behavioral session contained 60 target trials and 20 sham trials.

Training Session

Shaping and training were done as previously described (Rogalla et al., 2020). In order to teach the subjects to detect reverberated stimuli from dry stimuli, all subjects underwent training sessions. In training sessions, both initialization time of the trial and the sound pressure level of dry stimuli varied from easy (short initialization times and low sound pressure level) to difficult tasks. Furthermore, only the vocalizations of both mice species and bird 1 were used. After the delay time of the target stimulus and the sound pressure level were adapted to the experimental level, the vocalizations of bird 2 and bird 3 were added to the experimental sessions.

Analysis

Based on the signal detection theory, the hit rate and false alarm rate of a session were used to calculate the sensitivity d' (performance) for each session. All sessions with a false alarm rate greater than 25 % were excluded from further analysis (in total 150 sessions, see table 5.1). We used the Fishertest (with Bonferroni correction $\alpha = 0.0025$) in order to observe if the subjects were able to distinguish between dry and reverberated stimuli. Response time distributions for each animal and vocalization

were computed by discretizing the time it took the animals to leave the pedestal after the onset of the reverberated sound in 50 ms bins for all hit trials. For each animal, this distribution was corrected for putative random responses by subtracting the same distribution obtained from the false alarms. We compared differences among the distributions for different vocalizations and for the response times by using a generalized linear mixed-effects model and tested their estimated marginal means (https://github.com/jackatta/estimated-marginal-means).

Table 5.1.: Number of valid sessions for each subject and vocalization with a FA rate less than or equal 25 %.

subject ID	m 1	m 2	b 1	b 2	b 3
subject 1	7	9	6	7	6
subject 2	6	7	5	6	5
subject 3	8	14	9	12	9
subject 4	6	9	6	7	6

5.2.2. Electrophysiology

Subjects

All electrophysiological data were obtained from nine male mice. Animals were kept as described in section 3.1 and above except they were not food-deprived. At the time of the surgery, the mice were between 8 and 12 weeks old.

Implant Design and Surgery

The mice were equipped with a chronic implant (probe) for extracellular recordings. Implants were custom-made at our laboratory. The implant consisted of eight twisted-wire tetrodes (17 μm, Platinum/10 % Iridium California Fine Wire Company, Grover Beach, CA, US). For a set of chronic implants, we concentrically arranged around a 105 μm optic fiber (FG105LCA Multimode Fiber, Thorlabs, Newton, NJ, US) in order to stabilize the tetrodes. The probe was attached to a microdrive (Axona, London, UK) to move the probe within AC. The electrode tips protruded approx. 400 μm from the tip of the fiber. Surgery and post-operative procedure were carried out as described in section 3.2 and modified by Gothner et al. (2020).

Experimental setup and electrophysiology

All electrophysiological experiments were carried out in the setting as described in section 4.2.5 (Gothner et al., 2020).

All experiments took place in a customized double-walled sound-attenuated chamber (workshop of the University of Oldenburg). Animals were monitored throughout experiments using an infrared camera (Pi NoIR, Raspberry Pi foundation, Cambridge, UK). Mice were placed on a custom horizontal and acoustically transparent running wheel made out of wire mesh and were free to run during the experiments. A loudspeaker (XT 300 K/4, Vifa, Viborg, Denmark) was attached 45 cm above the running wheel and delivered amplified sound (A-S501, Yamaha, Hamamatsu, Japan). Sound stimulation was generated digitally at a sample rate of 192 kHz using custom software written in MATLAB (MathWorks, Natick, MA, US) and was D/A converted by a USB sound device (Fireface UC, RME, Haimhausen, Germany). The sound delivery was controlled using MATLAB (Gothner et al., 2020).

We recorded neural data extracellularly during auditory stimulation. Continuous raw voltage traces were amplified and digitized using a 32-channel headstage (RHD2132, Intan Technologies, Los Angeles, CA), recorded using an acquisition board (OpenEphys, www.open-ephys.org), and saved on a personal computer at a sample rate of 30 kHz for offline spike sorting and analysis. After an experimental session was completed, the probe was moved approx. 65 μm along the middle cortical layers using the microdrive attached to the implant and the tissue was allowed to settle for at least 3 hours. Data collection could last up to four months, recording up to 15 positions in each animal. Data collection was stopped when no primary-like responses could be detected anymore; criteria for primary-like responses were latency below 20 ms and reliable, clearly tuned responses to pure tone stimuli (Gothner et al., 2020).

Auditory stimuli

We used the same dry and reverberated natural animal vocalizations as described for behavior experiments with certain exceptions: we presented the complete sound duration of the stimuli, all dry and reverberated stimuli were randomly presented 20 to 30 times in one recording session using an interstimulus interval of 1 s and for each vocalization, we did not adjust the sound pressure level. For the electrophysiological setup, we up-sampled the sample rate to 192 kHz.

Analysis

All analyses were performed offline using MATLAB unless otherwise noted. Continuous raw voltage traces were spike-detected and -sorted using a latent-variable spike-sorting algorithm (Sahani, 1999) as previously described (Hildebrandt et al., 2017).

In order to visualize population responses, peri-stimulus time histograms (PSTHs) of all units (n = 2052) from all animals were calculated using a bin size of 10 ms. A preference index was defined as

the ratio between the response of the neuron to the first 500 ms of the reverberated stimulus $\langle r_{rev} \rangle$, divided by the rate during the presentation of the same, dry stimulus $\langle r_{dry} \rangle$. The responses of the units were classified as 'reverb' or 'dry preferring' if their preference index belonged to the highest or lowest quartile of the population and subsequently averaged for each vocalization.

Dry and reverb classification   For a population classification of dry and reverb preferring units, we used a 5-fold binomial logistic regression for each recording position. Therefore, we extracted the neuronal response of each unit and each trial during the first 500 ms after stimulus onset. Only units with a spiking rate between 2 and 150 spikes/s were involved in the binomial logistic regression (n = 1980 from 2495). All extracted rates were normalized with a mean of 0 and a standard deviation of 1. In order to compare the electrophysiological results with the behavioral results, we also calculated the sensitivity d' for the classification prosperity: based on the true context (dry/reverb) and the model prediction, we collected hits (reverb:reverb), misses (reverb:dry), correct rejections (dry:dry) and false alarms (dry:reverb). We compared differences among the distributions for different vocalizations as described for behavior analysis. We excluded experimental sessions (17 sessions excluded) with a p-value (Fisher-test) smaller than 0.05 and accuracy of decoding smaller than 66 %.

Mutual Information   In order to quantify the mutual information between the responses and either reverberation or vocalization ID, single-trial rates for each unit were calculated for the first 512 ms of each stimulus in bins ranging from 4 to 512 ms in logarithmic spacing. For each unit, a matrix [bins x trials x stimuli] was build with stimuli either binary for dry/reverb or numbers between 0 and 4 for the vocalization ID. These matrixes were used as the input to compute mutual information between the time-resolved responses and the stimuli (Magri et al., 2009). Information was either calculated for each unit separately or for the summed activity of all units at one position for each single trial.

Linear dimensionality reduction (LDA)   To investigate the optimal subspace for decoding of dry/reverb and vocalization ID, stimulus linear dimensionality analysis (LDA) was used on the single-trial data binned at 16 ms, using the function LinearDiscriminantAnalysis from the python scikit-learn library. Single-trial rates for each unit were normalized prior to dimensionality reduction. LDA was applied to all units from each animal, pooling all recordings at different positions. Labels for LDA were either reverb/dry as labels or vocalization IDs. This way we obtained single-trial trajectories for each animal vocalization in either on (reverb/dry) or 4 dimensions (vocalization ID).

Stimulus reconstruction   Reconstruction was done based on optimal prior reconstruction (Mesgarani et al., 2014), using a linear mapping between the output of the stimulus-ID-based LDA com-

ponents and the spectrogram. In short, a reconstruction filter is computed by minimizing the mean-squared error between stimulus and LDA components for the training data set (10 % of the data) and then used on the rest of the data for reconstruction. Both population responses and spectrograms were binned at 16 ms. Accuracy of reconstruction was measured as the maximum of the 2D cross-correlation between original and reconstructed spectrograms for each vocalization. We compared reconstructed spectrograms obtained from responses to reverberated vocalization to both reverberated and dry stimuli. For an unbiased estimate of the reconstruction, we used a 10-fold cross-validation.

5.3. Results

### 5.3.1. Mice discriminate reverberated from dry stimuli

In order to observe if animals can distinguish between dry and reverberated vocalizations (fig. 5.1 a), we implemented a Go/No-go paradigm for mice to report a reverberated stimulus out of a continuous sequence of dry stimuli (fig. 5.1 b). We calculated the sensitivity d'-value for each animal and vocalization (fig. 5.1 c). All four subjects were able to detect the reverberated stimulus out of the dry background significantly ($p < 0.001$, Fisher-test) for all vocalizations. The mean sensitivity d'-values differed consistently for all subjects among the vocalizations: all subjects had their best performance for mouse 2 (m2), and reverberation was overall subjects easier to detect for the two mice vocalizations than for the three bird vocalizations. Nevertheless, there are some differences: While the sensitivity d'-value of vocalization mouse 1 (m1) differs significantly compared to all of the other vocalizations ($p < 0.05$, estimated marginal means), the sensitivity d'-value of bird 3 (b3) differs significantly additionally to vocalization bird 1 (b1, $4.7 * 10^{-6}$, estimated marginal means). Since the different vocalizations differ strongly in their temporal structure, we wondered whether the achievement of the sensitivity d'-value could be reflected in the response time of the animals - the time it took for the subjects to leave the platform after the onset of the reverberated vocalization (fig. 5.1 d). For all but vocalization b3 response time distribution was similar: compared to vocalization b1 ($1.5 * 10^{-8}$, estimated marginal means), m1 ($p = 0.0301$, estimated marginal means) and m2 ($2 * 10^{-4}$, estimated marginal means), the subjects jumped significantly later (mean (s.e.) = 0.5272 s (0.0235)) from the pedestal.

Vocalization b3 is different from all the other vocalizations in that it is not strongly amplitude modulated and has a monotonous structure without any pulses.

5.3.2. Dry and reverberated stimuli cause different neuronal responses

Since the animals were able to detect reverberation in sequences of repeated vocalizations, we next asked what the underlying neural representation may be. Therefore, we presented those vocalizations to mice while they were awake and passively listening and we recorded their neuronal responses from core auditory cortex (fig. 5.2 a). Using a movable electrode probe (fig. 5.2 b), we were able to record neuronal responses from 2495 units in 9 animals.

Regarding the question if neurons respond differently to dry and reverberated stimuli and to gain an overview of all neuronal data, we first calculated a preference index (dry preferring or reverb preferring) for each unit in each vocalization and sorted the PSTHs by the preference index (fig. 5.2 c top:
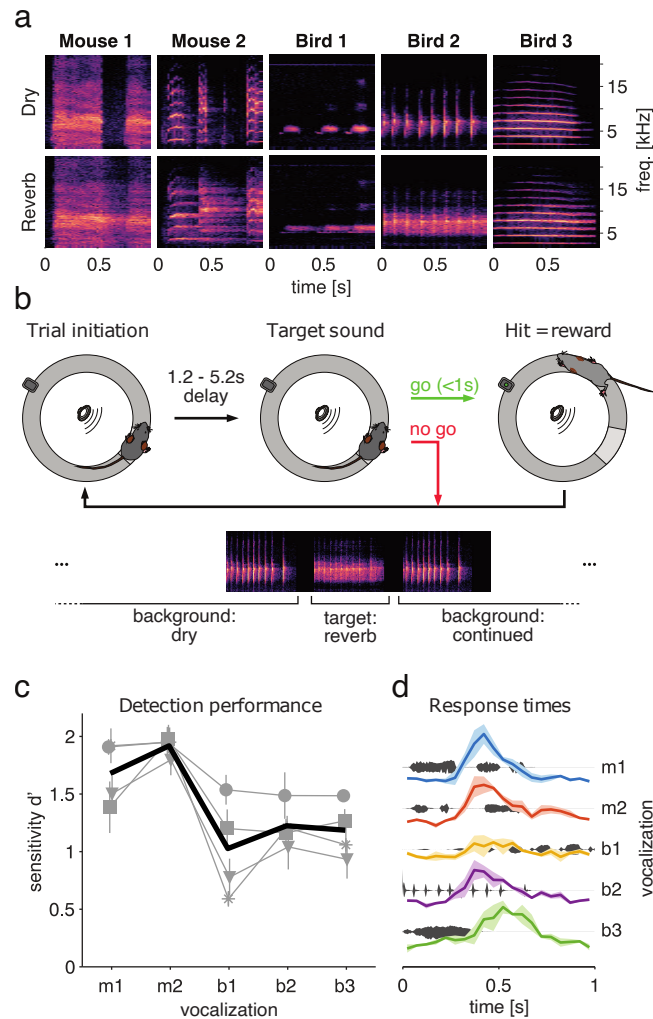
Figure 5.1.: **Mice are able to discriminate between dry and reverberated sounds.** **(a)**: Spectrograms of the natural vocalization used throughout the study. Shown are the 1 s of each stimulus used for the behavioral experiments. The top panel row shows the dry stimulus version, the bottom panel the same stimulus with added reverberation. **(b)**: Behavioral paradigm: mice had to detect a change from continuously repeated dry stimuli to the reverberated sound and indicate successful detection by jumping down from a small pedestal within 1 s after the stimulus onset. The dry background stimuli were level roved to exclude overall loudness as a cue. **(c)**: Detectability of reverberation quantified by the sensitivity d' for all four tested subjects (grey lines, mean ± s.e.m of all tested sessions), resolved by vocalization type. The thick black line is the grand mean over all animals. **(d)**: Distribution of the response times of the animals relative to the start of each stimulus, which is depicted in the background. The solid line is the mean distribution of all tested animals (n = 4), the shaded area depicts s.e.m. between the subjects.

dry preference, bottom: reverberation preference). Since the order of units within each vocalization between dry (left) and reverberated (right) sound is the same, we can already observe that some neurons' responses differ between dry and reverberated stimuli: reverberation preferred units (below red lines) are more likely to respond to reverberated stimuli (right) than to dry stimuli (left). Comparing the mean responses of the dry preferring units to the reverberation preferring units (fig. 5.2 d, 25 % quantile each), we not only observe that the neuronal activity of reverberation preferring units (right) is higher during reverberated stimuli (orange) furthermore, their neuronal activity is inhibited during dry stimuli (blue) as well. For dry preferring units (left) vice versa.
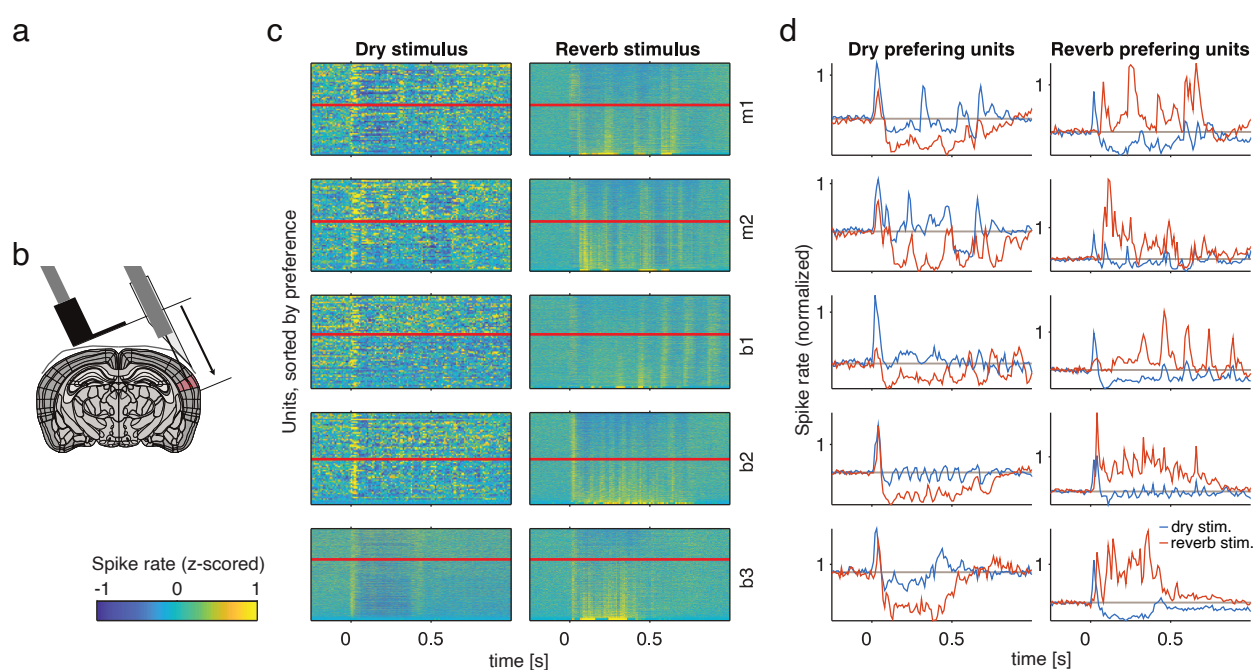
Figure 5.2.: **Units in auditory cortex respond differently to dry and reverberated sounds.**
(a): Recording setup: mice were chronically implanted with a moveable tetrode array. During the experiments, animals were free to run on a horizontal running wheel. **(b)**: Position of implanted tetrodes, allowing to record from multiple points along the medial-lateral axis from core fields of the auditory cortex. **(c)**: Population PSTHs in response to the five different vocalizations (n = 1952 (m1), 1978 (m2), 1967 (b1), 1956 (b2), 1957 (b3) units). Each row depicts the color-coded PSTH of a single unit. Single units are sorted by their preference for dry or reverberated sounds, the red lines indicate the border between 'dry' and 'reverb preferring' units. Order on the left (dry stimulus) and right side (reverberated stimulus) is the same. **(d)**: Mean PSTH of the top 25 % quantile of dry (left) and reverberation (right) preferring units, respectively. Blue traces display the responses to the dry stimulus, orange to the same, but reverberated stimulus. The grey line indicates the level of spontaneous activity.

5.3.3. Decoding of dry and reverberated stimuli based on single-trial population responses

If units with non-invariant representations of dry and reverberated stimuli within a neuronal population really exist, we should be able to reproduce our behavioral observation using the neuronal data: can we distinguish between dry and reverberated stimuli by neuronal responses?

Based on population response a correct prediction of the stimulus might be not as obvious as we might suggest (fig. 5.3 a, example population): only a few units clearly increase their firing rate in either of both stimulus conditions which suggests that they prefer firing for one of these condition. Studying the spike rate only is not possible to clearly distinguish between dry and reverberated stimuli for all trials (fig. 5.3 b). For example, for vocalization bird 1 (b1, $p = 0.1609$, Wilcoxon rank-sum test) the spiking rates alone can not predict the right stimulus condition. Furthermore, in vocalization m1, m2 and b2, the single-trial firing rates are even increased for dry stimuli compared to the reverberated stimuli. It is obvious that we can not define a good stimulus predictor based on single-trial firing rates.

In order to classify the preference of units, we modulated for each recording population a binomial logistic regression using the mean spike rate of each trial (up to 500 ms after onset) and unit. Thus, every unit obtains a weight-value which depicts the unit as dry preferring or reverberation preferring unit. The higher the weight of a unit, the more likely is the unit's preference for reverberated stimuli and vice versa (fig. 5.3 a right panel). Using these weights to emphasize the spike rates in each trial and unit (coefficient score), discrimination of dry and reverb stimuli became accurate: in the example, the coefficient score significantly differs between dry and reverberated stimulus condition (fig. 5.3 c) for all vocalizations ($p < 0.001$, Wilcoxon rank-sum test).

Comparing the predicted stimulus condition from the preference-classification to the true stimulus condition, we can calculate the sensitivity d'-value for each subject in each vocalization (like for behavior analysis) and display the accuracy of the regression (fig. 5.3 d): the higher the sensitivity d'-value the higher is the match rate of true and predicted stimulus condition. For all subjects, the pattern of the sensitivity d'-value is similar: The m2 and b2 vocalizations are the most successful classifications within the mouse stimuli, whereas vocalization b1 is the most erroneous one. Over all subjects, vocalization m1 and b1 differ significantly from the other vocalizations ($p < 0.001$, estimated marginal means). We already observed a similar pattern in the behavioral results (fig. 5.3 e): we gained best performances for both, behavioral (black line) and electrophysiology (blue line) within the mouse stimuli for m2 and within the bird stimuli for b2 and the worst performance for b1, even though the range of the behavioral observation is smaller compared to the classification results.
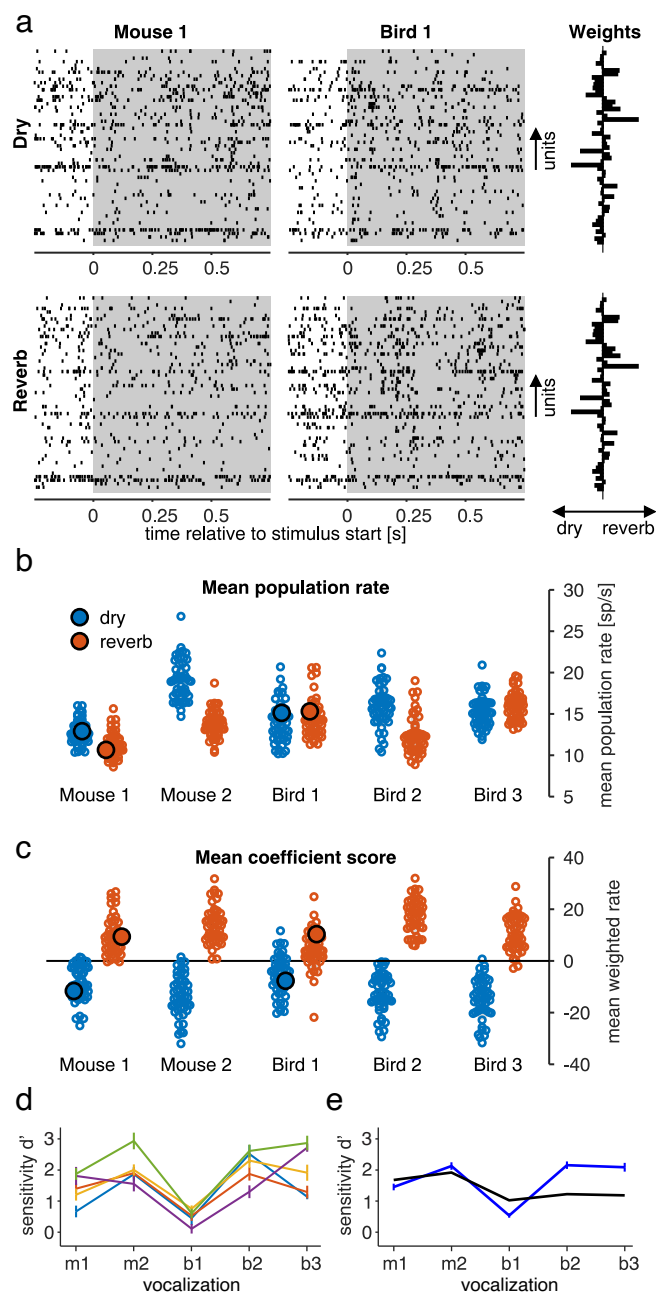
Figure 5.3.: **Classification of sounds into dry and reverberated based on single-trial population responses.** **(a)**: Example single-trial population responses to two different vocalizations in their dry and reverberated versions. The grey area indicates the presence of the stimulus. For the classification, only responses up to 0.5 s were used. On the right, the weights for each unit's rate for classification are shown - bars pointing to the left indicate that a higher rate in this unit is predictive of a dry stimulus, bars pointing to the right of the reverberated stimulus.

Figure 5.3.: **(b)**: Example for mean population rates trial-by-trial for dry and reverberated vocalizations, showing that there is no mean rate effect of vocalization that is consistent across different stimuli. Each dot is the mean rate of the population in a single trial, the black circles mark the examples in (a). **(c)**: When the mean coefficient score based on the weight shown in (a) is plotted instead of the mean rate, single-trials can be well classified into dry and reverberated. **(d)**: Mean classification performance for all tested animals resolved by vocalization, error bars are s.e.m. over positions. **(e)**: Comparison of the average performance for neural (blue) and behavioral classification performance (black, redrawn from fig. 5.1 c).

5.3.4. The deviation in population response explains the classification performance

In order to further understand which aspects of the population responses contribute to a dry/ reverberation discrimination, we calculated the mean firing rates of all single-trial rates per unit for all dry and reverberated stimuli separately (fig. 5.4 a). Instead of a bias of higher rates towards reverberated stimuli, we observed varying spreads of rates: the rate differences (rate distance) between dry and reverberated stimuli for bird 1 are smaller than for the other vocalizations. Since the mean classification performance was poorest for bird 1 as well (fig. 5.3 d), we compared both, the mean of rate distance (fig. 5.4 b top) and the standard deviation of rate distance (bottom) to the result of the classification performance: the deviation of the rates within the populations is highly predictive of the classification performance (r = 0.9466, $p = 0.0147$), but not the mean rate distance (r = -0.1378, $p = 0.8252$). Furthermore, the classification success for each single experimental session is highly correlated to the deviation of the population response (fig. 5.4 c bottom, r = 0.6015, $p < 0.0001$): the higher the deviation, the better is the classification performance. An explanation of the classification performance by means of the mean rate distance (Fig. c top, r = 0.026, $p = 0.6407$) is not possible.

Since the spread of rates within a population reflects our classification performance well, we were wondering where this disparity within the population came from. Therefore, we selected 10 % of the units with the lowest classification weights, which implicates dry preferring units (see fig. 5.3) and 10 % of the highest classification weights, which implicates reverberation preferring units (fig. 5.4 d) and we compared the mean firing rates of all single-trial rates per unit like before (fig. 5.4 e, top: low weights = dry preferring, bottom: high weights = reverberation preferring). Here we found, that the subset of dry preferring units (top) have an increased firing rate in dry stimuli, whereas the subset of reverberation preferring units (bottom) have an increased firing rate in reverberated stimuli.
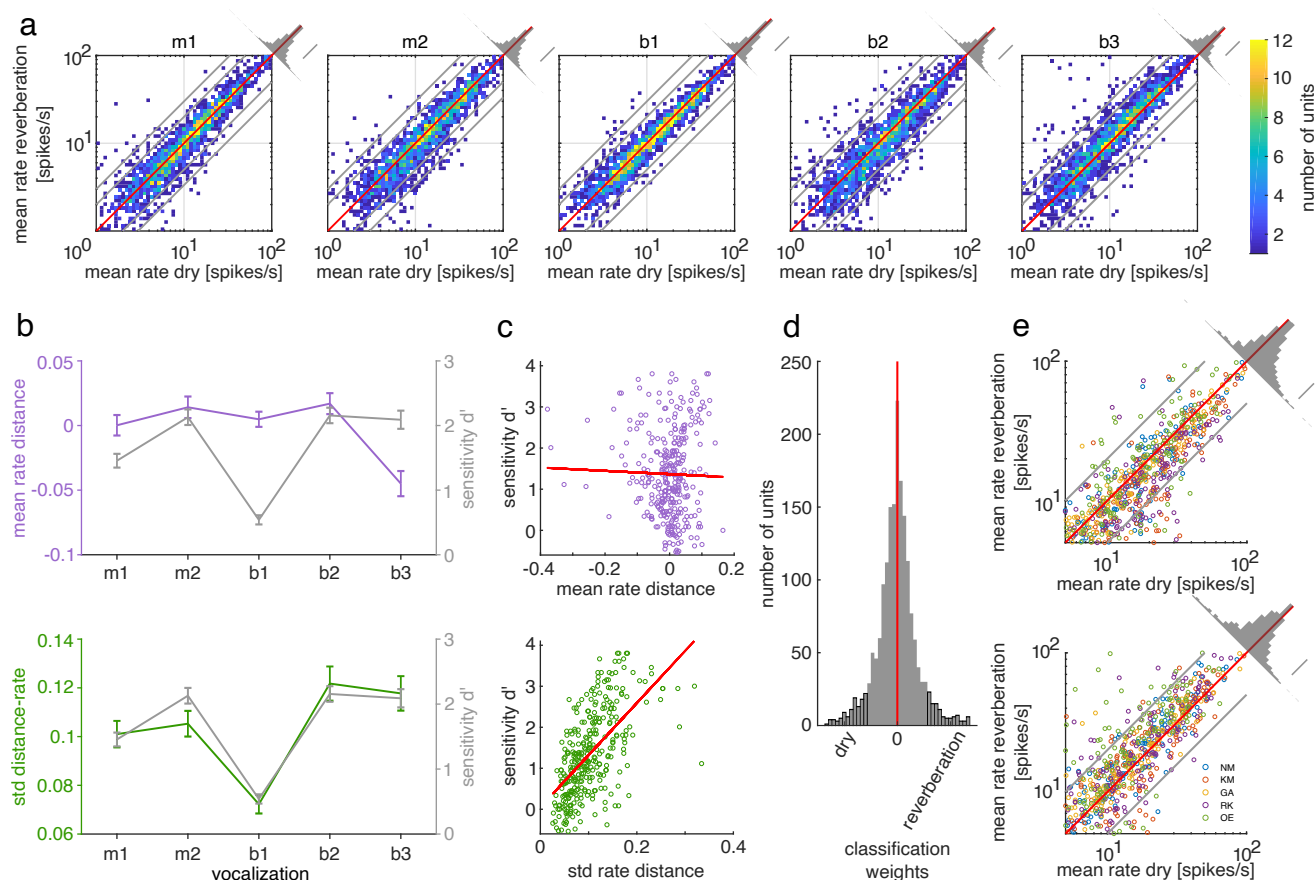
Figure 5.4.: **The classification performance of each vocalization can be explained by the disparity of population responses. (a)**: Comparison of the mean trial rates for each unit (n = 1980) for the dry and reverberated stimulus in each vocalization. The red diagonal line indicates equal rates in the dry and reverberated condition. Grey diagonal lines indicate a twice (threefold) as high rate for one of the stimulus conditions compared to the other one. Right upper corner: Distribution of rate differences (rate distance) between both stimulus conditions (bars = 200 units). **(b)**: Mean (top, purple) and standard deviation (bottom, green) of the rate distances (mean and s.e.m.) for each vocalization compared to the classification performance (grey). **(c)**: Classification performance (sensitivity d') compared to the means of the rate distances (top) and the standard deviations of the rate distances (bottom) in each position and vocalization (n = 325). **(d)**: Distribution of classification weights of all units (n = 1800). In (e), 10% of the lowest (dry) and highest (reverberation) weights were used (black edges). **(e)**: Like in a) (diagonal histogram bars = 50 units), but only units with low (top, n = 958) and high (bottom, n = 962) classification weights (see (d)).

5.3.5. Parallel processing of reverberation and sound identity

Both our behavioral and electrophysiological experiments showed that information about reverberation is present and can be used invariantly of sound identity. However, animals need to identify

sounds invariantly of context as well. We next asked whether and how parallel processing of context and sound identity can be found in mouse auditory cortex. We first evaluated the MI between single-unit responses or summed population activity and (1) reverberation irrespective of sound identity and (2) sound identity, independent of reverberation condition. To get an idea on the preferred time scales of encoding, we calculated MI in different time windows, ranging from 4 ms bins to the firing rate over 512 ms (fig. 5.5 d). As would be expected based on the successful classification, both single units and mean population responses contained information about reverberation, and this information was highest for the large time windows we had used for the classification. MI between reverberation and summed population activity at each position varied largely and improved encoding only slightly. This may be expected since summing improves trial-by-trial variability but sums reverb-preferring and dry-preferring units, eliminating the within-population variance in the population that we had shown to be crucial for decoding (fig. 5.4 c). For sound identity, on the other hand, summing over the populations improved MI between stimulus and neural response significantly (fig. 5.5 a, lower panel), and peaked at shorter time windows (between 32 and 64 ms), suggesting that the sum over dry- and reverb-preferring units may result in a more invariant representation, encoding sound identity with a neural code with higher temporal resolution than the one best for reverberation context.

We next asked whether we could decode stimulus identity invariantly of reverberation from the population in a similar manner as we were able to decode reverberation. We applied multinomial logistic regression with all units from a single animal as inputs and used different bin sizes (fig. 5.5 b). We were able to decode vocalization identity with high accuracy. Similar to the MI analysis, decoding performance peaked for shorter time window, and was best for 16 ms bins, further suggesting a neural code with higher temporal resolution for sound identity and a slower rate code for contextual information about reverberation.

It has been shown before that stimulus reconstructions from population responses to reverberated sounds in auditory cortex result in spectrograms that resemble dry rather than the original reverberated sounds (Mesgarani et al., 2014). Our results suggest that in the mouse, there does not seem to be such an invariant code. However, sound identity can still be decoded from the population reliably using logistic regression. We next asked whether there exists a projection of the population activity that would enable invariant reconstruction of the spectrograms of the vocalizations similar to what had been found in ferrets. To find such a projection, we performed a LDA, searching for those sub-spaces of the population activity that best discriminate between the vocalizations (LDA$_{id}$) or between reverberation and dry (LDA$_{reverb}$).

LDA$_{id}$ components were largely invariant to reverberation (fig. 5.5 c), but contained different aspects of the temporal structure of the vocalizations. The LDA$_{reverb}$ component on the other hand contained

little temporal details, but very well separated reverberated from dry sounds (Fig.c). Finally, we used LDA$_{id}$ projections for the reconstruction of spectrograms of the vocalization. An example of the reconstruction is displayed in figure 5.5 d: both responses to dry and reverberated sounds resemble much more the original dry than the reverberated stimulus, suggesting an invariant representation of the vocalization in the LDA$_{id}$ space. This observation was confirmed when we quantified the similiarity of the reconstruction to dry or reverberated spectrograms for all subjects and vocalizations (fig. 5.5 e). For all vocalizations except m1, reconstructions of responses to reverberated sounds were more similar to original dry then reverb for all 5 subjects. For m1 this was true for 4 out of 5 subjects.
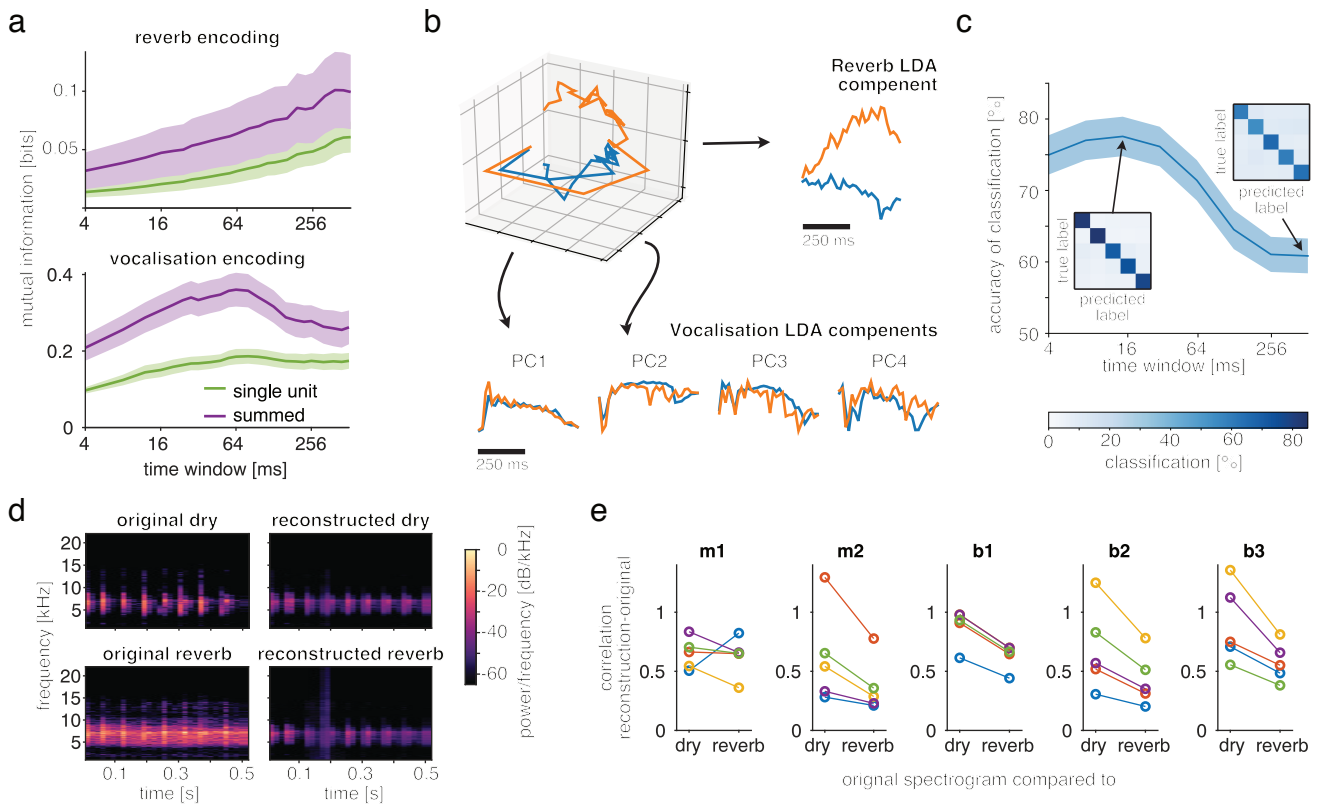
Figure 5.5.: **Decoding of vocalization identity.** (**a**): Encoding of information on reverberation (top) and vocalization identity (bottom), quantified mutual information between stimulus quality and either single units (top) or mean population (bottom) response. Mutual information was calculated for different time bins. Sold lines are mean values for all positions, shaded areas are s.e.m. over positions. (**b**): Example of decomposition into dimensions optimized for either reverb or vocalization. The 3D plot shows the mean path of the population response along with the first two vocalization components and the reverberation component for the b3 vocalization. Blue traces are dry, orange reverberated sounds. Upper right shows the time course of the reverb component in the dry and reverberated condition, the lower row shows all four vocalization identity PCs, largely invariant to reverberation condition. (**c**): Classification success for all five vocalization using different time bins. The insets show confusion matrices for 16 ms and 512 ms time windows. Vocalizations from left to right and top to bottom: m1, m2, b1, b2, b3. (**d**): Example of reconstruction of stimuli based on single-trial population data. For reconstruction, all units from each animal were pooled. On the left is the original spectrogram of vocalization b2, on the right, the average reconstructed spectrograms, based either on the responses to the dry (top) or reverberated vocalization (bottom). (**e**): The similarity of reconstruction, based on the responses to the (different colors, n = 5) reverberated stimulus for all recorded animals and all five vocalizations. Displayed is the correlation normalized to the correlation between the spectrogram reconstructed from the dry stimulus and the original dry spectrogram. For all vocalization, the spectrogram reconstructed from the responses to the reverberated sounds resembles more those of the original dry stimulus.

5.4. Discussion

Our goal was to investigate a mechanism behind reverberation coding and sound identification: how can we recognize reverberation and identify the sound simultaneously? Therefore, we presented a set of five different animal vocalizations, dry and reverberated, to mice in active-discrimination behavioral and passive-listening electrophysiological experiments. Our behavioral results show that mice can discriminate reverberated from dry sound (fig. 5.1) but differently well between the vocalizations. Recordings in AC revealed that some neurons respond differently to dry and reverberated stimuli (fig. 5.2). Within a neuronal population, neurons of different preferences contribute to a broad population response (fig. 5.4). By using this broad population response, we were able to decode both the stimulus context (dry/reverberation, fig. 5.3) and stimulus identity (fig. 5.5). Furthermore, the reconstruction of stimulus identity leads to invariant representations of the sound, independently from the context. Based on mutual information analysis, we used a different time window for stimulus identity classification and reconstruction compared to the context decoding. Hence, the encoding of sound context and identity is possible based on different time scales within the same population response.

5.4.1. Limitations

In our behavioral experiments, mice performed a Go/No-go paradigm in order to detect reverberated sound out of a background of dry stimuli. In order to minimize non-reverberated cues for this discrimination task, we adjusted the experimental setup in three steps:

To eliminate temporal cues of stimulus duration (dry stimulus is shorter than a reverberated stimulus), we shorten all stimuli to 1 s (1) and additionally, the subjects had a response window of only 1 s (2) after stimulus onset. Since adding reverberation to a sound, we have to be aware that the reverberated stimulus does not only change temporal aspects but concentrates more energy as well. To eliminate the cue of reverberated sound being more energetic than dry stimuli, we added level-roving to the dry stimuli (3) and increased their level of energy equal to and higher than the reverberated sound. In spite of reducing temporal and energical cues, we can not conclude that our subjects used further unknown cues for this discrimination task.

The analysis of neuronal data in this study is focused on population response. In population response, we show that the high energy of reverberated sound compared to dry sound does not necessarily lead to higher mean spiking rates (fig. 5.3, 5.4). On this basis, it is reasonable to suppose that reverberation coding is supported by complex neuronal adjustment. The quantitative and classification results (fig. 5.2, 5.3, 5.4) on single-neuron level show that spiking behavior to reverberation differ between neurons. In our context, we declared those neurons as dry or reverberation preferring neurons. This

observation could be a link to already described noise- and background-preferring neurons (Bar-Yosef and Nelken, 2007; Malone et al., 2017). Since our analysis focused on population response, the effect of reverberation on the single-neuron level remains fragmentary.

5.4.2. Connection to other previous work

We observed neurons with context-dependent preference. The response of dry and reverberation preferring neurons varied a lot between both stimulus conditions (fig. 5.2): after an onset response, neurons got even inhibited in the non-preferred condition. We were able to quantify this preference using the weighted values out of a simple binomial logistic regression (fig. 5.3). For the whole neuronal population, we found a normal distribution of preference weighted neurons (fig. 5.4). This leads to a broad population spiking response which was the necessary impact for the classification success. Furthermore, the lack of diversity in population response for vocalization b1 can explain both, the poor classification success and the worst discrimination performance in the behavioral experiments.

The existence of reverberation-depending neurons was already shown in the auditory cortex (Bar-Yosef et al., 2002; Bar-Yosef and Nelken, 2007). In their studies, Bar-Yosef presented original chirp vocalizations and their components like background only, echo only, noise only or main chirp component only to anesthetized cats and showed the importance of background in shaping the responses of cortical neurons. Furthermore, they described that some neurons responded strongly to echo or noise only but weaker during natural chirp. Although previous studies focused on background sensitivity (Las et al., 2005; Malone et al., 2017) the link between background-/noise-depending neurons and reverberation-depending neurons as well as the temporal-spectral impact on them (different deviations in population code between vocalizations) remains elusive.

Is it even reasonable to compare background and reverberation processing?

Nelken et al. (1999) showed that separable background (which is rather common in environment) can elicit comodulation masking release (CMR) that facilitates tone recognition within noise (Hall et al., 1984). On the contrary, reverberation contributes to self-masking that downgrades speech recognition (Nabelek et al., 1989). However, reverberation of a signal delivers information about the surrounding of the listener and the distance to the source (Traer and McDermott, 2016) which can be used by bats as echolocation (Griffin and Grinnell, 1958) or even by blind humans for orientation (Kellogg, 1962). In his study, Kellogg compared the success of echolocation in a setting of comparable discs in blind and sighted men using self-produced sound. Although all discs were placed at a certain distance in front of the participants, the blind participants turned their head to the left and the right during their echolocation task. Kellogg already observed a comparable behavior in dolphins (Kellogg, 1960) and

called it 'auditory scanning', which is a combination of echo-ranging and binaural localization. Nevertheless, binaural localization using reverberation is a well-studied phenomenon explained by the precedence-effect. The precedence-effect implies that the first (direct) signal wavefront that arrives the listener is the leading acoustic signal for sound localization (Wallach et al., 1949). These observations lead to the assertion that reverberation processing is stronger linked to sound localization than to noise processing.

Since the temporal aspect is a crucial cue within sound localization (ITD), it is reasonable to find temporal hints for reverberation within neuronal coding. We showed that mutual information was highest for sound identity and reverberation within different time windows in the population code (fig. 5.5) that indicates multiplexed population coding. Multiplex coding was already shown on the level of single-neurons for simple tone features and sound localization (Walker et al., 2011), noting that mutual information for azimuth localization was highest in AC. Within multiplex coding, the strength of reverberation (respectively the location of the sound source) could be adjusted by a temporal interval between the different information of identity and context.

A further indication for a possible sound localization component within reverberation processing is the robust stimulus reconstruction (fig. 5.5). Like in the study of Mesgarani et al. (2014), stimulus reconstruction by population response leads to the dry stimulus indicating that a lack of information about an azimuth shift in sound location displays an undistorted acoustic environment. Furthermore, Devore et al. (2009) presented ITD-sensitive neurons in the inferior colliculus of anesthetized cats, which respond differently to dry, moderate or strong reverberation at different azimuth locations.

Using sound localization to explain reverberation discrimination remains one question unanswered: How were our subjects in the behavior experiment able to discriminate between reverberated and dry sound?

Traer and McDermott (2016) analyzed the temporal and spectral aspects of natural reverberation and evaluated their results in reverberation discrimination tasks in humans. They conclude that reverberation itself provides statistical features for the auditory system to process an auditory scene analysis for reverberation. Depending on the identity of the dry sound those statistical features might be formed more or less distinctive. Since the spectral presence of vocalization b1 compared to the other vocalization is limited (fig. 5.1 a), the lack of frequency-depending convolution could provide means for the impaired discrimination performance of the subjects.

5.4.3. Outlook

Here, we showed that broad population response includes neurons with preferred reverberation or dry firing activity (1) and that stimulus reconstruction of these responses lead to a robust invariant stimulus representation (2). We further showed that mice can discriminate dry and reverberated sound (3). As described in detail (see Limitations), we excluded endogenous cues from the behavioral discrimination task in order to focus on reverberation features only. Further behavior experiments using different strengths and features of reverberation as described by Traer and McDermott (2016) would ensure our findings and develop further reverberation characteristics with an overall validity in mammals. Valid reverberation discrimination in animal experiments enables behavior experiments with parallel cortical recordings to analyze the role of attention in reverberation discrimination task. Since there are already studies based on sound localization in reverberant rooms, a link between both processes remains elusive.

Part III.

General discussion

6. General discussion

Auditory signals are omnipresent in the environment and may have a strong influence on behavioral reactions or perceptions. Before necessary information from auditory signals can be retrieved and used for behavior decisions, overall sensory information has to be processed first. This thesis gives insight in both how auditory information can be processed and retrieved. For information processing (chapter 4), the role of PV+ neurons for auditory processing has been analyzed. Enhancing the activity of those neurons in core auditory cortex enables flexible, divisive modulation of cortical responses across neurons and stimulus paradigms but preserved spectral and temporal response properties. Therefore, spectral and temporal neuronal properties are robust against external influences from PV+ neurons. Hence, modulation of PV+ neurons could serve as sensory gain control in auditory cortex, which is a computational function for e.g. foreground-background separation, selective attention and optimized sensory discrimination while keeping important acoustic information. For information retrieval (chapter 5), classification of stimulus reverberation-context or identity can be carried out by population responses using different timescales. Here, the organism can have flexible access to auditory information that is required. Context-preferred activity of some neurons within the population contribute to the successful classification for both context and identity classification. The reconstruction of the the stimulus identity based on the population response was accompanied by the loss of the information about the reverberation. All in all, this provides a means for multiplexed information representation or even parallel strategies from sound localization.

Neuronal robustness plays a major role in information processing and neuronal flexibility is crucial for information retrieval. Although neuronal robustness and flexibility imply to be mutually exclusive, both are central requirements for information processing and retrieval.

6.1. Neuronal robustness and computational flexibility in information processing and retrieval

Robustness and flexibility imply to be a contradiction. However, information processing and retrieval make use of both. Here it became evident that flexibility and robustness are not exclusive but rather complementary to each other. In order to prepare for that further discussion, the terms robustness and flexibility are explained in more detail first.

As the ability to resist influences without adapting (Wieland and Wallenburg, 2012) the robustness of a neuronal network creates the solid basis to contain information of different aspects. The neuronal code is less susceptible to unwanted disturbances. For example, in order to identify different musical instruments within one musical piece neuronal robustness is crucial. Acoustic sounds from the guitar differs to the acoustic sounds of the drums. Both instruments have acoustic characteristics which have to be remained during sensory processing. Flexibility is the quality to adapt a neuronal network or to offer different options. Hence, the ability of flexibility provides a way to modify different signals although resources (e.g. types of receptors, number of cells) are limited. Despite the fact that all resources are finite, the amount of possible reactions (e.g. behavior, attention, perception) is almost limitless. This indicates that flexibility is a fundamental component, which contributes to a high quantity and quality of any behavioral life.

As general partners, robustness and flexibility are not a contradiction. Hence, they can coexist in any system. Within auditory information processing and retrieval, they have to play particular roles in order to contribute to different tasks. In the following, these particular roles of flexibility and robustness are discussed for information processing and retrieval, respectively.

Flexible but robust: gain control via PV+ modulation

For auditory information processing (chapter 4), the effect of PV+ cells on cortical neurons was described. Increasing the activity of PV+ neurons leads to divisive modulation across cortical neurons whereas spectral and temporal characteristics of cortical neurons remain unchanged. Theses characteristics have to be robust against influences because they reflect important features of the detected sound. The robustness of a neuron depend on the input information (tonotopic routing from cochlea), anatomical arrangement of the cell body like morphology, passive and active membrane characteristics and location of synaptic transmissions. All in all, the intrinsic electrical activity of a neuron is as unique as a fingerprint (Llinas, 2014). Hence, robustness on cellular level makes neurons a highly input/output-specific tissue. In order to cover all possible sensory input, the performance of robust neurons has to increase. Since an increased number of neuronal structures would go beyond the lim-

its of capacity and space, an additional flexible component which maintain the performance over a broad range of input is a more capable solution. The flexible component in this study occurred as a mainly divisive reduction or enhancement of single-unit activity after PV+ cell manipulation while keeping their spectral and temporal properties robust. Those neurons were gain-modulated (or gain-controlled) by PV+ neurons. Gain modulation is primarily described as an integration mechanism of two or more information sources. Therefore, robust primary information can be adjusted by further information sources, like extrinsic information (e.g. audition and vision) or intrinsic information (e.g. audition and head position or audition and attention). This widespread information integration is important to create an overall realistic picture of the environment (Salinas and Thier, 2000; Salinas and Sejnowski, 2001).

In case of auditory information processing, PV+ neurons modulate the overall activity of cortical neurons and hence contribute to flexible adaption while spectral and temporal information of the sound may remain unchanged due to robust neuronal characteristics.

Robust but flexible: invariant representation without loosing the context

For auditory information retrieval (chapter 5), cortical population responses to different sound identities, which were reverberated or not (context), were described. On basis of different timescales it was possible to classify the stimulus context or the stimulus identity. This means that information about the identity and the context are located at different temporal places within the population code. The reconstruction of the stimulus identity upon the population response supports the observation: a reconstructed reverberated sound was more similar to the original dry stimulus than to the original reverberated one. Hence, information about identity and context are separately conserved within a neuronal population. On the one hand, the information about sound identity is invariant and robust against possible reverberation context. On the other hand, the information about reverberation is not lost but it is flexibly additionally retrievable if necessary. Both stimulus information are robustly conserved on different timescales within a population response and can be flexibly retrieved if required.

The order of conserved stimulus information across the time may depend on the priority of the information itself: the identity of a sound is more important (e.g. danger, harm) than the information about the sounds' reverberation (e.g. distance and environment). Hence, the neuronal information for sound identity is conserved within the population response early after stimulus onset (64 ms) compared to reverberation (approx. 500 ms, see Fig 5.5, A). The robust conservation of stimulus information across neurons and time delivers an easy option to extract required information (stimulus identity or context) flexibly.

Since robustness in information retrieval is reflected by neuronal activity within a particular timescale,

it is unclear how to retrieve these information flexibly. The possibility, that coordinate transformation is a good candidate for flexibility will be further explained. Here, an already existing coordinate system rotates around a given point (passive transformation), which takes the new coordinates from the transformed coordinate system (Morrison and Parker, 1987). Such a computational approach can be helpful when different reference points affect a behavioral action. For instance, reaching for a mug without shifting the gaze from the newspaper. The middle of the body as the target for the mug differs to the reference point of the gaze as well as the reference point of the arm and hand including muscle activities (Salinas and Sejnowski, 2001). Using coordinate transformation, robust information can take on multiple values (dimensions), depending on the coordinate frame and referring system. A robust neuronal code which already includes different information of a stimulus on different timescales (chapter 5) can further enlarge its multiplex representation by coordinate transformation. Possibly, in a different experimental setting, the information about the context (reverberation) can be further interpreted for sound localization by changing the reference point. Apparently, this could lead to an uncountable amount of possible (virtual) coordinate values of the neuronal code due to the number of possible changes of the coordinate system.

6.2. Conclusion

Sensory information processing and retrieval have to cope with different challenges. On the one hand, they have to resist unwanted disturbances, on the other hand, they have to be adaptable due to the environmental approach. The main task in information processing is the flexible integration of information from different sources without changing signal properties like the sound spectrum or temporal pattern. Those signal properties are ensured by neuronal properties on the level of single-cells. Processed information then can be retrieved and used for behavioral responses. Since any information about the current auditory environment exist, necessary information according the behavior task or requirement can be flexibly selected. Robustness and flexibility within the nervous system is no contradiction in sensory integration but a crucial combination that provides efficient, fast and stable computation for only limited capacity.
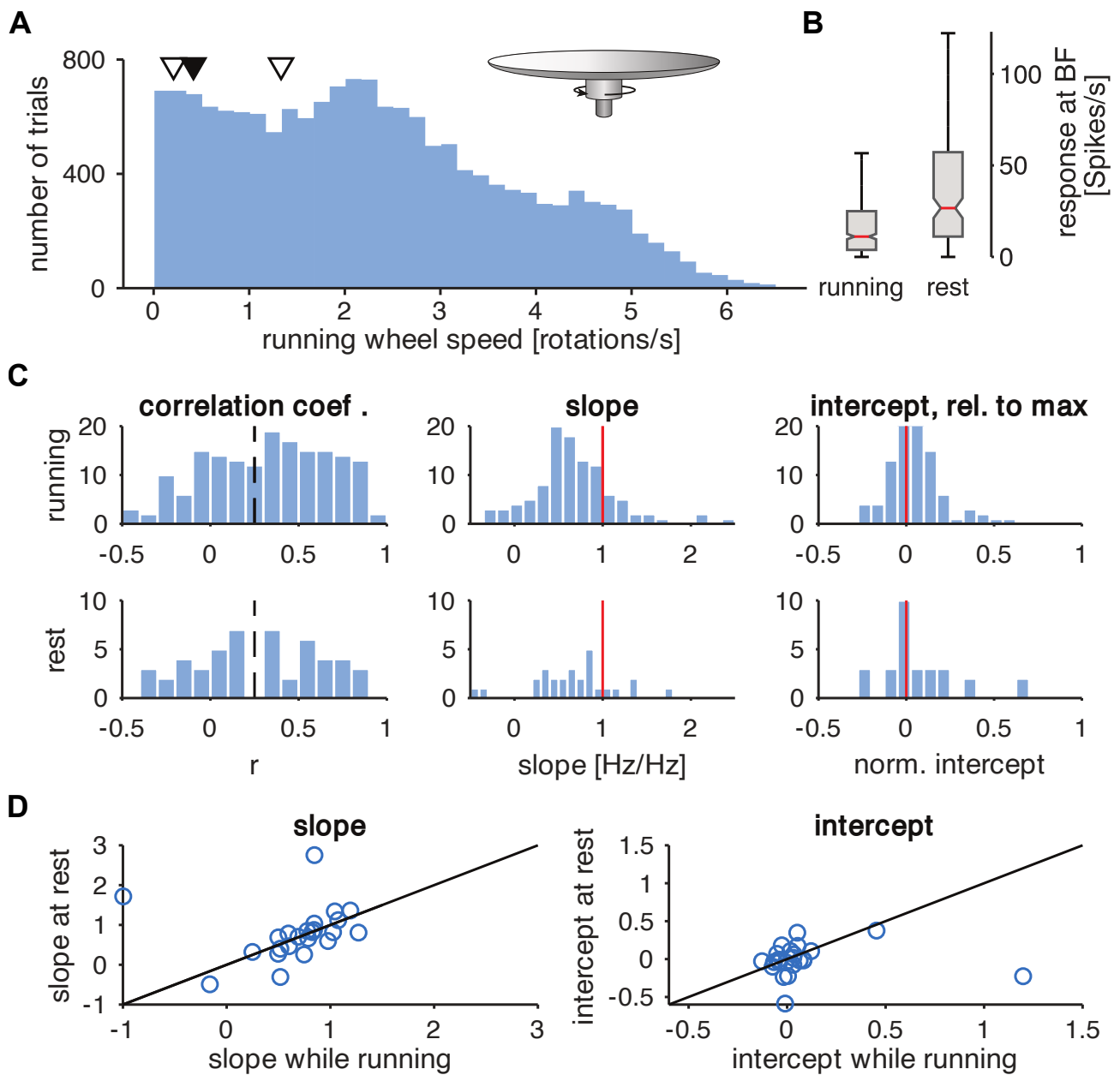
Appendix

Supplementary material

Figure S1.: **Effect of locomotion on divisive/subtractive scaling elicited by SSFO. (A)**: Distribution of mean running speeds per trial measured from rotation of the horizontal treadmill (inset). Running data was collected during neuronal recordings from 12 AC sites in two animals (23054 trials in total). Since there was no clear bimodal distribution in wheel rotation speed, three different thresholds for distinguishing "rest" from "running" activity were applied (triangles at 0.21, 0.42, and 1.33 rotations/s) to test for an effect of locomotion on SSFO modulation of neuronal activity. Filled marker shows threshold used for illustrations of analysis in panels B-D.

Figure S1.: **(B)**: Effect of locomotion on peak onset firing rate at best frequency under control conditions (red lines: medians, box: 25% and 75% quartiles, error bars: full range), showing a strong reduction in firing rate during trials with more running (11.1 vs 27.7 spikes/s, $p < 10^{-12}$, Wilcoxon rank-sum test). **(C)**: Histograms of results from major axis regression of the frequency response curves for SSFO • PV versus control trials (analysis as in Fig. 4.4), split into running and rest trials (upper and lower panels, respectively). Plots show data from all reduced units that could be tested at all frequencies in the respective activity condition only. (**(D)**: Relationship between regression fit parameters for rest versus running trials, for all units with complete data in both conditions. Solid lines represent equal values in both conditions. Slope values for rest and running trials were significantly correlated across units, not only for the 0.42 rotations/s running threshold used here ($r = 0.56$, $p = 0.0028$) but also for the other thresholds tested (0.21 rotations/s: $r = 0.36$, $p = 0.045$; 1.33 rotations/s: $r = 0.53$, $p < 0.0001$). For the intercept, correlations were weaker ($r < 0.3$ and $p > 0.1$ for all three threshold choices).
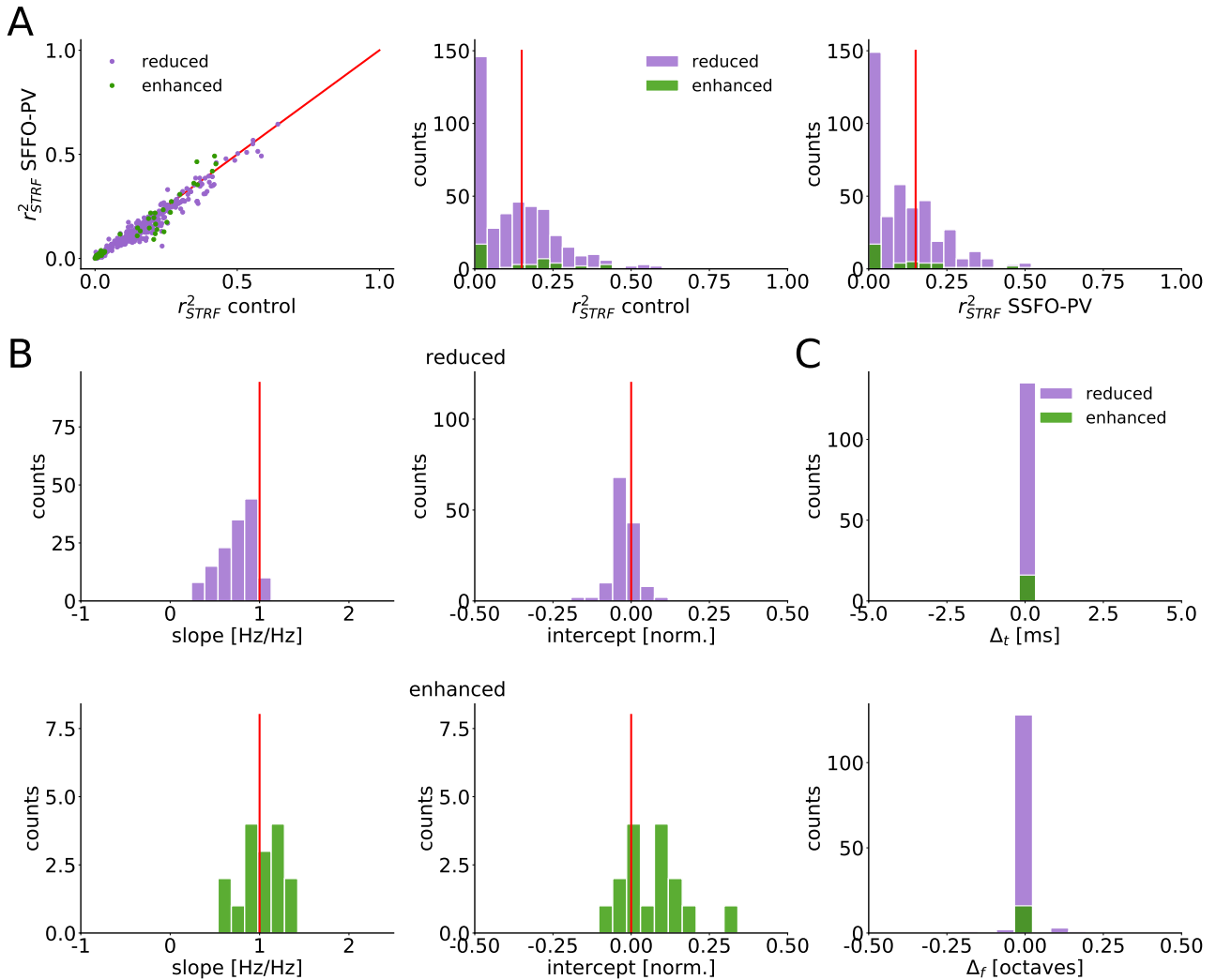
Figure S2.: **Units with coefficient of determination** $r^2 > 0.15$ **in STRF estimation have STRFs which are divisively scaled by PV-activation, while preserving their structure.** **(A)**: Coefficients of determination of STRF estimation in PV-activated versus control conditions (left). Coefficients of determination are highly correlated ($\rho \approx 0.976$) and have similar range in PV-activated versus control conditions. Note that 1% of the reduced units and 5% of the enhanced units have $r^2 < 0$ in PV-activated condition and are excluded for better visualisation of the bulk of the data. **(B)**: For reduced (top) and enhanced (bottom) units, slopes (left) and intercepts (right) of linear fits to STRF predicted activities in PV-activated versus control conditions. Only units with $r^2 > 0.15$ are included (enhanced units n = 16 (out of a total 44) and reduced units n = 135 (out of a total 419)). Results are robust to the choice of r^2 threshold (results not shown). **(C)**: For most units, sustained PV-activation does not shift the STRF in time or frequency.

Bibliography

Aizenberg, M., Mwilambwe-Tshilobo, L., Briguglio, J. J., Natan, R. G., and Geffen, M. N. (2015). Bidirectional regulation of innate and learned behaviors that rely on frequency discrimination by cortical inhibitory neurons. *PLoS Biol*, 13(12):e1002308.

Alitto, H. J. and Dan, Y. (2012). Cell-type-specific modulation of neocortical activity by basal forebrain input. *Front Syst Neurosci*, 6:79.

Atallah, B. V., Bruns, W., Carandini, M., and Scanziani, M. (2012). Parvalbumin-expressing interneurons linearly transform cortical responses to visual stimuli. *Neuron*, 73(1):159–70.

Bamann, C., Kirsch, T., Nagel, G., and Bamberg, E. (2008). Spectral characteristics of the photocycle of channelrhodopsin-2 and its implication for channel function. *J Mol Biol*, 375(3):686–94.

Bar-Yosef, O. and Nelken, I. (2007). The effects of background noise on the neural responses to natural sounds in cat primary auditory cortex. *Front Comput Neurosci*, 1:3.

Bar-Yosef, O., Rotman, Y., and Nelken, I. (2002). Responses of neurons in cat primary auditory cortex to bird chirps: effects of temporal and spectral context. *J Neurosci*, 22(19):8619–32.

Bathellier, B., Ushakova, L., and Rumpel, S. (2012). Discrete neocortical dynamics predict behavioral categorization of sounds. *Neuron*, 76(2):435–49.

Bean, B. P. (2007). The action potential in mammalian central neurons. *Nat Rev Neurosci*, 8(6):451–65.

Berndt, A., Yizhar, O., Gunaydin, L. A., Hegemann, P., and Deisseroth, K. (2009). Bi-stable neural state switches. *Nat Neurosci*, 12(2):229–34.

Bizley, J. K. and Cohen, Y. E. (2013). The what, where and how of auditory-object perception. *Nat Rev Neurosci*, 14(10):693–707.

Blackwell, J. M. and Geffen, M. N. (2017). Progress and challenges for understanding the function of cortical microcircuits in auditory processing. *Nat Commun*, 8(1):2165.

Boyden, E. S., Zhang, F., Bamberg, E., Nagel, G., and Deisseroth, K. (2005). Millisecond-timescale, genetically targeted optical control of neural activity. *Nature Neuroscience*, 8(9):1263–1268.

Busse, L., Wade, A. R., and Carandini, M. (2009). Representation of concurrent stimuli by population activity in visual cortex. *Neuron*, 64(6):931–42.

Caillard, O., Moreno, H., Schwaller, B., Llano, I., Celio, M. R., and Marty, A. (2000). Role of the calcium-binding protein parvalbumin in short-term synaptic plasticity. *Proc Natl Acad Sci U S A*, 97(24):13372–7.

Cant, N. B. and Benson, C. G. (2003). Parallel auditory pathways: projection patterns of the different neuronal populations in the dorsal and ventral cochlear nuclei. *Brain Res Bull*, 60(5-6):457–74.

Carandini, M. and Heeger, D. J. (2011). Normalization as a canonical neural computation. *Nat Rev Neurosci*, 13(1):51–62.

Cardin, J. A. (2019). Functional flexibility in cortical circuits. *Curr Opin Neurobiol*, 58:175–180.

Castro-Alamancos, M. A. and Connors, B. W. (1996). Short-term plasticity of a thalamocortical pathway dynamically modulated by behavioral state. *Science*, 272(5259):274–7.

Caviness, V. S., J. (1975). Architectonic map of neocortex of the normal mouse. *J Comp Neurol*, 164(2):247–63.

Cruikshank, S. J., Killackey, H. P., and Metherate, R. (2001). Parvalbumin and calbindin are differentially distributed within primary and secondary subregions of the mouse auditory forebrain. *Neuroscience*, 105(3):553–69.

Cruikshank, S. J., Lewis, T. J., and Connors, B. W. (2007). Synaptic basis for intense thalamocortical activation of feedforward inhibitory cells in neocortex. *Nat Neurosci*, 10(4):462–8.

de Villers-Sidani, E., Alzghoul, L., Zhou, X., Simpson, K. L., Lin, R. C., and Merzenich, M. M. (2010). Recovery of functional and structural age-related changes in the rat primary auditory cortex with operant training. *Proc Natl Acad Sci U S A*, 107(31):13900–5.

deCharms, R. C., Blake, D. T., and Merzenich, M. M. (1998). Optimizing sound features for cortical neurons. *Science*, 280(5368):1439–43.

DeFelipe, J. (1997). Types of neurons, synaptic connections and chemical characteristics of cells immunoreactive for calbindin-d28k, parvalbumin and calretinin in the neocortex. *J Chem Neuroanat*, 14(1):1–19.

Deisseroth, K., Feng, G., Majewska, A. K., Miesenbock, G., Ting, A., and Schnitzer, M. J. (2006). Next-generation optical technologies for illuminating genetically targeted brain circuits. *J Neurosci*, 26(41):10380–6.

Devore, S., Ihlefeld, A., Hancock, K., Shinn-Cunningham, B., and Delgutte, B. (2009). Accurate sound localization in reverberant environments is mediated by robust encoding of spatial cues in the auditory midbrain. *Neuron*, 62(1):123–34.

DeWitt, I. and Rauschecker, J. P. (2012). Phoneme and word recognition in the auditory ventral stream. *Proc Natl Acad Sci U S A*, 109(8):E505–14.

Di Pasquale, G., Davidson, B. L., Stein, C. S., Martins, I., Scudiero, D., Monks, A., and Chiorini, J. A. (2003). Identification of pdgfr as a receptor for aav-5 transduction. *Nat Med*, 9(10):1306–12.

Edeline, J. M. (2012). Beyond traditional approaches to understanding the functional role of neuromodulators in sensory cortices. *Front Behav Neurosci*, 6:45.

Encyclopaedia Britannica (2010). Image house-mouse. `https://www.britannica.com/animal/house-mouse/#media/1/273137/74904`. accessed May 13, 2020.

everyVECTOR (2009). vector paav-ef1a-dio ssfo-eyfp. `http://www.everyvector.com/sequences/show_public/15601#`. accessed May 14, 2020.

Fairhall, A. L., Lewen, G. D., Bialek, W., and de Ruyter Van Steveninck, R. R. (2001). Efficiency and ambiguity in an adaptive neural code. *Nature*, 412(6849):787–92.

Flotte, T. R. and Berns, K. I. (2005). Adeno-associated virus: a ubiquitous commensal of mammals. *Hum Gene Ther*, 16(4):401–7.

Fritz, J., Shamma, S., Elhilali, M., and Klein, D. (2003). Rapid task-related plasticity of spectrotemporal receptive fields in primary auditory cortex. *Nat Neurosci*, 6(11):1216–23.

Froemke, R. C. and Jones, B. J. (2011). Development of auditory cortical synaptic receptive fields. *Neurosci Biobehav Rev*, 35(10):2105–13.

Goodale, M. A. and Milner, A. D. (1992). Separate visual pathways for perception and action. *Trends Neurosci*, 15(1):20–5.

Gopaul, D. N. and Duyne, G. D. (1999). Structure and mechanism in site-specific recombination. *Curr Opin Struct Biol*, 9(1):14–20.

Gothner, T., Gonçalves, P. J., Sahani, M., Linden, J. F., and Hildebrandt, K. J. (2020). Sustained Activation of PV+ Interneurons in Core Auditory Cortex Enables Robust Divisive Gain Control for Complex and Naturalistic Stimuli. *Cerebral Cortex*. bhaa347.

Gow, D. W., J. (2012). The cortical organization of lexical knowledge: a dual lexicon model of spoken language processing. *Brain Lang*, 121(3):273–88.

Griffin, D. R. and Grinnell, A. D. (1958). Ability of bats to discriminate echoes from louder noise. *Science*, 128(3316):145–7.

Guo, F., Gopaul, D. N., and Van Duyne, G. D. (1999). Asymmetric dna bending in the cre-loxp site-specific recombination synapse. *Proc Natl Acad Sci U S A*, 96(13):7143–8.

Guo, W., Clause, A. R., Barth-Maron, A., and Polley, D. B. (2017). A corticothalamic circuit for dynamic switching between feature detection and discrimination. *Neuron*, 95(1):180–194 e5.

Haider, B., Krause, M. R., Duque, A., Yu, Y., Touryan, J., Mazer, J. A., and McCormick, D. A. (2010). Synaptic and network mechanisms of sparse and reliable visual cortical activity during nonclassical receptive field stimulation. *Neuron*, 65(1):107–21.

Hall, J. W., Haggard, M. P., and Fernandes, M. A. (1984). Detection in noise by spectro-temporal pattern analysis. *J Acoust Soc Am*, 76(1):50–6.

Hamilton, L. S., Sohl-Dickstein, J., Huth, A. G., Carels, V. M., Deisseroth, K., and Bao, S. (2013). Optogenetic activation of an inhibitory network enhances feedforward functional connectivity in auditory cortex. *Neuron*, 80(4):1066–76.

Harris, K. D. and Mrsic-Flogel, T. D. (2013). Cortical connectivity and sensory coding. *Nature*, 503(7474):51–8.

Hildebrandt, K. J., Sahani, M., and Linden, J. F. (2017). The impact of anesthetic state on spike-sorting success in the cortex: A comparison of ketamine and urethane anesthesia. *Front Neural Circuits*, 11:95.

Hippenmeyer, S., Vrieseling, E., Sigrist, M., Portmann, T., Laengle, C., Ladle, D. R., and Arber, S. (2005). A developmental switch in the response of drg neurons to ets transcription factor signaling. *PLoS Biol*, 3(5):e159.

Hubel, D. H. and Wiesel, T. N. (1962). Receptive fields, binocular interaction and functional architecture in the cat's visual cortex. *J Physiol*, 160:106–54.

Hudspeth, A. J. (1997). How hearing happens. *Neuron*, 19(5):947–50.

Inan, M. and Anderson, S. A. (2014). The chandelier cell, form and function. *Curr Opin Neurobiol*, 26:142–8.

Johnson, K. R., Erway, L. C., Cook, S. A., Willott, J. F., and Zheng, Q. Y. (1997). A major gene affecting age-related hearing loss in c57bl/6j mice. *Hear Res*, 114(1-2):83–92.

Kawaguchi, Y. and Shindou, T. (1998). Noradrenergic excitation and inhibition of gabaergic cell types in rat frontal cortex. *J Neurosci*, 18(17):6963–76.

Keifer, O. P., J., Gutman, D. A., Hecht, E. E., Keilholz, S. D., and Ressler, K. J. (2015). A comparative analysis of mouse and human medial geniculate nucleus connectivity: a dti and anterograde tracing study. *Neuroimage*, 105:53–66.

Keller, C. H., Kaylegian, K., and Wehr, M. (2018). Gap encoding by parvalbumin-expressing interneurons in auditory cortex. *J Neurophysiol*, 120(1):105–114.

Kellogg, W. N. (1960). Auditory scanning in the dolphin. *Psychol Rec*, 10:25–27.

Kellogg, W. N. (1962). Sonar system of the blind. *Science*, 137(3528):399–404.

Kepecs, A. and Fishell, G. (2014). Interneuron cell types are fit to function. *Nature*, 505(7483):318–26.

Keuroghlian, A. S. and Knudsen, E. I. (2007). Adaptive auditory plasticity in developing and adult animals. *Prog Neurobiol*, 82(3):109–21.

Kim, H., Ahrlund-Richter, S., Wang, X., Deisseroth, K., and Carlen, M. (2016). Prefrontal parvalbumin neurons in control of attention. *Cell*, 164(1-2):208–218.

Kuchibhotla, K. V., Gill, J. V., Lindsay, G. W., Papadoyannis, E. S., Field, R. E., Sten, T. A., Miller, K. D., and Froemke, R. C. (2017). Parallel processing by cortical inhibition enables context-dependent behavior. *Nat Neurosci*, 20(1):62–71.

Las, L., Stern, E. A., and Nelken, I. (2005). Representation of tone in fluctuating maskers in the ascending auditory system. *J Neurosci*, 25(6):1503–13.

Lee, S. H., Kwan, A. C., and Dan, Y. (2014). Interneuron subtypes and orientation tuning. *Nature*, 508(7494):E1–2.

Lee, S. H., Kwan, A. C., Zhang, S., Phoumthipphavong, V., Flannery, J. G., Masmanidis, S. C., Taniguchi, H., Huang, Z. J., Zhang, F., Boyden, E. S., Deisseroth, K., and Dan, Y. (2012). Activation of specific interneurons improves v1 feature selectivity and visual perception. *Nature*, 488(7411):379–83.

LeMasurier, M. and Gillespie, P. G. (2005). Hair-cell mechanotransduction and cochlear amplification. *Neuron*, 48(3):403–15.

Linden, J. F., Liu, R. C., Sahani, M., Schreiner, C. E., and Merzenich, M. M. (2003). Spectrotemporal structure of receptive fields in areas ai and aaf of mouse auditory cortex. *J Neurophysiol*, 90(4):2660–75.

Linden, J. F. and Schreiner, C. E. (2003). Columnar transformations in auditory cortex? a comparison to visual and somatosensory cortices. *Cereb Cortex*, 13(1):83–9.

Llinas, R. R. (2014). Intrinsic electrical properties of mammalian neurons and cns function: a historical perspective. *Front Cell Neurosci*, 8:320.

Lundstrom, B. N. and Fairhall, A. L. (2006). Decoding stimulus variance from a distributional neural code of interspike intervals. *J Neurosci*, 26(35):9030–7.

Magri, C., Whittingstall, K., Singh, V., Logothetis, N. K., and Panzeri, S. (2009). A toolbox for the fast information analysis of multiple-site lfp, eeg and spike train recordings. *BMC Neurosci*, 10:81.

Malmierca, M. S. (2003). The structure and physiology of the rat auditory system: an overview. *Int Rev Neurobiol*, 56:147–211.

Malone, B. J., Heiser, M. A., Beitel, R. E., and Schreiner, C. E. (2017). Background noise exerts diverse effects on the cortical encoding of foreground sounds. *J Neurophysiol*, 118(2):1034–1054.

Markram, H., Toledo-Rodriguez, M., Wang, Y., Gupta, A., Silberberg, G., and Wu, C. (2004). Interneurons of the neocortical inhibitory system. *Nat Rev Neurosci*, 5(10):793–807.

McGinley, M. J., David, S. V., and McCormick, D. A. (2015). Cortical membrane potential signature of optimal states for sensory signal detection. *Neuron*, 87(1):179–92.

McGovern, S. (2020). Room impulse response generator. `https://www.mathworks.com/matlabcentral/fileexchange/5116-room-impulse-response-generator`. MATLAB Central File Exchange. Retrieved May 22, 2020.

Mesgarani, N. (2013). *Stimulus Reconstruction from Cortical Responses*, pages 1–3. Springer New York, New York, NY.

Mesgarani, N., David, S. V., Fritz, J. B., and Shamma, S. A. (2014). Mechanisms of noise robust representation of speech in primary auditory cortex. *Proc Natl Acad Sci U S A*, 111(18):6792–7.

Metherate, R., Cox, C. L., and Ashe, J. H. (1992). Cellular bases of neocortical activation: modulation of neural oscillations by the nucleus basalis and endogenous acetylcholine. *J Neurosci*, 12(12):4701–11.

Metzger, D. and Chambon, P. (2001). Site- and time-specific gene targeting in the mouse. *Methods*, 24(1):71–80.

Meyers, E. M. (2013). The neural decoding toolbox. *Front Neuroinform*, 7:8.

Miyamae, T., Chen, K., Lewis, D. A., and Gonzalez-Burgos, G. (2017). Distinct physiological maturation of parvalbumin-positive neuron subtypes in mouse prefrontal cortex. *J Neurosci*, 37(19):4883–4902.

Mizrahi, A., Shalev, A., and Nelken, I. (2014). Single neuron and population coding of natural sounds in auditory cortex. *Curr Opin Neurobiol*, 24(1):103–10.

Moore, A. K. and Wehr, M. (2013). Parvalbumin-expressing inhibitory interneurons in auditory cortex are well-tuned for frequency. *J Neurosci*, 33(34):13713–23.

Moore, A. K., Weible, A. P., Balmer, T. S., Trussell, L. O., and Wehr, M. (2018). Rapid rebalancing of excitation and inhibition by cortical circuitry. *Neuron*, 97(6):1341–1355 e6.

Morrison, M. and Parker, G. (1987). A guide to rotations in quantum mechanics. *Australian Journal of Physics*, 40(4):465–498.

Mountcastle, V. B. (1997). The columnar organization of the neocortex. *Brain*, 120 (Pt 4):701–22.

Munoz, W. and Rudy, B. (2014). Spatiotemporal specificity in cholinergic control of neocortical function. *Curr Opin Neurobiol*, 26:149–60.

Nabelek, A. K., Letowski, T. R., and Tucker, F. M. (1989). Reverberant overlap- and self-masking in consonant identification. *J Acoust Soc Am*, 86(4):1259–65.

Nagel, G., Szellas, T., Huhn, W., Kateriya, S., Adeishvili, N., Berthold, P., Ollig, D., Hegemann, P., and Bamberg, E. (2003). Channelrhodopsin-2, a directly light-gated cation-selective membrane channel. *Proceedings of the National Academy of Sciences of the United States of America*, 100(24):13940–13945.

Nelken, I., Rotman, Y., and Bar Yosef, O. (1999). Responses of auditory-cortex neurons to structural features of natural sounds. *Nature*, 397(6715):154–7.

Ozeki, H., Finn, I. M., Schaffer, E. S., Miller, K. D., and Ferster, D. (2009). Inhibitory stabilization of the cortical network underlies visual surround suppression. *Neuron*, 62(4):578–92.

Pakan, J. M., Lowe, S. C., Dylda, E., Keemink, S. W., Currie, S. P., Coutts, C. A., and Rochefort, N. L. (2016). Behavioral-state modulation of inhibition is context-dependent and cell type specific in mouse visual cortex. *Elife*, 5.

Panzeri, S., Macke, J. H., Gross, J., and Kayser, C. (2015). Neural population coding: combining insights from microscopic and mass signals. *Trends Cogn Sci*, 19(3):162–72.

Paterna, J. C., Feldon, J., and Bueler, H. (2004). Transduction profiles of recombinant adeno-associated virus vectors derived from serotypes 2 and 5 in the nigrostriatal system of rats. *J Virol*, 78(13):6808–17.

Paul, A., Crow, M., Raudales, R., He, M., Gillis, J., and Huang, Z. J. (2017). Transcriptional architecture of synaptic communication delineates gabaergic neuron identity. *Cell*, 171(3):522–539 e20.

Perel, S., Sadtler, P. T., Oby, E. R., Ryu, S. I., Tyler-Kabara, E. C., Batista, A. P., and Chase, S. M. (2015). Single-unit activity, threshold crossings, and local field potentials in motor cortex differentially encode reach kinematics. *J Neurophysiol*, 114(3):1500–12.

Petrie, K. A., Schmidt, D., Bubser, M., Fadel, J., Carraway, R. E., and Deutch, A. Y. (2005). Neurotensin activates gabaergic interneurons in the prefrontal cortex. *J Neurosci*, 25(7):1629–36.

Phillips, E. A. and Hasenstaub, A. R. (2016). Asymmetric effects of activating and inactivating cortical interneurons. *Elife*, 5.

Polack, P. O., Friedman, J., and Golshani, P. (2013). Cellular mechanisms of brain state-dependent gain modulation in visual cortex. *Nat Neurosci*, 16(9):1331–9.

Poorthuis, R. B., Enke, L., and Letzkus, J. J. (2014). Cholinergic circuit modulation through differential recruitment of neocortical interneuron types during behaviour. *J Physiol*, 592(19):4155–64.

Posluszny, A. (2019). Updating the picture of layer 2/3 vip-expressing interneuron function in the mouse cerebral cortex. *Acta Neurobiol Exp (Wars)*, 79(4):328–337.

Puig, M. V., Watakabe, A., Ushimaru, M., Yamamori, T., and Kawaguchi, Y. (2010). Serotonin modulates fast-spiking interneuron and synchronous activity in the rat prefrontal cortex through 5-ht1a and 5-ht2a receptors. *J Neurosci*, 30(6):2211–22.

Purves, D., Augustine, G. J., Fitzpatrick, D., Hall, W., LaMantia, A., McNamara, J., and Williams, S. (2004). *Neuroscience. 3nd edition*. Sinauer Associates.

Rabinowitz, N. C., Willmore, B. D., King, A. J., and Schnupp, J. W. (2013). Constructing noise-invariant representations of sound in the auditory pathway. *PLoS Biol*, 11(11):e1001710.

Rabinowitz, N. C., Willmore, B. D., Schnupp, J. W., and King, A. J. (2011). Contrast gain control in auditory cortex. *Neuron*, 70(6):1178–91.

Riedemann, T. (2019). Diversity and function of somatostatin-expressing interneurons in the cerebral cortex. *Int J Mol Sci*, 20(12).

Robles, L. and Ruggero, M. A. (2001). Mechanics of the mammalian cochlea. *Physiol Rev*, 81(3):1305–52.

Rogalla, M. M., Rauser, I., Schulze, K., Osterhagen, L., and Hildebrandt, K. J. (2020). Mice tune out not in: violation of prediction drives auditory saliency. *Proc Biol Sci*, 287(1919):20192001.

Ruff, D. A. and Cohen, M. R. (2017). A normalization model suggests that attention changes the weighting of inputs between visual areas. *Proc Natl Acad Sci U S A*, 114(20):E4085–E4094.

Sahani, M. (1999). *Latent variable models for neural data analysis*. PhD thesis, California Institute of Technology.

Sahani, M. and Linden, J. F. (2003). Evidence optimization techniques for estimating stimulus-response functions. In *Advances in neural information processing systems*, pages 317–324.

Salinas, E. and Sejnowski, T. J. (2001). Gain modulation in the central nervous system: where behavior, neurophysiology, and computation meet. *Neuroscientist*, 7(5):430–40.

Salinas, E. and Thier, P. (2000). Gain modulation: a major computational principle of the central nervous system. *Neuron*, 27(1):15–21.

Sauer, B. and Henderson, N. (1988). Site-specific dna recombination in mammalian cells by the cre recombinase of bacteriophage p1. *Proc Natl Acad Sci U S A*, 85(14):5166–70.

Schneider, D. M., Nelson, A., and Mooney, R. (2014). A synaptic and circuit basis for corollary discharge in the auditory cortex. *Nature*, 513(7517):189–94.

Seybold, B. A., Phillips, E. A. K., Schreiner, C. E., and Hasenstaub, A. R. (2015). Inhibitory actions unified by network integration. *Neuron*, 87(6):1181–1192.

Seybold, B. A., Stanco, A., Cho, K. K., Potter, G. B., Kim, C., Sohal, V. S., Rubenstein, J. L., and Schreiner, C. E. (2012). Chronic reduction in inhibition reduces receptive field size in mouse auditory cortex. *Proc Natl Acad Sci U S A*, 109(34):13829–34.

Shaner, N. C., Steinbach, P. A., and Tsien, R. Y. (2005). A guide to choosing fluorescent proteins. *Nat Methods*, 2(12):905–9.

Sherrington, C. S. (1906). Observations on the scratch-reflex in the spinal dog. *J Physiol*, 34(1-2):1–50.

Smith, E. C. and Lewicki, M. S. (2006). Efficient auditory coding. *Nature*, 439(7079):978–82.

Stiebler, I. (1987). A distinct ultrasound-processing area in the auditory cortex of the mouse. *Naturwissenschaften*, 74(2):96–7.

Stiebler, I., Neulist, R., Fichtel, I., and Ehret, G. (1997). The auditory cortex of the house mouse: left-right differences, tonotopic organization and quantitative analysis of frequency representation. *J Comp Physiol A*, 181(6):559–71.

Swanson, O. K. and Maffei, A. (2019). From hiring to firing: Activation of inhibitory neurons and their recruitment in behavior. *Front Mol Neurosci*, 12:168.

Tharwat, A., Gaber, T., Ibrahim, A., and Hassanien, A. E. (2017). Linear discriminant analysis: A detailed tutorial. *Ai Communications*, 30:169–190,.

Thompson, A. M. and Schofield, B. R. (2000). Afferent projections of the superior olivary complex. *Microsc Res Tech*, 51(4):330–54.

Toussay, X., Basu, K., Lacoste, B., and Hamel, E. (2013). Locus coeruleus stimulation recruits a broad cortical neuronal network and increases cortical perfusion. *J Neurosci*, 33(8):3390–401.

Traer, J. and McDermott, J. H. (2016). Statistics of natural reverberation enable perceptual separation of sound and space. *Proc Natl Acad Sci U S A*, 113(48):E7856–E7865.

Tremblay, R., Lee, S., and Rudy, B. (2016). Gabaergic interneurons in the neocortex: From cellular properties to circuits. *Neuron*, 91(2):260–92.

Tronche, F., Casanova, E., Turiault, M., Sahly, I., and Kellendonk, C. (2002). When reverse genetics meets physiology: the use of site-specific recombinases in mice. *FEBS Lett*, 529(1):116–21.

Walker, K. M., Bizley, J. K., King, A. J., and Schnupp, J. W. (2011). Multiplexed and robust representations of sound features in auditory cortex. *J Neurosci*, 31(41):14565–76.

Wallach, H., Newman, E. B., and Rosenzweig, M. R. (1949). The precedence effect in sound localization. *Am J Psychol*, 62(3):315–36.

Wieland, A. and Wallenburg, C. (2012). Dealing with supply chain risks: Linking risk management practices and strategies to performance. *International Journal of Physical Distribution and Logistics Management*, 42(10):887–905.

Williamson, R. S., Ahrens, M. B., Linden, J. F., and Sahani, M. (2016). Input-specific gain modulation by local sensory context shapes cortical and thalamic responses to complex sounds. *Neuron*, 91(2):467–81.

Wilson, D. A. (2001). Receptive fields in the rat piriform cortex. *Chem Senses*, 26(5):577–84.

Wilson, N. R., Runyan, C. A., Wang, F. L., and Sur, M. (2012). Division and subtraction by distinct cortical inhibitory networks in vivo. *Nature*, 488(7411):343–8.

Xu, X., Roby, K. D., and Callaway, E. M. (2010). Immunochemical characterization of inhibitory mouse cortical neurons: three chemically distinct classes of inhibitory cells. *J Comp Neurol*, 518(3):389–404.

Yizhar, O., Fenno, L. E., Davidson, T. J., Mogri, M., and Deisseroth, K. (2011a). Optogenetics in neural systems. *Neuron*, 71(1):9–34.

Yizhar, O., Fenno, L. E., Prigge, M., Schneider, F., Davidson, T. J., O'Shea, D. J., Sohal, V. S., Goshen, I., Finkelstein, J., Paz, J. T., Stehfest, K., Fudim, R., Ramakrishnan, C., Huguenard, J. R.,

Hegemann, P., and Deisseroth, K. (2011b). Neocortical excitation/inhibition balance in information processing and social dysfunction. *Nature*, 477(7363):171–8.

Zhang, F., Wang, L. P., Boyden, E. S., and Deisseroth, K. (2006). Channelrhodopsin-2 and optical control of excitable cells. *Nat Methods*, 3(10):785–92.

Zhang, Y., Meyers, E. M., Bichot, N. P., Serre, T., Poggio, T. A., and Desimone, R. (2011). Object decoding with attention in inferior temporal cortex. *Proc Natl Acad Sci U S A*, 108(21):8850–5.

Zhou, M., Liang, F., Xiong, X. R., Li, L., Li, H., Xiao, Z., Tao, H. W., and Zhang, L. I. (2014). Scaling down of balanced excitation and inhibition by active behavioral states in auditory cortex. *Nat Neurosci*, 17(6):841–50.

Publication

Sustained Activation of PV+ Interneurons in Core Auditory Cortex Enables Robust Divisive Gain Control for Complex and Naturalistic Stimuli

Tina Gothner [1,+], Pedro J. Gonçalves [2,3,+], Maneesh Sahani [3], Jennifer F. Linden [4], K. Jannis Hildebrandt [1,5]

[1] Department of Neuroscience, University of Oldenburg, Oldenburg, Germany, 26126

[2] Max Planck Research Group Neural Systems Analysis, Center of Advanced European Studies and Research (caesar), Bonn, Germany, 53175

[3] Gatsby Computational Neuroscience Unit, University College London, London, UK, W1T 4JG

[4] Ear Institute and Department of Neuroscience, Physiology, & Pharmacology, University College London, London, UK, WC1E 6BT

[5] Cluster of Excellence Hearing4all, University of Oldenburg, Oldenburg, Germany, 26129

[+] these authors contributed equally to the work

Inhibitory interneurons have been shown to provide a powerful means for neuromodulatory adjustment of cortical processing. Despite advances in our understanding of the roles of cortical interneurons, we lack an understanding of how sustained activation of inhibition changes cortical computation. Here, we show that sustained activation of the largest group of cortical interneurons, PV+ cells, enables divisive gain control - one of the most fundamental adjustments of sensory processing. While previous studies on potential roles of inhibition used transient optogenetic activation, we employed a technique enabling prolonged activation for up to several minutes, a timescale typical for many neuromodulatory processes. Using this approach, we show that robust division generalizes to complex and naturalistic sounds, verifying the potential ecological relevance of the mechanism.

Original Research Article

Contributions of collaborators

Study: Sustained Activation of PV+ Interneurons in Core Auditory Cortex Enables Robust Divisive Gain Control for Complex and Naturalistic Stimuli

The data collection was supported by B.Sc. H. Hosseini and B.Sc. D. Gonschorek, Master's students of the program Neuroscience at University of Oldenburg.

The analysis of spectro-temporal receptive fields (Fig 4.5) was done and kindly provided by Dr. P.J. Gonçalves (member of Max Planck Research Group Neural Systems Analysis, Center of Advanced European Studies and Research (caesar), Bonn, Germany).

Study: A Multiplex Population Code for Sound Identity and Context in Core Auditory Cortex

The behavioral experiments were done by Charlotte Sigg, Bachelor's student of the division Auditory Neuroscience at University of Oldenburg.

The data collection of electrophysiology experiments was supported by B.Sc. D. Gonschorek, Master's students of the program Neuroscience at University of Oldenburg.

The analysis of mutual information and stimulus reconstruction (Fig. 5.5) was done and kindly provided by Dr. K.J.Hildebrandt (Auditory Neuroscience, Department of Neuroscience, University of Oldenburg, Oldenburg, Germany).

Danksagung

Es ist für mich keine Selbstverständlichkeit, dass dieses Werk entstanden ist. Daher möchte ich mich hier bei allen Personen bedanken, die mich bei dieser Arbeit tatkräftig unterstützt haben.

Meinen ersten Dank möchte ich an meine Arbeitsgruppe richten, insbesondere an Dr. Jannis Hildebrandt, der mir dieses Projekt ermöglicht, mich unterstützt und geleitet hat. Hatte ich den roten Faden aus den Augen verloren, hat er ihn mir wieder in die Hand gelegt. Vielen Dank für alle wervollen Erfahrungen, die mich geprägt haben und mich zu dem gemacht haben, der ich jetzt bin. Meinen Kollegen Meike Rogalla und Lasse Osterhagen möchte ich für die Kurzweiligkeit, für viele Stunden fachlicher Diskussionen und geselligen Fröbeleien danken.

Dr. Jutta Kretzberg und ihrer Arbeitsgruppe möchte ich für die Unterstützung danken, die ich mit unter schon weit vor der Doktorarbeit erhalten hatte. Herzlichsten Dank für spannende Projekte, kreative Ideensammlungen und natürlich vielen Dank für die Aufnahme in die Arbeitsgruppe als externes (Familien-)Mitglied. An dieser Stelle möchte ich mich explizit bei Dr. Go Ashida für die tolle wissenschaftliche und menschliche Unterstützung bedanken.

Es ist nicht immer schlimm, wenn man Berufliches und Privates nicht trennen kann. Vielen Dank an Dr. Lena Köpcke und Sonja Meiser für Kaffeepausen mit Diskussionshintergrund, fachliche Spieleabende und eine rund-um-die-Uhr Gesprächshotline für alle Hoch und Tiefs.

Ein mir sehr wichtiger Dank geht an all meine Freunde und an meine Familie in Süddeutschland, die geduldig auf meine Rückkehr gewartet haben und mich nach fünf Jahren Abstinenz wieder herzlich willkommen hießen.

Das größte und wichtigste Dankeschön gilt Tilman, der mich in allen erdenklichen Phasen zeitintensiv, sachlich und emotional unterstützt hat und mir immer zur Seite stand. In guten, wie in schlechten Zeiten.

Für meinen Papa.

Eidesstattliche Erklärung

Hiermit versichere ich, dass ich diese Arbeit selbständig verfasst und keine anderen als die angegebenen Quellen und Hilfsmittel benutzt habe. Außerdem versichere ich, dass ich die allgemeinen Prinzipien wissenschaftlicher Arbeit und Veröffentlichung, wie sie in den Leitlinien guter wissenschaftlicher Praxis der Carl von Ossietzky Universität Oldenburg festgelegt sind, befolgt habe.

Nürnberg, den 18.01.2021

Tina Gothner